Mass Spectrometric Imaging for Biomedical Tissue Analysis

Kamila Chughtai and Ron M. A. Heeren*

FOM-Institute for Atomic and Molecular Physics, Science Park 104, 1098 XG Amsterdam, The Netherlands

Received January 13, 2010

Contents

1. Introduction 3237
   1.1. Mass Spectrometry 3237
   1.2. Mass Spectrometric Imaging 3238
   1.3. MSI—Basic Principles and Ionization Techniques 3238
      1.3.1. Matrix Assisted Laser Desorption/Ionization 3239
      1.3.2. Secondary Ion Mass Spectrometry 3239
      1.3.3. Desorption Electrospray Ionization 3241
      1.3.4. Other Desorption and Ionization Techniques for MSI 3241
   1.4. Advantages of MSI 3242
   1.5. Limitations of MSI 3242
   1.6. MSI—Applications 3243
2. Methodological Description and Current Improvements 3243
   2.1. Biological Sample Preparation 3243
      2.1.1. Biological Sample Handling 3243
      2.1.2. Tissue Preparation 3245
      2.1.3. Matrix Application 3248
      2.1.4. Staining 3253
      2.1.5. Contaminants 3253
   2.2. MSI Instrumentation and Processing Tools 3254
      2.2.1. Mass Analyzers 3254
      2.2.2. Software for MSI 3256
   2.3. Application of Ion Mobility Separation for Mass Spectrometric Imaging 3257
   2.4. Microscope vs Microprobe Mode of Image Acquisition 3258
   2.5. Profiling vs Imaging 3258
   2.6. Tags 3259
3. Applications of Mass Spectrometric Imaging 3259
   3.1. Application of MSI in Disease Pathology 3260
   3.2. Application of MSI in Biological Sciences 3261
   3.3. Application of MSI in Proteomics/Peptidomics 3263
   3.4. Application of MSI in Metabolomics 3265
   3.5. Application of MSI in Lipidomics 3266
   3.6. Application of MSI in Pharmacokinetic Studies 3269
   3.7. MSI 3D Imaging 3271
4. Future Perspectives 3272
5. Abbreviations 3272
6. Acknowledgments 3273
7. References 3273

* Corresponding author. Telephone: +31-20-7547 100. Fax: +31-20-7547 290. E-mail address: heeren@amolf.nl.

1. Introduction

1.1. Mass Spectrometry

A mass spectrometer is described as the smallest weighing scale ever used in the world.[1] Mass spectrometry (MS) is a unique technique that has an interdisciplinary nature, which freely crosses the borders of physics, chemistry, and biology. Mass spectrometry is a great scientific tool due to its capabilities to determine the mass of large biomolecular complexes, individual biomolecules, small organic molecules, and single atoms and their isotopes. Right from the time of its invention in the first decade of the 20th century, mass spectrometry has undergone tremendous improvements in terms of its sensitivity, resolution, and mass range. It currently finds applications in all scientific disciplines, such as chemistry, physics, biology, pharmacology, medicine, biochemistry, and bioagro-based industry.

Introduction of "soft" ionization sources such as electrospray ionization (ESI) by Fenn et al.[2] and matrix-assisted laser desorption/ionization (MALDI) by Karas et al.[3] in the 1980s revolutionized mass spectrometry, as it offered the capability to analyze large intact biomolecules. As such, MS became an irreplaceable tool for the biological sciences. The development of both ESI and MALDI made possible the ionization of smaller biomolecules such as drugs and metabolites as well larger biomolecules such as lipids, peptides, and even proteins.[2,4] The molecular weight (M_w) ranges we use in this review are defined as follows. The low M_w range includes elements and molecules from 1 to 500 Da. Molecules with M_w between 500 and 2000 Da fall in the medium M_w range. All molecules with $M_w > 2000$ Da are considered to be part of the high molecular weight class. It goes beyond the scope of this review to cover all developments in MS. Rather this review focuses on one of the latest, rapidly developing innovations in MS, namely mass spectrometric imaging (MSI). This young technique takes benefit from all methodological and technological developments in general MS over the last decades. Over the last 20 years MSI has transformed from an esoteric, specialist technology studied by few researchers only to a technique that now finds itself at the center stage of mainstream MS. Over the last years the technology has matured to find applications in many different areas, with instrument developments taken up by all MS instrument manufacturers resulting in a rapid rise of the number of research groups active in this area. A thorough review of the area is therefore timely and needed to offer a starting point for all newcomers to the field. In this paper we describe and review approximately 20 years of MSI development from the perspective of its application to biomedical imaging. We will emphasize the key research steps and pitfalls that determine

10.1021/cr100012c
Published on Web 04/28/2010

Kamila Chughtai obtained her first M.Sc. degree in biotechnology at Maria Curie-Sklodowska University in Poland. In 2005 she joined Prof. Elizabeth Ann (Lee) Fortunato's research group at University of Idaho and in 2007 graduated as a M.Sc. in Microbiology, Molecular Biology, and Biochemistry. She returned to Poland to become a research assistant in the Department of Medical Genetics of The Children's Memorial Health Institute in Warsaw. At present, she is a Ph.D. student in Ron M. A. Heeren's group focused on mass spectrometric imaging of breast cancer. Her research interests include the application of various imaging techniques for molecular biology of cancer, revealing the role of DNA repair machinery in human genomic instability syndromes as well as during viral infections.

Ron M. A. Heeren obtained a Ph.D. degree in technical physics in 1992 at the University of Amsterdam on plasma−surface interactions. After two years of postdoctoral work on FTICR mass spectrometry, he joined the MOLART research team at the FOM-Institute for Atomic and Molecular Physics as a project leader, heading the instrumental developments for paint cross-section analysis in early 1995. In 1999 he started a research group focusing on macromolecular ion physics with high resolution mass spectrometry and the development of imaging mass spectrometry at AMOLF. In 2001 he was appointed professor at the chemistry faculty of Utrecht University, lecturing on the physical aspects of biomolecular mass spectrometry. He is an active participant in The Netherlands Proteomics Centre and the Virtual Laboratory or e-sciences. His academic research interests are the fundamental studies of the energetics of macromolecular systems, conformational studies of noncovalently bound protein complexes, virtual laboratory technology, and the development and validation of new mass spectrometry based proteomic imaging techniques for the life sciences. The mass spectrometric imaging facility at FOM-AMOLF under his supervision is used to study neurodegenerative diseases, the molecular basis of cancer, and several drug metabolic projects, including innovative nanoparticle based drug delivery systems.

the outcome of biological applications of this relatively new *label free* biomolecular imaging technique in life sciences.

1.2. Mass Spectrometric Imaging

MSI allows the rapid detection, localization, and identification of many molecules from the most complex, biological sample surfaces. It emerged as a response to the demand for spatial information about biomolecules detected by conventional mass spectrometry. The MSI instrumentation, methods, and protocols have been developed to study the spatial distribution of endogenous compounds such as lipids or proteins and exogenous compounds such as polymers or pharmaceutical compounds on complex surfaces. It is a *label free* technique that can deliver detailed understanding of biological processes on different length scales, from subcellular to multicellular level and from organs to whole biological systems. Although MSI takes advantage of all modern developments in MS, the concept already existed before the development period reviewed here. In particular, in the field of physics, secondary ion mass spectrometry (SIMS) was used extensively to study semiconductor surfaces and the like. It was not until the introduction of MALDI-MSI in 1997 by Caprioli et al.[5] that the current rapid developments of methodologies, instrumentation, and software used for imaging of biological samples started. Now, peptide and protein profiling directly from biological tissue samples is almost routine already, while the first images of whole tissue sections were shown only in 2001, illustrating the speed of application development.[6]

SIMS has also seen limited application for imaging biological samples.[7,8] The development of liquid metal ion guns (LMIG) as a primary ion source for SIMS experiments in the 1990s revolutionized SIMS imaging. It realized a much wider scope of applications of high spatial resolution MSI of biological surfaces.[9]

The third ionization method used for MSI evolved recently in the form of desorption electrospray ionization (DESI). This relatively new technique has emerged from the lab of Cooks and co-workers in 2004.[10]

These three desorption and ionization methods, MALDI, SIMS, and DESI, lay at the heart of modern MSI developments. In the next section, we will review the basic principles of MSI and its desorption and ionization techniques in more detail to provide a thorough basic understanding before discussing their many different applications in section 3.

1.3. MSI—Basic Principles and Ionization Techniques

Mass spectrometric imaging is essentially a four step process. It involves sample preparation, desorption and ionization, mass analysis, and image registration. All four elements need to be carefully controlled and monitored to generate meaningful images. Sample preparation is a key to any analytical technique. Its special requirements for MSI will be extensively discussed in section 2.1 of this review. After introduction of the samples into an MSI instrument, the biomolecules first are desorbed and ionized from the surface. This is achieved through exposure of the surface to a laser beam (LDI/MALDI), a primary ion beam (SIMS), or a charged droplet flux (DESI). The ionized molecules are subsequently mass separated inside the mass analyzer. This can be a time of flight (TOF), Fourier transform ion cyclotron resonance (FTICR), linear quadrupole (Q), or Orbitrap instrument or any of the available mass spectrometric systems that can be interfaced with these desorption and ionization sources. The different nature of these instruments renders different mass spectral quality and information, which will be discussed in detail in section 2.2 of this review. The whole surface of the sample is examined during a MSI experiment to collect mass spectral information about the molecular

composition and distribution of the analyzed molecules at every point. The resulting molecular ion distributions are presented in the form of ion images.

In the life sciences there is a growing demand for a technique or tool capable of visualizing macromolecular distributions directly from biological samples. So far, MSI is the only technique that generates high resolution biomacromolecular images directly from tissue sections and without the need for labels.[9]

1.3.1. Matrix Assisted Laser Desorption/Ionization

Matrix-assisted laser desorption/ionization mass spectrometry (MALDI-MS) is a dramatic improvement of laser desorption/ionization mass spectrometry (LDI-MS). It is a powerful method that allows the analysis and detection of a wide range of biomolecules directly from tissue sections. MALDI is an ionization technique that is capable of producing intact higher M_w ions through the use of a pulsed laser beam combined with energy absorbing matrix molecules. In nonimaging MALDI analysis, the analyte is mixed with an excess of chemical matrix: usually, the analyte is a small organic acid at a molar matrix to analyte ratio of 10^3-10^5:1.[11] The role of the matrix is to absorb the majority of the laser energy, leading to explosive desorption of the matrix crystals, together with incorporation of analyte into the gas phase without degradation of the analyte. The matrix also aids the ionization of analyte molecules in the gas phase due to the presence of protons from added acids such as trifluoroacetic acid (TFA). The first reported LDI-MS experiments were performed using a fine powder of cobalt metal in glycerol as the matrix for the observation of ions with a mass over charge ratio (m/z) of 34 000.[12] Soon afterward, MALDI-MS results of serum albumin (67 000 Da) were reported using nicotinic acid as the matrix.[13] MALDI has low femtomole to attomole sensitivity and a mass range up to 100 kDa, and it is routinely used for the analysis of metabolites, lipids, peptides, and proteins.[1,11]

Molecular imaging of tissue sections with MALDI-MSI requires the tissue surface to be covered by a solution of a low M_w organic compound (matrix). On-tissue application of this matrix solution results in *in situ* extraction of biomolecules from the biological sample. The subsequent evaporation of the solvent from the matrix solution causes the crystallization of the matrix and incorporation of the analyte molecules into growing crystals. The matrix is always applied in concentrations well above the surface analyte concentrations. The resulting crystal surface is irradiated with pulsed laser light of sufficient fluence, leading to desorption and ionization of matrix and analyte molecules, as schematically indicated in Figure 1. The incorporation of the analyte into the matrix crystals ultimately prevents fragmentation of larger analyte molecules during desorption through the reduction of the direct interaction of the analyte molecules with the laser light. The matrix molecules absorb the laser energy and facilitate the explosive desorption and ionization process. Fragmentation of the acidic matrix molecules typically leads to an excess of protons above the surface that in turn result in gas-phase ion−molecule reactions producing pseudomolecular ions.

During a MALDI-MSI experiment the laser beam is rastered across the surface of the matrix covered tissue, which allows desorption and ionization of biomolecules. The ablation crater is estimated to have a depth of 1 μm or more, depending on laser fluence.[9] The position of the laser beam

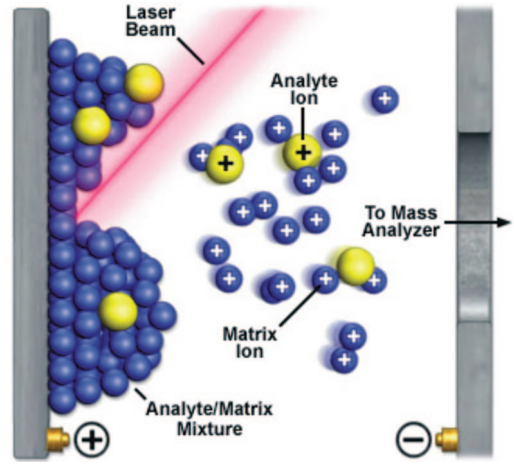

Figure 1. Schematic representation of the MALDI desorption and ionization process. Reprinted with permission from ref 339. Copyright 2008 National High Magnetic Field Laboratory.

on the surface is usually varied by moving the target plate while the laser beam remains fixed in an optimized position with respect to the inlet of the mass spectrometer. The introduction of N_2 (337 nm) or neodymium-doped yttrium aluminium garnet (Nd:YAG) (355 nm) lasers with repetition rates of 200−1000 Hz and typical pulse lengths of 3 ns or less shortened the time needed for sufficient data acquisition.[14] To make MALDI-MSI a practical application, the laser spot size was reduced from 100−150 to 20 μm.[15] Further laser spot size reduction and micrometric spatial resolution was achieved with a MALDI instrument equipped with a highly focused laser.[16] Focusing of the laser beam to the diameter of a single cell (approximately 7 μm) has also been reported by Holle et al. in 2006.[17] Unfortunately, the improvement in resolution decreased sensitivity. Laser intensity modulation within the laser spot, such as implemented in the SmartBeam technology, is used to enhance the signal-to-noise ratio in a MALDI imaging MS experiment. The use of an acousto-optic modulator or a programmable liquid crystal phase modulator can create random patterns of hot spots in solid state lasers, similar to those naturally found in a plasma based laser such as a nitrogen laser.[18] It combines the sensitivity, resolution, ease of a nitrogen laser use, focusing ability, variable beam diameter, and high repetition rate of common solid state lasers.

The time needed to obtain images from the sample depends on the number of analyzed spots, the repetition rate of the laser (Hz), and the data collecting and processing speed of computers. On modern state of the art MALDI mass spectrometers equipped with lasers operating at 1 kHz, a whole-body mouse or rat section would take less than 4 h to image.[19]

MALDI-MSI is a leading method for recording intact peptide and protein distributions because it can detect hundreds of peptides and proteins directly from tissue sections due to its high sensitivity, large tolerance for salts and other contaminants, a wide mass range, little fragmentation, *label free* detection method, and easy data interpretation because the majority of ions are singly protonated $[M + H]^+$.

1.3.2. Secondary Ion Mass Spectrometry

SIMS is a desorption and ionization technique used for MSI which utilizes a primary ion beam (e.g., metal ions) to produce secondary ions from the surface of the sample as

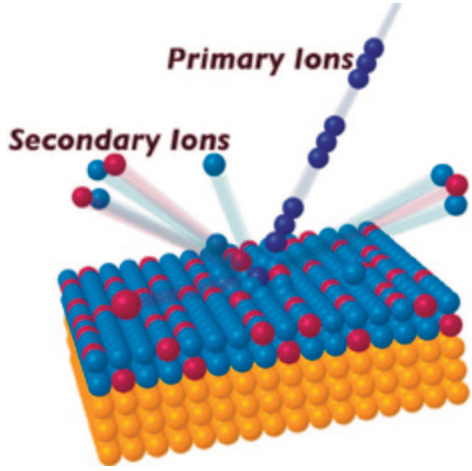

Figure 2. Schematic representation of the SIMS desorption and ionization process. Reprinted with permission from ref 340. Copyright 2010 NESAC/BIO and University of Washington.

schematically shown in Figure 2. For this purpose an ion column is used that produces, accelerates, conditions, focuses, and steers a primary ion beam. This primary ion beam can be focused as sharply as 50 nm, depending on the primary ion beam current, the M_w, and the charge state of the primary ions. The energy of the primary ions deposited into the surface is substantially higher than the energy deposited into the surface by a laser beam during LDI or MALDI experiments. SIMS therefore often yields extensive fragmentation of surface molecules. However, as ion beams can be focused with much higher precision than a laser beam, SIMS is a unique tool for high spatial resolution MSI of elements and small organic molecules in different organelles in the cell.[9,20]

SIMS imaging of biological materials was principally developed by Winograd et al. and by Todd et al.[15,21] This ionization method yields chemical information on lower M_w species at very high spatial resolution (less than 10 nm has been reported).[22] A collision cascade transfers the energy of the primary ions to the sample surface. Typical energies of the primary ions are in the range of 5−25 keV, which are much higher compared to bond energies of surface molecules. This results in extensive fragmentation of molecules and bond breaking near the collision site, producing essentially only the emission of atomic particles. When moving away from the primary collision site, less fragmentation occurs. A small fraction of intact molecules is subsequently ejected from the first layers of the surface if the surface binding energy is overcome. In most cases, the molecules are found to desorb from within 5−10 nm of the impact point. Most molecules are emitted as neutrals, and only approximately 1% of them are charged. Depending on the electron configuration of the surface molecules, both positive and negative ions can be generated. An important parameter in SIMS is the damage cross section: this is a measure of the surface area affected by the impact of a single primary ion. The impact of a primary ion damages the molecules close to the point of impact. Resampling the damaged areas would provide chemical information about the damaged areas and not the surface. In order to ensure that the chemical information corresponds to the pristine surface, very low primary ion doses ($<10^{13}$ ions cm^{-2}) are used. Within this regime, less than 1% of the top surface layer of atoms (or small molecules) receives a primary ion impact. Statistically it is unlikely that the same area is sampled twice; consequently, the mass spectrum provides chemical information about the unchanged (static) surface. This type of SIMS is known as static SIMS, and the ion dose limit constitutes the static SIMS limit. Above this limit, the technique is referred to as dynamic SIMS. This review will concentrate on static SIMS; unless otherwise stated, SIMS refers to static SIMS.

The current developments in primary ion guns used for MSI predominantly employ monatomic primary ions (Ar^+, Ga^+, In^+, Au^+, Xe^+, Bi^+). The development of softer primary ion beams such as C_{60}^+, SF_5^+, Bi_3^+, Au_n^+, and Cs_n^+ [23,24] extends the applicability of SIMS for larger M_w species. These polyatomic primary beams are able to desorb secondary ions from the sample surface without extensive fragmentation. As a result, they are more suitable for the analysis of intact biomolecules from tissue surfaces.[14,22] The secondary ions are introduced into a mass analyzer after acceleration using a high voltage acceleration system. The polarity of the accelerator is employed to select if positive or negative ions are analyzed. A TOF system is most commonly used for mass determination in SIMS, although alternate approaches, such as those based on a magnetic sector mass analyzer, are also employed. The primary ion source must provide short pulse widths (subnanosecond) to yield secondary ions with minimal time dispersion for TOF analysis. The energy and angular dispersion of the secondary ions that originates with the emission process can be compensated using focusing elements such as an ion mirror or reflectron. The reflectron focuses the secondary ions through a retarding electric field in the middle of the flight path, resulting in improved mass resolution. After mass separation, the secondary ions are focused onto a detector. The detector consists of a microchannel plate for ion-to-electron conversion, a scintillator for electron-to-photon conversion, and a photomultiplier, which is placed outside the vacuum chamber.

A wide range of samples can be analyzed by this surface specific technique, which is extremely sensitive to any sample preparation treatment. The sample preparation protocol for the SIMS imaging experiment requires only mounting of the tissue section on an indium tin oxide (ITO)-coated glass slide without any further washing steps. The sample must be stable under ultrahigh vacuum (UHV) conditions, which ensures that both the primary and secondary ions travel from their origin to their final destination without undergoing collisions. The surface morphology of the sample can affect the generation of secondary ions. Samples with surfaces as flat as possible are desired in order to avoid possible shadow effects.

Several surface modification methods have been developed that can enhance the production of intact secondary ions in a SIMS experiment. The application of a thin metal coating for metal assisted-SIMS (MetA-SIMS) or the application of an energy moderating matrix for matrix enhanced-SIMS (ME-SIMS) prevents fragmentation of surface molecules by primary ion beam impact.[25,26] Both techniques will be discussed in the following paragraph, as they enable the use of SIMS for the analysis of intact biomolecules such as lipids and peptides.

MetA-SIMS employs metallization of (organic) samples with a thin layer of silver, gold, or platinum, and it has been shown to increase secondary ion yields of intact molecular ions in SIMS.[27,28] It provides increased sensitivities for larger analytes (<5 kDa) as diverse as fatty acids, lipids, and peptides. In addition, the thin metal layer provides a conductive contact, thus effectively converting insulating samples into conducting samples, thereby removing the need

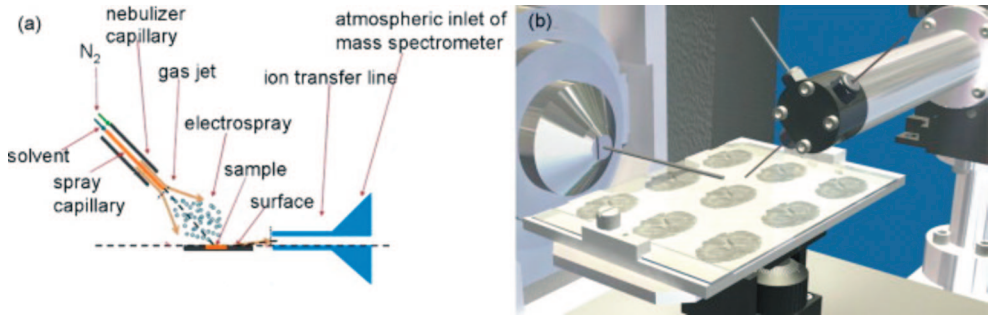

Figure 3. Desorption electrospray ionization (DESI). (a) Schematic representation of the DESI desorption and ionization process; (b) brain tissue imaging analysis using DESI. Reprinted with permission from ref 314. Copyright 2008 Elsevier.

for charge compensation.[9] A complication of using sample metallization is that the ions observed are frequently adducts with the metal and metal clusters.

ME-SIMS can be considered as a combination of MALDI and SIMS. The organic acid is applied on the surface, which enhances the ionization efficiency of larger molecules in a very similar manner as MALDI.[9,29] Standard MALDI matrixes can be used for ME-SIMS, such as 2.5-dihydroxybenzoic acid (DHB), which results in signal intensity enhancement for a wide range of molecular species. One of the advantages of ME-SIMS is that it is both easy and cheap to implement. In ME-SIMS, standard SIMS instrumentation and MALDI sample preparation protocols can be used.[26]

The apparent limitations of SIMS are the lack of sensitivity of the mass range over 1000 *m/z*, due to in-source fragmentation of complex molecules and/or decreased ionization yield and very few or no information on hydrophilic metabolites. Mass spectra obtained by SIMS can be more complicated for interpretation than those from MALDI due to extensive fragmentation of molecules. In addition, SIMS instruments do not operate in MS/MS mode, which limits identification of molecules.[30] Given the current state of the technique, it does not seem possible to liberate, ionize, and detect intact, low abundance proteins with SIMS or ME-SIMS.[9] However, new developments in instrumentation may lead to an increase in the SIMS mass range. One such example is a new system for MSI which used MeV ion beams, termed MeV-secondary ion mass spectrometry (MeV-SIMS).[31] MeV-SIMS demonstrated a more than 1000-fold increase in molecular ion yield from a peptide sample (1154 Da), compared to keV ion irradiation.

The rapid development of SIMS MSI offered new possibilities in biotechnology and biological research with applications in medicine and pathology.[32] SIMS found numerous applications, such as imaging of unicellular organisms[20,33,34] and single cells,[7,35−39] chromosomes,[40] embryos,[41] different organs, such as kidney,[42−44] brain,[45−49] prostate,[15] adipose tissue,[32,50,51] cockroach, and snail tissue,[26] and distribution of herbicide on a leaf.[52] There are also medical applications of SIMS, such as analysis of biomaterial implants,[53] a mouse model of Duchenne muscular dystrophy,[54,55] retinopathy,[56] the cornea and conjunctiva,[57] cardiovascular diseases,[58,59] and human breast cancer cell lines[60] and 3D imaging of tumors and oocytes.[61,62]

Pharmacokinetic studies of the accumulation of pharmaceuticals in cancer cells[63,64] or molecular imaging of vitamins in neurons[65] were also performed using SIMS. In addition, archeological studies of thousand-year-old Peruvian mummies[66] or art[67] can benefit from this technique. Two recent reviews presented SIMS as an imaging technique.[32,68]

1.3.3. Desorption Electrospray Ionization

DESI, an ionization method developed by R.G. Cooks in 2004,[10] can be used for MSI analysis in an ambient environment.[69] Contrary to MALDI and SIMS, which operate under high vacuum (HV) or UHV conditions, DESI is employed under atmospheric pressure (AP). DESI is a combination of two MS ionization methods: electrospray ionization (ESI) and desorption ionization (DI). Instead of a laser beam or a primary ion beam, DESI uses energetic, charged electrosprayed solvent droplets to desorb the molecules from the sample surface. Figure 3 illustrates the operational priniciple of DESI and its implementation on a linear trap quadrupole (LTQ)-based mass spectrometer. The formation of molecular ions from secondary droplets occurs either by ion emission (ion evaporation model)[70] or by evaporation of neutral solvent molecules (charged residue model).[71] As a result, gaseous ions are produced in a process similar to ESI. So the solid samples analyzed by DESI produce multiply charged ions in the form of $[M + nH]^{n+}$ or $[M - nH]^{n-}$, which is a characteristic feature of the ESI method.

For DESI imaging, the sample is either placed onto a target (e.g., microscope glass slide) or analyzed *in situ*.[72−74] The most common DESI probe design allows a lateral resolution of better than 400 μm on rat brain tissue.[69] A recent spray design theoretically predicts an improvement in achievable lateral resolution of 40 μm.[75] MALDI routinely provides a higher spatial resolution but requires more complicated sample preparation. The first MSI experiments used DESI to profile plant tissue for alkaloid distributions using a line scan.[10] These experiments were followed by line profiles of thin sections of liver tissue.[69] Although there are still damage, sensitivity, and resolution issues to address, the technique holds the promise of soft, local, liquid atmospheric desorption and ionization. This could resolve one of the problems often forwarded by biologists, namely the desire to perform imaging experiments away from the harsh vacuum environment of the mass spectrometer.[9]

DESI was applied to study lipids,[72] endogenous and drug metabolites,[76] alkaloid content in plant tissue,[10] natural products in algae,[77] and antifungal molecules in seaweed.[78] DESI was also combined with an ion mobility TOF mass spectrometer to probe the conformations of proteins desorbed from an insulating surface.[79]

1.3.4. Other Desorption and Ionization Techniques for MSI

Several other desorption and ionization methods are described in the literature that find their application in MSI,

such as laser desorbtion ionization (LDI),[16,80] surface enhanced laser desorption (SELDI),[81] nanoparticle-assisted laser desorption/ionization (nano-PALDI),[82] matrix-enhanced surface-assisted laser desorption/ionization (ME-SALDI),[83] and nanostructure initiator mass spectrometry (NIMS).[84]

One of the desorption and ionization techniques that is gaining popularity for MSI is laser ablation inductively coupled plasma MS (LA-ICP-MS). This technique is capable of quantitative imaging of elemental distributions generated from surfaces. A comprehensive review of this methodology has been published recently to which the interested reader is referred.[85]

Combinations of different desorption and ionization technologies are being developed to enable local desorption and ionization in the ambient environment. Although these techniques, such as matrix assisted laser desorption electrospray ionization (MALDESI),[86] laser ablation electrospray ionization (LAESI),[87] and infrared MALDI (IR-MALDI),[88] have great potential, they have not yet resulted in routine MSI applications.

1.4. Advantages of MSI

MSI offers a unique tool box for sample surface analysis. Several methods offer high spatial resolution biomolecular analysis. The achievable spatial resolution depends on the ionization technique used; for example, typically MALDI allows probing spots as small as 25 μm in diameter,[6] while a NanoSIMS ion beam can be focused to the size of 50 nm in diameter.[20] With a typical mammalian cell size of 10 μm, MALDI collects spectra covering approximately four cells per image point while SIMS can probe subcellular structures.[89] Special approaches such as the utilization of a high resolution 1 μm coaxial objective or 600 nm microscope mode imaging[16] can be used to overcome some of these spatial resolution limitations. However, these instruments are not widely available yet, and the experiments at extremely high spatial resolution can suffer from the lack of sensitivity.

Modern mass spectrometers are capable of separating and detecting ions with very high mass resolution. Resolving power $(m/dm)_{50\%}$ in excess of 10^5 is routinely available on commercial instruments. High mass resolving power can be used to reveal spatial features that remain hidden with low resolution technologies.[90] Ion mobility separation (IMS) combined with mass spectrometry allows the gas-phase separation of isobaric ions or molecules with similar nominal mass during an MSI experiment.[91]

MSI takes full advantage of high sensitivity MS instrumentation to image molecules present at very low concentrations inside the cells. At present the instruments are capable of detecting molecules present in concentrations as low as 500 attomol, which facilitates detection of components from a single cell.[92] The sensitivity of MS instruments was estimated by spotting a protein solution (insulin) on brain tissue, which resulted in detection of a minimal signal obtained from a spot of insulin at a concentration of 12 fmol/mm.[293] With the laser spot diameter of 50 μm, this resulted in an absolute detection level of 25 attomol per image point. This sensitivity is in a range where it can be used to detect biomolecules present in tissue sections.

In order to visualize different classes of biomolecules present inside the cells, the instruments must be able to detect a broad range of ions, from very low M_w ions such as drugs and metabolites to large M_w ions of intact proteins. In theory, TOF mass analyzers can mass separate all ions without molecular weight limits.

MS instruments can also be used for imaging unknown compounds present in the biological sample without any *a priori* knowledge or labels. This is a key advantage of MSI, as unknown molecules can subsequently be identified using tandem mass spectrometry. For this purpose, an ion of interest (parent ion) is fragmented and its fragments (daughter ions) are mass analyzed. This type of analysis is also known as tandem MS, MS^n, or MS/MS because it involves two or more mass spectrometers: the first mass spectrometric separation is used for the selection of the ion of interest, prior to fragmentation in the collision cell, and the second mass spectrometer is used to mass analyze the fragments generated. Tandem MS can also be utilized for MSI analysis.

Another advantage of MSI is that molecules are detected directly from the biological sample without complicated preparation steps. Normally the protocol for MSI requires a short tissue wash followed by matrix application for MALDI and ME-SIMS.[22] Conventional SIMS typically uses no sample surface modification whatsoever.

The time of sample analysis is also a crucial aspect of any imaging technique. In the case of MSI, the image acquisition time depends on the selected spatial resolution, the repetition rate of the MALDI laser, and the area sampled. The data acquisition of an average imaging experiment lasts from minutes to several hours depending on the instrumentation utilized. The process is fully automated and normally does not require any supervision.

1.5. Limitations of MSI

The sensitive nature of MSI instruments requires that the samples remain stable at room temperature (RT) as well as in HV. Unfortunately some molecules degrade at RT within a couple of minutes.[89] The sample preparation process must be carried out as fast as possible without exposing the samples to the air, moisture, or high temperature. Also, all types of sample treatment, including cutting, washing, digestion, or matrix application, possess the risk of sample contamination and molecular diffusion, which can affect the reproducibility of the data, complicate their analysis, or affect the quality of the image. The spatial resolution of a MALDI image can also be affected by the matrix crystal size, which typically is above 10 μm.[94,95] The image quality can be compromised by the presence of matrix clusters and their alkali metal ion adducts, which complicates detection of compounds in the 500−1400 Da range.[96] SIMS does not require matrix or any sample washing steps, but its extensive in-source fragmentation limits the size of the ions detected to 1000 m/z.[14,97]

Biological tissue represents an extremely complex and challenging sample for direct analysis by MSI. The multiple molecules present in a tissue section (e.g., proteins, lipids, oligonucleotides, carbohydrates, small organic molecules, matrix ions, and salts) can negatively influence each others' desorption and ionization efficiency and prevent optimal detection. This phenomenon is called ion suppression and was reported by a number of authors.[98,99] The presence of ion-suppressing phenomena differentially attenuates the ionization process and can limit the number of detected molecules.[100] Ionization suppression occurs when one analyte is present in great excess over another or ionizes more easily than others. For example, components such as lipids, carbohydrates, and salts can promote adduct formation and

affect cocrystallization of biomolecules with matrix, which affects the quality of the mass spectra and number of biomolecules detected by MS.[94] Some other examples show that MS spectra can also be dominated by easily ionizing hemoglobin chains desorbed from highly vascularized tissues such as heart.[95] Such signals can significantly compromise other protein signals in the spectrum. This phenomenon can be minimized by careful tissue removal during the surgical process to avoid tissue contact with blood, washing of the tissue surface to remove hemoglobin, or, in the case of profiling (see Profiling vs Imaging), avoiding the analysis of the highly vascularized regions of the tissue.[95] On the other hand, the presence of low level ion signals from hemoglobin chains can be used as an internal calibrant.[95]

Ion suppression and adduct formation can decrease the quality of MSI analyses. However, the efforts to remove nonprotein components may affect the integrity of the surface and cause diffusion of analytes.[22] Great care has to be taken that proper control experiments are conducted before drawing any conclusion from a given MSI experiment.

The theoretically unlimited mass range of TOF mass analyzers starts in practice at 600 Da, with an upper limit around 25−30 kDa, because the lower mass region is partially obscured by ions from the matrix while the sensitivity drops rapidly for bigger molecules.[89] This can be ameliorated through the utilization of smart matrices such as *meso*-tetrakis(pentafluorophenyl) porphyrin (F20TPP) that have no low M_w peaks, nor does it lead to cluster formation.[101]

1.6. MSI—Applications

MSI has a broad scope of applications and is being successfully applied in biology, pathology, medicine, and pharmacology.[102,103] Key features that make MSI a practical tool in these different domains of the life sciences are the *label free* nature of molecular imaging, high sensitivity, high resolution, and its capability to visualize in parallel the distribution of many molecules of interest.

The popularity of MSI augmented quickly as a result of its almost unlimited range of applications. Samples for MSI can be obtained from any type of organism, ranging from bacteria and plants to animal and human tissues. This technique has been used to examine samples of different biological origins, from single cells[7,35,36,104] to whole animal body sections,[19,91,105,106] from both normal[107−109] as well as pathological specimens,[110−112] from organisms at different developmental stages, such as fertilized oocytes,[113] embryos,[41] and adult animals.[114] A detailed review of MSI applications in different fields of life science is presented in section 3.

2. Methodological Description and Current Improvements

2.1. Biological Sample Preparation

In this section we present the key practical aspect of MSI, the preparation of biological samples. Several crucial preparation steps such as sample handling, washing, matrix application, and on-tissue digestion will be discussed. This will be followed by an in-depth description of mass spectrometric instruments and software used for imaging. New instrumental developments that challenge the boundaries of MSI, such as IMS, microscope and microprobe modes of image acquisition, and their application in MSI, are briefly discussed. In this section, we will also explore and explain the difference between profiling and imaging modes of MSI.

2.1.1. Biological Sample Handling

The MSI sample handling protocols must maintain the integrity and spatial organization of the molecules in biological samples. Collection and treatment procedures need to be sufficiently fast to prevent rapid tissue degradation. The samples for MSI come from a variety of biological sources. They can originate from the resection of an organ or tissue, a whole animal body dosed with a pharmaceutical compound, individual cells, or clusters of cells isolated by laser capture microdissection (LCM) or contact blotting of a tissue on a target membrane. The sample degradation process starts immediately after the blood/oxygen flow to an organ has ceased, even prior to tissue removal (see Sample Degradation). This implies that samples must be properly and timely collected, processed, and stored before MSI analysis.

Types of Samples. All kinds of biological samples can be subjected to MSI, ranging from single cells,[20,115] to bacterial colonies,[33,116,117] to animal embryos,[41] to tissues from different plants[77,78,118,119] or animal organs,[114,120] to rodent whole body sections.[19,68,91,98,106] Different fresh, snap-frozen,[121,122] alcohol preserved,[123] or formaldehyde-fixed and paraffin-embedded (FFPE)[124−130] samples were used for MSI. To date, the most imaged tissue type is a rodent brain. This is due to its small size and characteristic internal structure and the ease with which it can be sectioned.[131] Additionally, the symmetrical nature of the brain provides a very good internal control of the imaging process. Other types of animal organs were also subjected to MSI analysis. The sample list shows the imagination of the researchers involved. It consists of a large variety of biological tissue types, from the more difficult to section, air filled lungs,[76] heart,[132] kidney,[42] tumor samples of different origin (glioma,[133,134] breast cancer,[128,135] prostate cancer,[112] ovarian cancer,[136] lung tumor[122]), human biopsies and resected tissue from surgery,[50,137] to cells from cell culture[37,138] or LCM.[139]

Sample Storage. The most common first step used in MSI protocols is tissue storage utilizing snap-freezing of the material and storage at −80 °C. Tissue biopsies, organs, or whole organisms, e.g. zebra fish, should be frozen immediately after collection in order to preserve the sample's morphology and minimize protein degradation through endogenous enzymatic proteolysis, oxidation of biomolecules, or changes in the metabolome of the cells.[100,140] However, the freezing process can lead to sample cracking and fragmentation, as different parts of the tissue cool down at different rates and ice crystals may form. To avoid sample damage, the tissue may be loosely wrapped in aluminum foil and frozen in liquid nitrogen, ethanol, or isopropanol at temperatures below −70 °C by gently lowering the tissue into the liquid over a period of 30−60 s. This preserves the shape of the tissue and also protects the biological tissue components from degradation.[95]

It is also important to avoid tissue deformation during storage, which usually occurs due to wrapping of the tissue in plastic film or storing it in a tube.[100]

Whole tissues may remain frozen in a freezer at −80 °C for at least a year with no significant degradation.[95] After one year of storage, even at −80 °C, it is difficult to obtain good peptide/protein spectra from tissues.[95,141] This phenom-

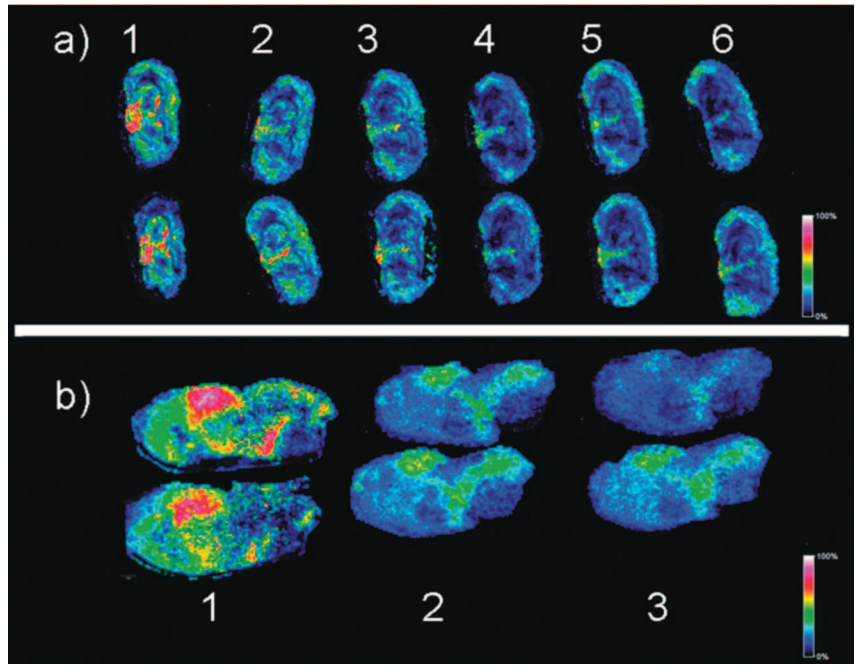

Figure 4. Degradation of molecular species during a time course of incubation of the tissue at RT visualized by MALDI-MSI. (a) Coronal sections of mouse brain warmed on the target slide for 0, 0.5, 1, 1.75, 2.75, and 5.25 min. Upper and lower series are from two separate technical replicates. (b) Parasagittal sections of mouse brain incubated for 5 min. Sample 1 was heat treated (Denator system) to denature proteins immediately after tissue collection. Sample 2 is the corresponding untreated tissue. Sample 3 was heat treated on the slide after sectioning and thaw mounting. Reprinted with permission from ref 89. Copyright 2008 Wiley Interscience.

enon of tissue aging is especially important for samples collected and stored over a long time period in medical centralized tissue repositories. It is very important to optimize and standardize the protocols for medical applications of MSI. Especially when it is not always possible to analyze freshly prepared samples.[141] A number of innovative protocols for MSI of fresh and aged biomedical samples have been recently developed.[123] The second most common form of tissue preservation found in medical tissue banks are FFPE tissue blocks. They are usually kept at RT, which leads to degradation of nucleic acids, metabolites, and many biomolecules other than proteins cross-linked by formaldehyde. The cross-linking, in turn, hampers easy desorption and ionization. These samples require special protocols ensuring removal of MS incompatible paraffin, digestion of cross-linked proteins, and correct identification of imaged molecules.[128]

Sample Degradation. In MSI the quality of biological samples is of great importance. Unfortunately, many molecules present in functional tissue undergo rapid degradation just after tissue dissection or even during agonal states of animals. Several factors, including pre- and post-mortem factors, can affect tissue quality.[142] Premortem factors include prolonged agonal states, perfusions, use of drugs, infections, tumors, hypoxia, and seizures. Post-mortem factors that influence tissue quality include post-mortem interval (PMI), which is the period from death to freezing of the tissue for long-term storage at −80 °C,[142] storage temperature, and duration of the storage as well as tissue processing and handling.

Molecular degradation studies show that endogenous proteolytic degradation resulting from the natural activity of enzymes including calpains, cathepsins, and those of the proteasome complex is already extensive at 3 min post-mortem.[143,144] It has also been demonstrated that the levels of several post-translational modifications (PTMs) in brain tissue are significantly changed within minutes post-mortem.[145,146] Post-mortem degradation of glycerophospholipids (GPLs) was observed within 15 min by MSI in a series of mouse brains extracted at different times, presumably because of stimulation of phospholipases A (PLAs) under ischemic (restricted blood supply) conditions.[107] Most studies concentrated on protein degradation have been conducted on animal (mouse, rat) brains, due to their availability. In these studies, either specific proteins were targeted, such as phosphorylated signal proteins, pre- and postsynaptic proteins, G-proteins, synaptophysin, microtubule-associated proteins, and calpain, or samples were analyzed in a more holistic proteomics approach.[147−149]

The study of endogenous degradation processes in human prefrontal cortex tissue showed that most human brain proteins are quite stable with respect to post-mortem factors, such as PMI and storage temperature. Nevertheless, the storage temperature seemed to significantly influence certain protein levels. Raising the storage temperature from 4 °C to RT increased the number of degraded proteins from 17 degraded proteins at 4 °C to 54 degraded proteins at RT.[142] This is indicative of the effect of temperature on naturally occurring post-mortem protein degradation. The majority of the identified proteins belonged to the functional classes of structural or metabolic proteins, which appear to degrade very easily during post-mortem delay.[142]

Figure 4a shows the time dependent loss of signals detected by MSI of rodent brains.[89,150] To prevent/minimize the molecular degradation process, some strategies such as *in vivo* fixation through focused microwave irradiation have been applied in MSI. However, the application of the focused microwave instrument is limited to smaller samples such as organs from small rodents and optimized for the brain tissue samples.[151−153]

Recently, a novel tissue stabilization system (Stabilizor T1, Denator AB, http://www.denator.com) was developed

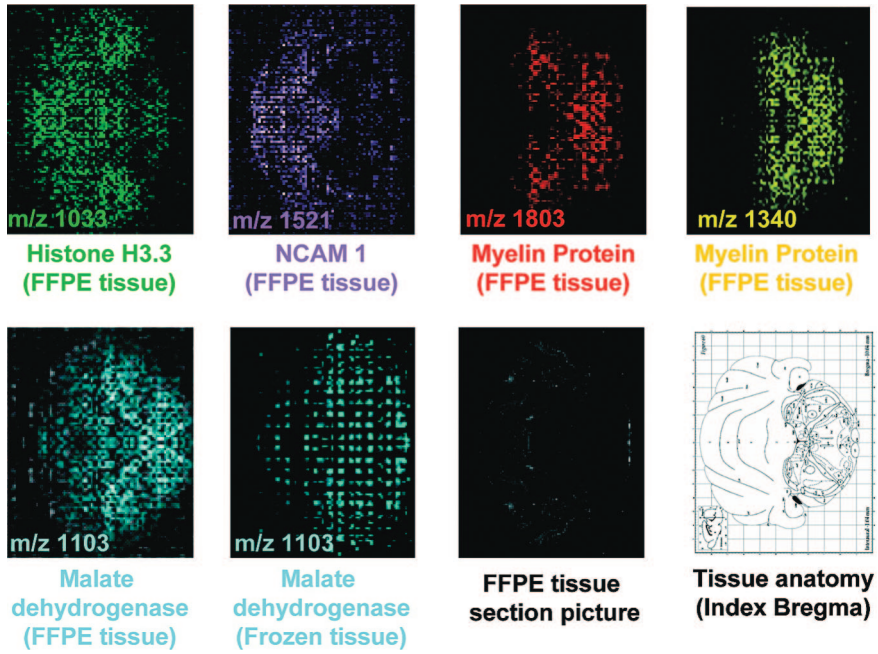

Figure 5. MALDI molecular images obtained from a 2-year-old FFPE rat brain tissue section subjected to on-tissue trypsin digestion. Reprinted with permission from ref 127. Copyright 2007 American Chemical Society.

by Denator Biotechnology and can be used for MSI samples.[154] Figure 4b illustrates the stabilizing effect of thermal treatment of biological tissue using this instrument. Substantial degradation is observed without this treatment. The instrument handles any type of tissue sample, both fresh and frozen, and utilizes a combination of heat and pressure, which prevents sample deformation while thermally inactivating/denaturing the enzymes responsible for rapid degradation of biomolecules in the tissue. The temperature of the sample is rapidly raised up to 90 °C but does not exceed 95 °C in any part of the sample.

Some other specific protocols need to be developed to meet the requirements of certain samples. For example, some tissues collected for MSI can contain drugs that are light-sensitive. To prevent the photodegradation of these components before analysis, the section should be kept in the dark.[95]

2.1.2. Tissue Preparation

Fixation. The majority of samples used for MSI are fresh, snap-frozen, chemically unmodified tissue sections. Unfortunately, it is not always possible to obtain fresh tissue for imaging experiments because many, especially medical samples, are routinely formaldehyde or alcohol fixed just after dissection and before any analysis. Due to protein cross-linking introduced by formalin fixation, the MSI analysis of FFPE tissues is difficult. The development of protocols useful for imaging and a recovery of polypeptides from FFPE samples allowed access to the different tissue banks, which store the samples in the form of paraffin blocks.[124−128] A successful example of the application of such a protocol employing on-tissue proteolytic digestion for biomedical imaging of FFPE brain sections is shown in Figure 5. The protocols must include a paraffin removal step followed by tissue digestion. The sample's analysis and data interpretation must consider the oxidation and degradation processes as well as effects of fixation and removal of paraffin on molecular structures.[128] All these aspects must be taken into account when old samples, large sample sets, or patient cohorts are going to be compared. This also implies that the profiling results of a 100-year-old FFPE tissue biopsy obtained from a patient with amyloidosis, presented by Seeley et al. in 2008, have to be dealt with with great caution.[134] This puts contraints on the analysis of large existing sample collections using MSI, as in many cases the history of these samples is not well-known. If it is unknown how long the sample was kept at RT and under ambient conditions, it is impossible to compare the MSI results from such samples with the MSI results from comparable modern samples, which typically display well-defined states of the proteome.

Alternative fixation methods rely on heat stabilization of tissues, which causes favorable protein denaturation (see Sample Degradation) or the preservation of samples in an alcohol bath. Figure 6 illustrates a comparison of MSI results between fresh frozen and ethanol-preserved brain tissue.[123]

A new method of tissue fixation using RCL2/CS100, which is a non-cross-linking, nontoxic, and nonvolatile organic fixative suitable for shotgun proteomic analyses and tissue imaging, was published by Mange et al. in 2009.[155]

Embedding. The embedding of the tissue in a supporting material allows easy handling and precise microtoming of sections. For histological applications, tissues cut on cryostat microtomes are usually embedded in the optimal cutting temperature (OCT) polymer. However, materials such as OCT, agar, sucrose, 2% (wt/vol) carboxymethylcellulose (CMC), and other polymer-based embedding media typically used for histological applications ionize easily during MS analysis and act as significant ion suppressors, as shown in Figure 7.[95,131] To minimize tissue tearing, the use of ice or gelatin as embedding material is recommended. Gelatin provides a much cleaner signal background compared with OCT.[156]

A large number of FFPE biological samples has been collected and stored in many tissue banks worldwide. Paraffin present in the samples suppresses ionization and must be removed before tissue analysis using a xylene wash. An MSI protocol employing dewaxing and hydration steps of such samples has been published by Lemaire et al. in 2007.[127]

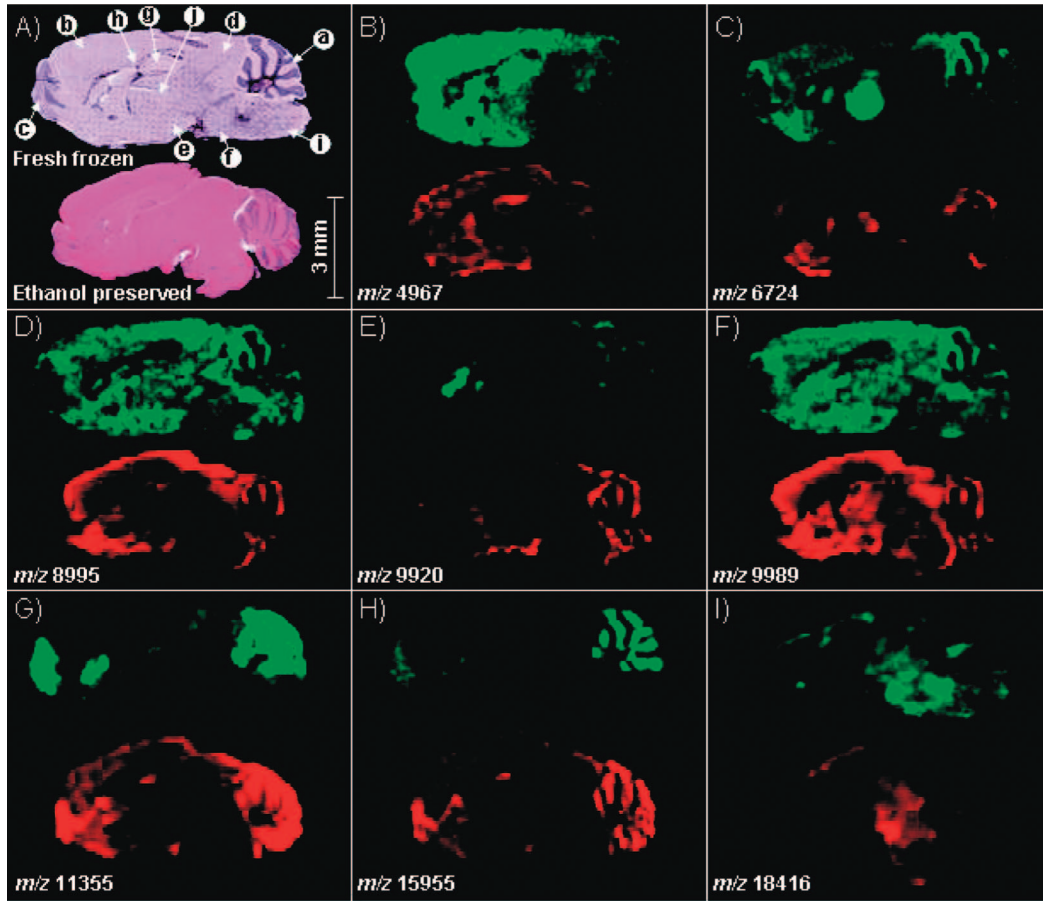

Figure 6. MALDI IMS analysis of fresh-frozen and ethanol-preserved sagittal mouse brain sections. (A) Photomicrographs of the sections after H&E staining: (a) cerebellum, (b) cerebral cortex, (c) main olfactory bulb, (d) midbrain, (e) hypothalamus, (f) pons, (g) hippocampal formation, (h) corpus callosum, (i) medulla, (j) thalamus. (B−I) Corresponding ion density maps from a subset of proteins observed in common from both sections. Reprinted with permission from ref 123. Copyright 2008 American Chemical Society.

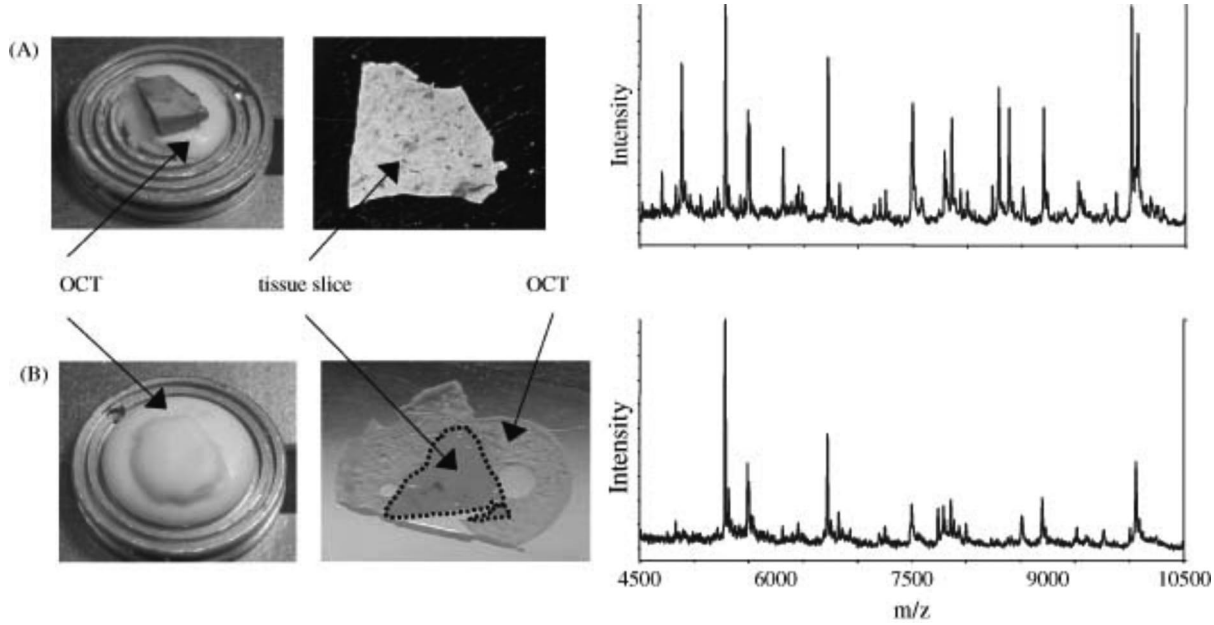

Figure 7. Analysis of the effect of OCT on MALDI signals from rat liver. (A) Procedure where OCT is used to adhere the tissue to the sample stage but does not come into contact with the sliced tissue. The resulting spectrum shows many intense signals between *m*/*z* 4500 and 10 500. (B) The tissue was embedded in OCT and attached to the sample stage. The resulting spectrum contains only about half of the signals as that in part A. Reprinted with permission from ref 95. Copyright 2003 Wiley Interscience.

Sectioning. For MSI the tissue sections are usually 5−20 μm thick. Thinner sections tear easily, while thicker sections, although easier to manipulate, may not be electrically conductive and take longer to dry, which can cause cracking and warping of the sections.[95] Thus, tissues are usually sliced to a thickness of the diameter of a mammalian cell (10−20 μm), so that the majority of the cells in the slice are cut open, exposing the intracellular contents for analysis.[95]

However, the thinner tissue sections, cut at 2−5 μm, have been recommended for the analysis of molecules in the larger molecular weight range of 3−21 kDa.[89,157] Tissue blocks are mounted to the cryo-microtome's cutting stage and sliced with a stainless steel microtome blade. The disposable blades used for sectioning are often packaged with a very thin film of oil between each blade, which potentially can be a source of sample contamination. To avoid contamination from this oil, it is recommended to rinse the blades with methanol and acetone prior to tissue sectioning.[100] The sample stage temperature is typically maintained between −5 and −25 °C, depending on the tissue type. Tissues with high fat content, e.g. brain, require lower temperatures to achieve high quality sections.[158] For example, samples such as breast tissue or visceral fat tissue can coagulate during sectioning at warmer cryo-microtome temperatures.[95]

Tissue Attachment. In order to perform MSI analysis, the tissue sections must be attached to an electrically conductive steal plate or glass slide. Conductive substrates are used to properly define the electric extraction field that will accelerate the ions produced from the surface.

In the past, tissue sections were thaw-mounted on flat metallic target plates such as aluminum, stainless steel, and gold-coated plates, with the last offering a fairly nice contrast for visualization of major histological features from the sections. However, opaque target plates were not suitable for microscopic visualization of the section. These plates have been replaced by conductive ITO-coated glass slides, coated with a 130 Å film of indium−tin oxide for electrical conductivity.[159] The transparent glass slides provide the possibility of microscopic observation of the MALDI samples.

There are two approaches for tissue attachment to these substrates: the use of an adhesive double-sided conductive tape or thaw-mounting. The tape binds the section to the target while thaw mounting attaches the tissue by warming the reverse of the target to produce a localized warm patch. The first method requires special care to avoid trapping air bubbles, which can affect the image acquisition. The latter method reduces the risk of sample contamination and tissue loss during the washing step. However, the thaw mounting method can cause significant variation in mass profiles due to rapid degradation of molecules during the tissue attachment process. Thaw mounting may not be good enough for additional procedures involving polar solvents (see Washing of Tissue).

Transfer of the tissue slice to a target plate or glass slide can be accomplished in several ways. One of the methods recommends cooling the plate by placing it in the cryo-microtome chamber at −15 °C before sectioning.[95] The tissue section is picked up using forceps for thicker sections or an artist's brush for thinner sections and transferred onto the cold plate. The plate and tissue section are then quickly warmed together. This method prevents loss of water-soluble proteins, since all ice crystals remain on the tissue section surface and not on the cryo-microtome cutting stage. The second method uses a plate held at RT that is placed over the frozen section. In this case, the ice crystals remain on the cutting surface. Sections transferred with this method may give poorer mass spectra, especially in the case of imaging water-soluble molecules.

Properly performed thawing does not cause any significant delocalization of the proteins, which is proved by traditional biochemical assays such as immunohistochemistry and autoradiography.[95] Regardless of the tissue transfer and attachment method used, the section must be transferred to the plate with great care without introducing any scratches, tears, or rolled-up edges. The mounted section should be immediately dried in a vacuum desiccator for 30 min to avoid moisture condensation that could cause delocalization of proteins.

Results of MSI often are compared to the histopathological information of the imaged tissue. During sectioning of the sample, an adjacent tissue section is collected on a regular microscopic slide for histological staining in order to correlate morphological information with the mass spectrometric images. In order to visualize tissue histology prior to MSI, protocols utilize optically transparent glass slides, coated with a thin conductive layer (ITO-coated glass slides) together with MSI friendly tissue staining protocols (e.g., methylene blue, cresyl violet).[160] This enables the microscopic evaluation of a tissue section by a pathologist followed by the molecular imaging of the same section by MSI. Another approach involves removal of the matrix from the tissue section followed by hematoxylin and eosin (H&E) staining of the same sample on an ITO slide in order to visualize the morphology of the tissue.[100,131] In this case, the visualization of microscopic structures may not be easy and depends strongly on the quality of the sample surface after completion of the MSI experiment. Samples used for SIMS or examined with the MALDI approach usually can be successfully stained and subjected to microscopic examination.

Washing of Tissue. Washing is required to remove unwanted molecules and salts from the surface of the tissue. Salts are released from ruptured cells or interstitial fluids during sectioning and suppress ionization through direct ionization or adduct formation with the proteins and peptides.[89] The standard washing steps usually employ a brief 70% ethanol wash to remove salts and debris followed by a 90−100% ethanol wash to dehydrate and temporarily fix the tissue.[94,95,160] The ethanol wash does not cause any significant delocalization of proteins due to its fixative properties.[95] A wash with an organic solvent such as chloroform or xylene is recommended for many tissues that have a high lipid content.[89,141] Lipid removal simplifies mass spectra in the medium mass range (500−1000 m/z), thus allowing the identification of low mass peptides that are usually masked by the high abundance of lipid peaks.[141] Washing protocols using organic solvents are acclaimed not to cause any delocalization or extraction of peptides or proteins but also not to reduce salt adducts.[141]

The washing method must be optimized for the specific MSI application, since different classes of molecules require different treatment. For example, peptide analysis may require an additional step of tissue treatment which includes 30 s of washing in 90% ethanol, 9% glacial acetic acid, and 1% deionized water.[161,162] Tissue samples washed in ethanol can be stored in a closed container at RT for up to 6 h without noticeable degradation observed in the MALDI spectra.[94] Some molecules can be detected only if washing has not been performed. In order to visualize all possible molecules, a combination of different tactics can be tested.

The washing method is an important aspect in sample preparation. Usually either the slide, with a tissue sample mounted on it, is immersed in the washing solution or the solution is applied on top of the tissue by pipet.[95] Immersion

of the slide in the washing solution brings a risk of tissue loss, especially if the section was not properly mounted on the slide.

On-Tissue Digestion. The current practical upper limit of TOF-mass analyzers is 30 kDa (the theoretical limit is much larger for singly charged species), which limits the detection to approximately half of all proteins present in tissue.[163] With approximately 2000 proteins expressed in a typical mammalian cell,[164] 1000 additional proteins could potentially be imaged if TOF-mass analyzers were able to detect an unlimited mass range. On-tissue digestion is often performed in order to bring more proteins into the MS range. This requires the local application of a proteolytic enzyme on the surface of the tissue section. Optimal enzyme activity requires the sample to remain moist at temperatures ranging from RT to 37 °C for an incubation period of 1 h up to several hours (e.g. overnight) depending on the research target and protocol used. Excess liquid applied in conjunction with the enzyme can lead to analyte diffusion during the incubation process. In order to prevent diffusion of peptides, two methods of enzyme application were optimized: spray-coating or spotting. During spray-coating the entire surface of the sample is covered with the solution of the enzyme. In this case, the spatial resolution is limited by a combination of diffusion and the diameter of the laser spot. The spotting of the enzyme prevents analyte diffusion and can be used if no extremely high spatial resolution is required.[161] In this case, small solution volumes, e.g. 100 pL, are deposited on an area of 100 μm diameter on the surface of the tissue. The digestion process and diffusion of analytes occurs exclusively within the spotted area. The size and distribution of enzyme spots limits the spatial resolution of the MS image. The protocol for on-tissue digestion for both frozen as well as FFPE samples has been recently published by Djidja et al.[128]

Other methods of protein digestion involve tissue blotting through a PVDF membrane with trypsin immobilized on the surface, followed by capture of the resulting peptides onto a second PVDF membrane, which maintains some degree of spatial resolution.[161,165] This procedure is referred to as the molecular scanner.[166] The lack of sensitivity and spatial resolution resulting from the blotting process in this approach result in limited pratical applicability.

Protein digestion typically yields peptides in the range of 400−3500 Da, a range where instrumental sensitivity is higher than that for intact proteins.[167] The mass spectrum of trypsin digested tissue is more complicated in the low mass region, due to simultaneous detection of peptides and overlapping signals from ionized lipids, matrix clusters, and smaller biomolecules.

On-tissue digestion results in the detection of multiple peptides derived from a number of proteins present in the tissue section. Protein identification can be performed using tandem MS instruments which have capabilities for efficient fragmentation of selected peptides, allowing the identification of the original protein. However, the chemical and molecular complexity of tissue may deliver multiple peptides at each nominal mass. As a consequence, except for highly abundant peptides, identification by MS/MS may prove difficult, due to fragments originating from different peptides. Tandem MS analysis of peptides may also be complicated by overlapping isobaric lipid ions. The recently developed IMS-MSI technique proved to be useful in the separation of isobaric ions that cannot be separated by conventional MS instruments (see Application of Ion Mobility Separation for Mass Spectrometric Imaging).[91]

2.1.3. Matrix Application

Matrix solution must be applied on the surface of the tissue before MALDI and ME-SIMS analysis. The matrix solution consists of three components: (a) an organic solvent such as methanol or acetonitrile, (b) an organic acid (the matrix) such as sinapinic acid (SA), and (c) TFA. The organic solvent extracts the molecules from the tissue and quickly evaporates, allowing matrix crystal formation from the weak organic acid.[22] The extracted molecules are incorporated into growing matrix crystals. The addition of TFA increases the amount of available protons for ionization and augments the number of intact pseudomolecular ions formed from the surface. During MSI analysis, the surface of the sample is probed with an appropriate laser beam or primary ion beam. The energy of the beam is absorbed by the matrix crystals, which evaporate quickly, releasing the trapped molecules. The matrix plays an active role in the ionization of the analytes.[168] The ionized molecules are typically singly charged $[M + H]^+$.

The choice of matrix (organic acid) applied on the tissue section depends on the mass range analyzed and chemical properties of analytes. Many different types of matrices are used for MALDI-MSI. An overview of the matrices used for MSI can be found in a number of MALDI and sample preparation reviews.[22,99,169] They commonly include derivatives of benzoic acid, cinnamic acid, and picolinic acid.[170−173] Sinapinic acid (3,5-dimethoxy-4-hydroxycinnamic acid, SA) is routinely used for higher M_w proteins while α-cyano-4-hydroxycinnamic acid (CHCA) is more common for lower M_w molecules such as peptides.[95,174] For phospholipids and drug analysis, matrices such as 2,6-dihydroxyacetophenone (DHA)[11] or DHB are used.[174,175]

The matrices can also be used in combination, such as SA in combination with 20% DHB, which provided good crystallization and a relatively homogeneous matrix layer across all organ tissues and resulted in detection of hundreds of protein signals from analyzed tissues.[19]

More effective matrix systems for MSI experiments are being developed. For example, a new class of ionic solid and ionic liquid matrices for MALDI-MSI has been developed.[176] Solid ionic matrices are obtained from the equimolar reaction mixture of acidic crystalline matrices such as CHCA, SA, or DHB with different bases such as aniline or *N*,*N*-dimethylaniline. Lemaire et al.[177] performed MALDI imaging on rat brain sections comparing the ionic matrix CHCA/aniline with regular CHCA. The application of an ionic matrix resulted in higher signal intensity and sensitivity, better image quality and peptide localization, reproducibility, and higher resistance to laser ablation.

The organic matrices absorb the energy of the laser beam in the UV-wavelength range, resulting in efficient desorbtion and ionization of the matrix material.[178] The ionization of the matrix and related clustering processes create strong background signals in the low mass region of the spectrum, which complicates the MALDI-MSI analysis of low M_w compounds. In order to lower the chemical noise at low mass ranges, higher molecular weight porphyrin based matrices (in the mass range from 566.70 to 1531.96 Da) have been used for MALDI analysis of vitamins and drugs.[179,180] Gold nanoparticles (AuNPs) with a size range of 2−10 nm can also be used as new generation matrices for high resolution

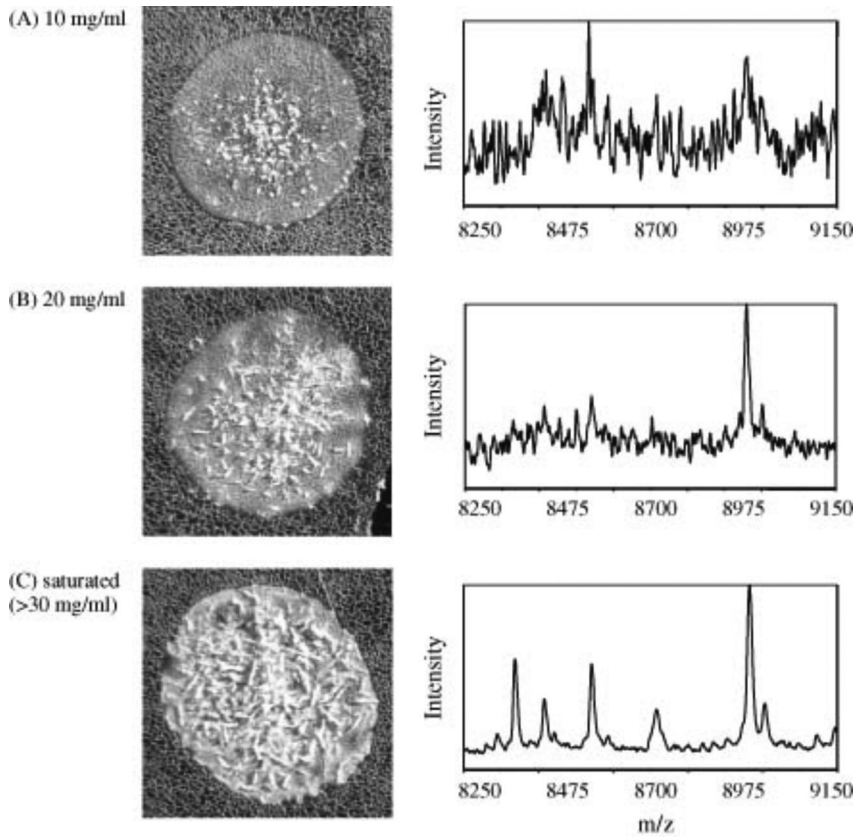

Figure 8. Analysis of matrix crystallization from solutions of different matrix concentration. Solutions of sinapinic acid in 50:50 acetonitrile/0.1% TFA in water at concentrations of (A) 10 mg/mL, (B) 20 mg/mL, and (C) saturated (>30 mg/mL). The spectra obtained from solutions spotted on mouse liver tissue sections showed that the greater the concentration of matrix, the greater the crystal coverage, and the better the resulting mass spectrum. Reprinted with permission from ref 95. Copyright 2003 Wiley Interscience.

imaging. They do not ionize easily but allow desorption and ionization of analytes, with minimum background signal coming from the matrix itself.[181] Su et al. compared bare and functionalized AuNPs with DHB, and they showed the successful detection of small carbohydrates with a molecular weight up to *m*/*z* 500 with AuNPs.[182] The background interference from matrices occurs as a result of their high concentration in comparison to analyte concentrations and the fact that clusters of matrix molecules also ionize and are detected together with analytes.

Recently, a new matrix, containing the coumarin moiety (7-mercapto-4-methylcoumarin), was used for MSI analysis of small molecular compounds such as choline alkaloids from the areca nut with decreased background interference in the mass range below *m*/*z* 600.[183]

The concentration of the matrix in solution must be carefully considered before matrix application. If the concentration is too low, the analyte may diffuse from its original position before crystallization or there will not be a sufficient amount of organic acid to form proper crystals. Too high a matrix concentration could result in rapid crystal formation and a limited time for analyte extraction and incorporation. Depending on the specific application, the matrix concentration range is 10−30 mg/mL SA for protein analysis and 10−20 mg/mL CHCA for peptide analysis.[174] The results from a comparison between three different SA matrix concentrations, in Figure 8, showed that a saturated matrix solution (>30 mg/mL) yielded the highest number of ion signals with the best mass spectral appearance.[95]

In the same study a series of saturated SA solutions with varying organic solvent/water combinations were deposited on a mouse liver section and analyzed by MALDI-MS in order to show the effect of solvent composition on the resulting mass spectra. Solvent combinations consisted of acetonitrile, ethanol, methanol, isopropanol, and acetone in different solvent/water proportions. Two solvent solutions, 50:50 acetonitrile/water and 50:50 ethanol/water, were recommended as good general solvents for different types of tissue samples.[95] More nonpolar solvents such as methanol or isopropanol can be used to analyze more hydrophobic surface molecules.[174]

As this study showed, the TFA concentration also affects the MS signals and corresponding results of direct tissue analysis. This study found that a concentration range of 0.3−1% TFA maximizes the total number of proteins analyzed.[95] However, in most current MSI protocols used to analyze different classes of biomolecules, TFA is used at a lower concentration of 0.1%.[4,184]

Hydrophobic proteins, such as membrane-bound or transmembrane proteins, are generally not easily extracted and cannot be detected during MSI analysis. Methods for dissolving molecules in organic/water solutions are ineffective for this class of molecules. For tissue imaging and profiling, the application of MS-compatible detergents (such as octyl β-D-glucopyranoside (*n*-octyl glucoside) or 3-[3-(1,1-bisalkyloxyethyl)pyridin-1-yl]propane-1-sulfonate (PPS)) to the tissue surface significantly enhanced detection of membrane/lipophilic proteins.[128,185]

The size of the crystals can influence the sensitivity of MSI detection. Usually, too small crystals lead to lower sensitivity for detecting intact biomolecules in MALDI-MSI. In ME-SIMS small crystals assist in obtaining higher spatial

resolution. ME-SIMS only samples the top 50 nm of the matrix surface and sputters less than 1% of the surface area in the static SIMS mode (see section 2.2.1 for the explanation of static vs dynamic SIMS) whereas MALDI typically ablates much more material both in depth and in surface area. Ultimately, the choice of matrix crystal size is determined by a combination of desorption and ionization technique used, required spatial resolution, and required sensitivity.

In order to obtain bigger crystals, a sufficiently long incubation time is required. Longer incubation allows the solvent to extract the biomolecules of interest from the tissue surface into the droplet prior to crystal formation. There are two parameters that influence the formation of matrix crystals: the speed of solvent evaporation and the time of matrix incubation. Slower solvent evaporation leads to bigger crystals.[9] This process depends on the solvent to water ratio. The higher the concentration of the solvent, the faster its evaporation. Slow crystallization can also be achieved by keeping the sample after matrix deposition at 4 °C for 1 h. This process results in lower noise mass spectra, as already pointed out by Stoeckli et al.[186] The matrix incubation time should be sufficient for effective solvent evaporation after each round of its application; too fast matrix application leads to analyte diffusion, due to an excess of solvent solution present on the surface of the tissue. The amount of solvent applied on the tissue should allow efficient extraction of biomolecules without diffusion of analytes. On the other hand, too big crystals (>100 μm) cover a large area of the tissue. As a result, molecules are extracted from many cells at a time and the spatial resolution of the MS image is negatively affected. For example, a 100-nL droplet dries to form a 900-μm diameter crystalline spot and extracts proteins from about 1000 individual cells.[95] Smaller matrix spots are necessary to increase the spatial resolution of the image, since it is limited by two key parameters: spot size and laser beam diameter. Larger spots require larger sample step sizes between laser shots, while smaller spots allow decreased sample step sizes. With spot diameters smaller than the laser beam, the imaging resolution is generally limited to the laser beam diameter (50−150 μm).

Smaller matrix spots and better coverage of the tissue with the matrix material were obtained by applying a thin layer of mechanically ground SA particles on the surface of the tissue section.[94] The seeded matrix produced more homogeneous ion signals throughout each matrix spot and reduced the number of droplets required to obtain matrix spots with good crystal coverage.

The crystallization process is heavily influenced by the presence of salts and surface-active compounds such as carbohydrates, lipids, or excessive amounts of hemoglobin.[94,176] The local concentration of these interfering substances may lead to differences in the crystallization process, crystal heterogeneity, decreased signal quality, and formation of analyte-rich matrix crystals called "sweet spots" or "hot spots" as well as crystals formed exclusively by matrix and containing no or very little analytes.[176] Rinsing of the tissue section with ethanol prior to matrix application removes salts from the sample's surface and improves the crystallization process. It has been demonstrated that different salt/matrix compositions locally lead to the formation of different pseudomolecuar ion types and different degrees of fragmentation.[187] Another important aspect of effective matrix crystallization is the choice of the matrix, since different matrices give different crystal patterns. Evaluation of the three most common matrices, SA, CHCA, and DHB, presented in Figure 9, showed that the pattern of SA crystallization is the most uniform and provides an even layer of crystals over the spotted area.[95] In comparison, DHB formed crystals on the rim of the drying droplet which may compromise the quality of the image. With high repetition rate lasers (typically 200 Hz or more), the fast and accurate generation of averaged molecular profiles for each spot on the tissue surface became possible.

Matrix Application Methods. The matrix solution can be deposited on the tissue section as individual droplets (spotted) or as a homogeneous layer (coated). The method of matrix deposition depends on the spatial resolution required for the analysis. Both methods are focused on homogeneous crystallization of the smallest possible crystals trapping the largest amount of analytes without any diffusion of molecules. Both methods, spotting and spraying, can be performed either manually or automatically. Automated devices offer better reproducibility and control over extraction processes, which allows comparison between different samples. Both spotting and spraying parameters must be experimentally optimized for every tissue type, since the quality of MSI depends on matrix coverage, wetness of the surface during matrix application, and thickness of the crystal layer, with all of these parameters being surface dependent. In both cases, multiple passes of matrix application are necessary to coat the entire tissue, but excess amount of matrix (overcoating) can suppress the analyte signal.[174] The matrix layer can be monitored under a microscope until an even coating with small crystals is achieved. To check the homogeneity of the matrix coating and to correct for uneven matrix distributions, an internal calibrant, typically a peptide in the same mass range as the analyte of interest, can be added to the matrix solution.[165]

Matrix deposition methods developed at the FOM-Institute for Atomic and Molecular Physics (AMOLF) for different matrix deposition devices and high-resolution MSI were reviewed by Altelaar and Heeren in 2009.[188] Here, the most popular spotting and spraying devices currently available for MSI are presented.

Spotting. The spotting of the matrix solution onto the tissue section limits diffusion of the analytes to the spot size. Manual spotting can be done using a micropipet that delivers microliter (μL) droplets generating spots of approximately millimeter size. Robotic spotting deposits picoliter (pL) droplets and provides a spot size of around 100−200 μm, which allows MSI at a resolving power of approximately 200 μm.[89,189]

Two popular automated spotting devices utilize two different types of droplet ejectors: inkjet-style piezonozzles and focused acoustic dispensers. General matrix deposition guidelines for both types of spotting devices have been described.[94,161] Both ejectors can release 100 pL droplets that dry on the tissue to a 100−150 μm diameter spot. The resolution of MSI analysis is in this case limited by the size of matrix spots, which is generally larger than the size of the focused laser spots.[190] Smaller, closely spaced droplets are best for high resolution images and effectively limit analyte migration to the area covered by the droplets, but they are harder to generate and evenly sample with the desorption laser. Larger droplets spread on the sample surface, increase the possibility of analyte diffusion within the matrix spot, and are better suited to profiling rather than imaging.[94] Spotting devices allow multiple rounds of droplet

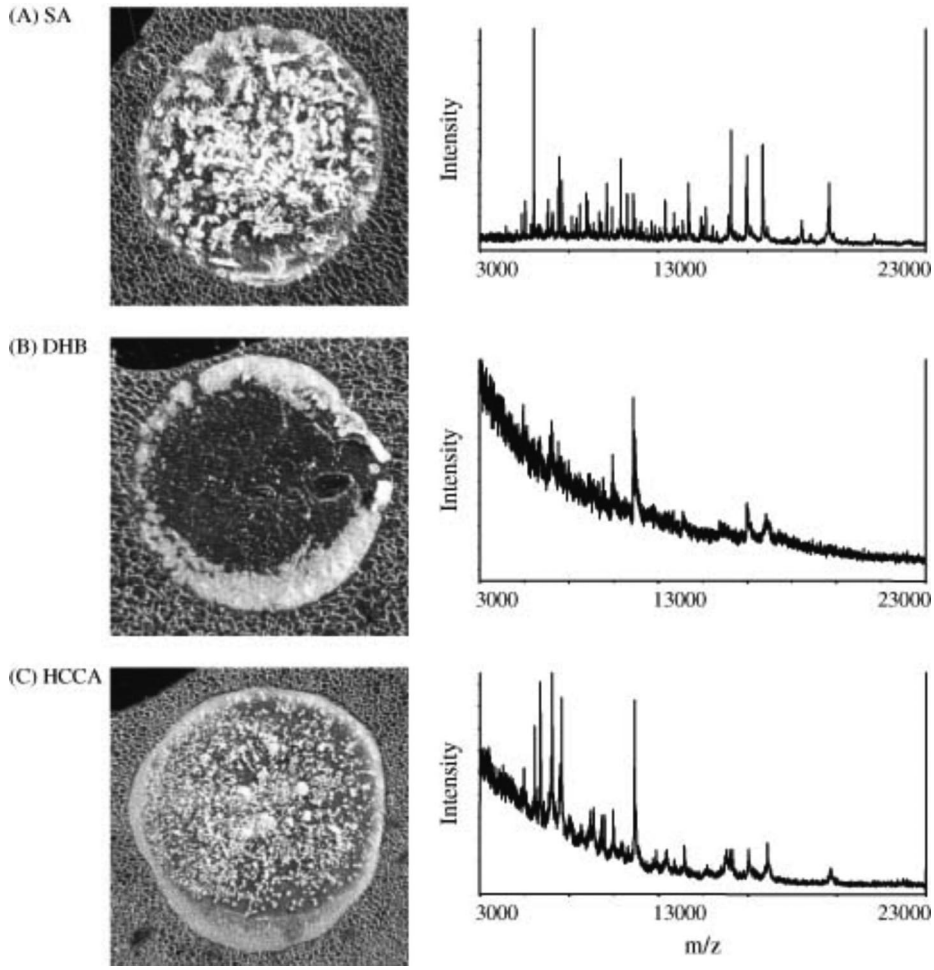

Figure 9. Analysis of matrix crystallization on tissue. Comparison of three different matrices, (A) SA, (B) DHB, and (C) HCCA, at the concentration 20 mg/mL (in 50:50 acetonitrile/0.1% TFA in water). SA and HCCA form dense crystals on the tissue, while DHB crystallizes on the rim of the spot. Reprinted with permission from ref 95. Copyright 2003 Wiley Interscience.

deposition, which can be performed at the same location to increase analyte extraction from the tissue. A number of devices are available for generating and accurately depositing droplets onto a surface. Matrix spotting devices such as CHIP (Shimadzu) are equipped with inkjet-style piezonozzles, which were first applied to the fabrication of microarrays of DNA, proteins, and other bioactive molecules.[176] Another automated method for matrix deposition, a desktop inkjet printer with a six-channel piezoelectric head that delivered 3 pL droplets, was presented by Baluya et al. in 2007.[191] The comparison of different matrix deposition methods, such as electrospray, airbrush, and inkjet, showed that the mass spectral images gathered from inkjet-printed tissue specimens were of better quality and more reproducible than those from specimens prepared by the electrospray and airbrush methods. The significant limitation of inkjet dispensers is the clogging of the capillary when spotting highly concentrated matrix solutions.

Focused acoustic dispensers utilize acoustic energy to generate very small droplets of matrix on tissue sections. Matrix solution is kept in a reservoir which is constructed from an acoustically transparent membrane that is coupled to a piezotransponder by way of a column of water. The sound wave produced by the transponder reaches the surface of the matrix solution in the reservoir, which ejects droplets of matrix with a volume of approximately 120 pL. These droplets are then collected on the tissue section held inverted over the matrix reservoir. Since the droplets are ejected from a large surface reservoir, there is no possible clogging.[94,100] A robot capable of acoustic droplet ejection (RapidSpotter; Picoliter Inc., Sunnyvale, CA) is being used to eject picoliter-sized matrix droplets onto the surface of the tissue, effectively coating the section. This technique results in a crystal surface similar to that of electrosprayed surfaces, but it allows multiple rounds of precise droplet deposition. This matrix application method deposits droplets which can remain wet longer and minimizes molecule delocalization to the area of droplet. Another spotting device, an Acoustic Reagent Multispotter (Labcyte Inc., Sunnyvale, CA), consists of an acoustic ejector, a translational stage with a lateral precision of 3 μm, and video telescopes integrated under software control.[94]

The matrix spotters can also be divided into contact and noncontact deposition devices.

Contact deposition methods require a pin or capillary to physically contact the sample for droplet deposition, which can introduce cross-contamination. The reproducibility of spotting small amounts of liquid using pins or microcapillaries can be low.

Noncontact printing devices such as piezoelectric, thermal ink jet, solenoid valves, and pulsed field ejectors do not have these limitations. Microdroplets are ejected from small capillaries onto the tissue by applying pressure pulses without any contact between capillary and the sample.[94]

Spraying. Spray coating is employed to cover the surface of the sample with a fine distribution of small droplets of

matrix solution. After drying of these droplets, a homogeneous thin film of solid matrix crystals is formed. Spraying devices deposit a matrix mist on the tissue surface, which results in much smaller droplets than those generated by spotting devices. This approach provides smaller crystal sizes ($\ll$100 μm) and allows higher image resolution.[9] Both manual (pneumatic sprayer, airbrush, or thin-layer chromatography (TLC) sprayer) and automated (robotic pneumatic sprayer, vibrational sprayer, electrospray) spray coating methods have been developed. Automated methods yield more reproducible results and provide more uniform application conditions. Currently, one fully automated vibrational sprayer system (ImagePrep, Bruker Daltonik GmbH, Bremen, Germany) is commercially available.

The spray coating delivers smaller crystal sizes but less reproducible matrix deposition and higher chance of analyte diffusion in comparison to spotting application methods if the surface is wetted too much. The advantage of spray coating is the size of the crystals formed, which are typically around 20 μm, not larger than the diameter of the focused laser beam. A more even coating can be obtained when the final spray consists of only solvent, allowing predeposited matrix crystals to redissolve and recrystallize, which increases the incorporation of analytes in the final crystals.[158] The smallest crystal size, $\ll$5 μm, can be obtained using electrospray deposition, which has been shown to yield subcellular resolution in ME-SIMS experiments.[27]

Both spotting and spraying of the matrix take place at RT, but spotting needs more time than spraying, which can cause degradation of some molecules during the matrix application process. Additionally, matrix application by coating covers the whole surface of the tissue section with a layer of matrix solution and requires a more careful application protocol than spotting.

Alternative Matrix Application: Solvent-Free and Matrix-Free Methods. Some other matrix application methods for MSI have been tested. One of them is sublimation, which was successfully used for matrix application and resulted in the formation of very small crystals. A protocol using sublimation for matrix deposition was reported in 2007 and provided a homogeneous coating of matrix that allowed the generation of high resolution phospholipid images from tissue.[192] The sublimation apparatus is relatively simple and became commercially available. The key advantage of sublimation deposition in comparison to other matrix application techniques is the elimination of diffusion of the analyte molecules because no solvent is used during the matrix deposition step. Another advantage is the increased purity of the matrix and the reduction of the crystal size.[193] Sublimation of matrix for imaging of peptides and proteins requires rewetting of the surface to enable surface extraction of these analytes.

Another alternative matrix application method optimized for detection of proteins involved cocrystallization of matrix with analyte acquired through placing a tissue section upon a drop of SA matrix dissolved in 90% ethanol and 0.5% Triton X-100.[4] After solvent evaporation, a seed layer of sinapinic crystals was added as a dispersion in xylene, followed by application of additional layers of SA added as solutions in 90% ethanol followed by 50% acetonitrile. An increased mass range between 25 kDa and 50 kDa of proteins was obtained from tissue sections such as kidneys, heart, lung, and brain of different rodent species.

Some variants of matrix application methods, such as covering the complete area with a large matrix volume at 4 °C followed by a drying step at RT or complete immersion of the sample in a matrix solution followed by a drying step, were tested, but both caused extensive protein diffusion.[93] However, the first method yielded very strong ion signals while the second provided a very thin layer of crystals and modest signal intensity.

Desorption-ionization on silicon (DIOS) was implemented in MSI.[194,195] This matrix free approach was introduced in 1999 by the Siuzdak group[196] predominantly for the analysis of small M_w compounds by using silicon surfaces prepared via a galvanostatic etching procedure on a Si wafer. The physical properties of the silicon material (high area surface, UV absorption) are crucial for the desorption/ionization process. A DIOS based MSI experiment requires the transfer of analytes to the DIOS surface by direct contact with the tissue of interest. After removal of the tissue, a mass spectral image can be acquired.

Colloidal graphite-assisted laser desorption/ionization (GALDI) MS has been demonstrated to work in MSI.[197] The method requires spraying of graphite nanoparticles onto the surface of the tissue. The sensitivity, suppression of ionization, and optimum distribution of the particles must be improved in order to apply this method on a broader scale.

Carbon nanotubes (CNTs) are another desorption and ionization method with potential application for MSI.[198,199] They are generated *in situ* by chemical vapor deposition. This method gives minimal interference, but this has not been shown to work on proteins or peptides.

Nanostructure-initiator mass spectrometry (NIMS) employed clathrates.[92,84] Clathrate nanostructures provided a spatial resolution comparable to MALDI-MSI, while maintaining the soft nature of MALDI. In this method, "initiator" molecules trapped in nanostructured surfaces (clathrates) release and ionize intact molecules adsorbed on the surface. This surface can be used together with both ion and laser beam irradiation.

Finely ground matrix particles which were filtered directly onto the tissue through a 20 μm stainless steel sieve are another variant of a dry-coating, solvent-free matrix deposition employed in MSI.[175] The analysis of phospholipids from mouse brain sections revealed that the results from dry matrix deposition shown in Figure 10 were identical to results from TLC spray-coated sections. However, dry matrix deposition resulted in simpler and faster sample preparation with virtually no analyte delocalization. This approach provided highly reproducible results and eliminated the variation caused by operator differences.

Another method of solvent-free matrix deposition involved coating of the tissue section with a thin layer of seed matrix, but in that case, a painter's brush was used to distribute the ground matrix, such as SA, on the tissue surface.[94] Excess material was removed using a gentle blow of compressed air in a laboratory hood. Observation of the tissue under a microscope indicated a high density dispersion of 0.3$-$3 μm particles across the section. The experiment comparing dry coating and regular coating using airbrush in Figure 11 showed that the solvent free matrix application technique was more beneficial for MALDI imaging of lipids, since solvent was necessary for extracting peptides from tissue samples.[156]

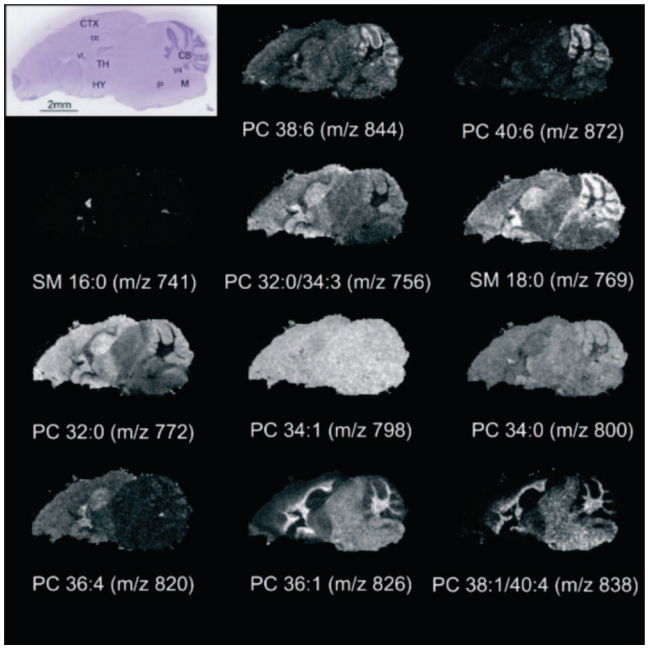

Figure 10. An optical image of H&E-stained sagittal mouse brain section showing the anatomy of the brain and selected ion images from a dry-coated serial sagittal section showing the phospholipid patterns in the brain: CB, cerebellum; CC, corpus callosum; CTX, cerebral cortex; HY, hypothalamus; M, medulla; P, pons; TH, thalamus; V4, fourth ventricle; VL, lateral ventricle; PC, phosphatidylcholine; SM, sphingomyelin. Reprinted with permission from ref 175. Copyright 2008 Elsevier.

2.1.4. Staining

Staining of MSI tissue sections helps to correlate the data obtained from imaging experiments with tissue histology. Staining can be done either before or after an MSI experiment. If staining is performed before MS measurements, the protocol must contain MS friendly histological dyes such as cresyl violet or methylene blue.[158,160] Hematoxylin and eosin (H&E) staining protocols, which are the most commonly used staining protocols in clinical pathology, cannot be used prior to MSI analysis, since these dyes affect the quality of the mass spectra.[158] H&E staining can be performed after MSI measurements, following matrix removal from the surface of the sections. Matrix removal can be achieved by immersing the glass slide in a 70% ethanol solution for approximately 1 min followed by dehydration of the section in a graded ethanol series before H&E staining.[100]

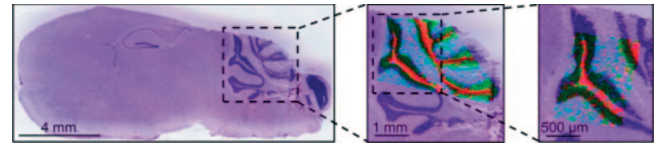

Figure 12. High-resolution MALDI images of a mouse cerebellum. The left panel shows the H&E-stained optical image of a mouse brain section. The overlaid phospholipid images show the localization of PC(40:6) (*m*/*z* 872 in light blue) to the cerebellar cortex, PC(36:1) and PC(38:4) (*m*/*z* 826 in the middle and *m*/*z* 810 on the left in red) to the cerebellar nucleus, and PC(38:6) (*m*/*z* 844 in green) to the granule cell layer. Reprinted with permission from ref 175. Copyright 2008 Elsevier.

The morphology of the sample must also be visualized before tissue profiling experiments, since only specific regions of the heterogeneous sample are subject to analysis (see Profiling vs Imaging). When staining cannot be performed, e.g. the tissue section was mounted on a steel plate, correlation of the MSI data with the sample morphology of the sample can be accomplished by using two adjacent sections: one for histology (on a glass slide) and one for MSI analysis. An example resulting from this approach is shown in Figure 12. However, visual coregistration between both sections can be complicated due to differences in the structure of adjacent tissue sections. Morphologically and functionally distinct regions of heterogeneous tumor samples are interesting objects for MSI analysis for medical diagnostics. Studies of different regions of lung and breast tumor sections resulted in the detection of many differences on the biomolecular level.[122,135] In both cases, the adjacent H&E stained tissue sections were used to select the regions of interest (ROIs) prior to profiling.

2.1.5. Contaminants

After successful tissue preparation, the sample is introduced and analyzed in a mass spectrometer, which results in detection of hundreds of different ions. The correct identification of detected peaks is the next biggest challenge. The increasing sensitivity of MSI instruments allows detection of molecules from the tissue present at very low concentration. Along with the biomolecules, many contaminants introduced during sample preparation steps will be

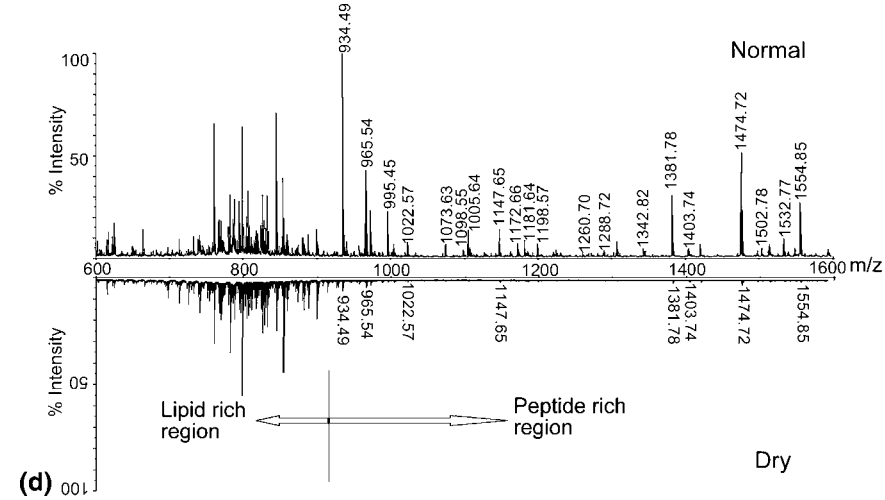

Figure 11. Comparison of dry matrix spraying and regular matrix spraying for lipid and neuropeptide detection from *C. borealis* brain. Reprinted with permission from ref 156. Copyright 2009 Elsevier.

ionized and detected as well. Among the most often detected contaminants of biological samples are the impurities present in the solvents used for tissue washing and matrix deposition, salt adducts, keratin, or polymers such as OCT or polyethylene glycol (PEG). A recently published review of common MS contaminants contains a broad list of unwanted ions of different origin.[200] In this paper, the contaminants are classified into two groups. The first group contains proteinaceous interferences or contaminants, which include e.g. enzymes used in sample preparations, keratins, and other abundant, involuntarily introduced proteins or instrument-induced peptide fragment interferences. Nonproteinaceous interferences or contaminants such as matrix clusters in MALDI-MS, adducts, solvents and polymeric interferences, plasticizers, and additives have been grouped in a second category of contaminants.

Ion mobility MS, high-field asymmetric waveform ion mobility spectrometry (FAIMS), and matrix-free laser desorption/ionization techniques including desorption/ionization on silicon (DIOS), DESI, or direct analysis in real time (DART) are some techniques that are helpful in minimization or elimination of certain background interferences.[200] In addition to that, all steps of tissue preparation should be carefully performed, which includes the use of gloves and clean lab glassware. Every MS analysis should also include blank tests such as system-, solvent-, method-, matrix-, and equipment blanks.[200]

2.2. MSI Instrumentation and Processing Tools

2.2.1. Mass Analyzers

Technological improvements in mass spectrometric instrumentation have enabled various high throughput peptide and protein screening applications in a large variety of samples. Proteomics as a scientific field that has emerged over the past decade has been a major driving force. Approaches such as shot-gun proteomics, quantitative proteomics, top-down proteomics, and chemical proteomics[201] have all developed out of mass spectrometric innovations. Imaging mass spectrometry is taking the same advantage of these innovative technological developments. In this section we will discuss some of these innovations from a more instrumental perspective, highlighting their respective benefits in MALDI or SIMS analysis of tissue. Table 1 provides an overview of the most commonly used mass spectrometers for MSI together with their characteristic performance indicators.

Time of Flight Mass Spectrometry. The majority of MSI experiments are performed on TOF systems. Stephens and co-workers introduced the TOF-MS in 1946,[202] and since then the TOF analyzer has been combined with SIMS ion sources and with MALDI sources. TOF-MS offers good transmission ratio (50−100%), sensitivity, dynamic mass range, and repetition rate. The first high mass resolving power imaging experiment with a TOF-SIMS in a scanning microprobe mode was published in 1991.[203] The reported secondary ion images were obtained from a polymer surface with an average M_w of 1400 m/z.

TOF analyzers allow the separation of ionized accelerated molecules according to their molecular masses. Generated by the ionization beam in the source, ions characteristic of the surface species are accelerated by an electric field between the conductive support (and sample) and the extraction grid (10−25 kV) to the same kinetic energy. Therefore, the ions arrive at the detector with different speeds, which are inversely proportional to their mass over charge values. Three main TOF analyzer geometries are defined in order to increase the sensitivity, mass accuracy, and mass resolving power. These entry geometries are linear, reflectron, and orthogonal. The linear geometry is commonly used in TOF imaging mass spectrometry and provides the highest sensitivity and mass range. The reflectron geometry utilizes an electrostatic mirror that compensates velocity differences obtained during desorption and ionization processes in the source. This compensation results in a substantial improvement of the mass resolving power as high as 60 000 fwhm (full width at half maximum). The use of a reflectron typically limits the mass range, and in imaging studies, it is predominantly used to analyze singly charged ions with a molecular weight in the range of 15−20 000 Da. Although a highly sensitive and rapid molecular weight profiling technique, MALDI-TOF has limited mass measurement accuracy (MMA) and resolving power and lacks the capability to perform effective tandem mass spectrometry experiments for peptide sequencing.[204] This changed with the introduction of an alternative TOF geometry, using orthogonal acceleration, by the group of Guilhaus.[205] The orthogonal acceleration (oa-TOF) approach allowed the decoupling of the ion source from the mass analyzer and led to the introduction of hybrid analyzers that combine a quadrupole mass analyzer with a TOF-MS, the so-called qTOF geometry. These oa-TOF or qTOF systems revolutionized the application of TOF-MS systems for structural analysis with tandem mass spectrometry. Combined with the

Table 1. Characteristic Performances of Different Mass Analyzers for Imaging MS[a]

analyzer	mass resolving power	m/z range low	m/z range high	transmission (%)	detection	pixel acquisition frequency
time-of-flight[b]	10^3-10^4	0	150K	50−100	parallel	>10 Hz
FTICR[c]	10^4-10^6	20	5K−10K	20−90	parallel	>1 Hz
(linear) ion traps[d]	10^2-10^3	50	4.5K	1−80	sequential	<10 Hz
triple-quad[e]	10^2-10^3	0	1−5K	1−80	SRM/MRM/sequential	>100 Hz
magnetic sector[f]	10^2-10^3	0	5K	<2	single ion/array detection	<1 Hz

[a] Generally, the type of desorption and ionization technique will affect the performance of a mass spectrometer. The numbers in this table are to be considered to provide a general impression of what the analyzer is minimally capable of in a standard MALDI-MSI. [b] The mass range of a ToF system is limited by detection efficiency only. Using special high mass detectors, the high mass limit can be extended to several MDa. [c] The mass limits in FTICR-MS are detemined by the magnetic field strength. The numbers in the table are provided for a 7 T system. [d] Ion traps usually have a low mass cutoff depending on the radio frequencies and mass analysis methods used. Linear ion traps are often hybridized with a second mass analyzer for multiplexed parallel tandem MS analysis. [e] Triple quadrupoles have the same limitations as single quadrupoles but in multiple reaction monitoring (MRM) the analytical quadrupoles have a fixed and narrow m/z transmission range so that the transmission for that specific reaction channel is substantially higher and the analysis is faster, as no sequential scanning is needed. [f] Magnetic sector instruments are not used for MALDI but mainly for dynamic SIMS. In that case, one or more selected ions are continuously imaged at high sensitivity. In the scanning mode, a sector instrument is impractical for imaging MS. As a result, most ions are discarded and transmission is low.

improved mass accuracy, this geometry is extremely useful for imaging mass spectrometry. The most recent development in this field is the introduction of ion mobility spectrometry (see Application of Ion Mobility Separation for Mass Spectrometric Imaging). An alternative approach for structural analysis with a TOF-MS system is the combination of two TOF-MS mass spectrometers coupled together in a so-called TOF-TOF configuration. The first TOF system is used to select a precursor ion for fragmentation, and the second TOF system is employed for rapid, parallel fragment analysis.

Fourier Transform Ion Cyclotron Resonance Mass Spectrometry. The FTICR MS technique is based on the determination of the ion cyclotron frequencies of ions trapped in a Penning trap. The mass to charge ratio of the ions is determined from this frequency in first approximation by the equation $\omega_c = qB/m$, where ω_c is the reduced cyclotron frequency in rad/s, q the elemental charge in C, B the magnetic field in T, and m the molecular weight in kg. In FTICR MS experiments, the ions can be generated directly inside the ion trap or the ions can be generated externally and transported to the ion trap. The latter approach has the advantage that a multitude of ion sources can be used. The ion trap (or ICR cell) generally consists of two trap electrodes, two excitation electrodes, and two detection electrodes. The trap electrodes define a parabolic trapping potential that confines the ions axially. Typical trapping potentials are of the order of ± 1 V. Radially, the ions are confined by the magnetic field in which the ICR cell is positioned. After ions have been trapped and stored for a variable time (which can be as short as a few milliseconds and as long as a few hours), the ion cyclotron motion is excited by the application of a rf (radio frequency) excitation pulse on the excitation electrodes. As a result of this time-varying electric field, the ions experience a net outward force which causes the ions to increase their cyclotron radius. More important, at the same time, the ion motion also becomes coherent. The coherently orbiting ions induce a corresponding image charge in the detection electrodes. The ICR signal is measured by digitizing the voltage difference between the two detection electrodes as a function of time. This signal is often referred to as the ICR transient. Fourier transformation of the time-domain transient results in the cyclotron frequency spectra, which can subsequently be converted into mass spectra.

Fourier transform mass spectrometers (FTMSs) offer several unique advantages including high mass resolving power, high MMA, and multistage MS/MS capabilities. Furthermore, the ability to trap and store ions while allowing additional ions to be introduced into the ion cyclotron resonance (ICR) cell makes it possible to accumulate ions from multiple MALDI ionization events in the FTICR cell prior to detection. Such in-cell ion accumulation (ICA) methods produce a significant signal-to-noise improvement over the more commonly used signal averaging methods.[204]

Sub-part-per-million MMA and mass resolutions greater than 100 000 allow, in theory, the detection and identification of a greater number of metabolites.[206] Recently, it was shown for the first time that direct identification capabilities required for biomolecular imaging studies can be realized by the implementation of FTICR MS at 7 T for molecular imaging.[90] FTICR MS delivers a unique combination of high mass spectral resolution and tandem mass spectrometric capabilities.[90] This combination allows the mass spectral separation of different species from complex systems while tandem mass spectrometry is employed to dissociate selected molecular ions for structural determination. The extreme resolution offered by FTICR MS allows the visualization of spatial details that remain hidden under lower mass spectral resolution conditions.

Other groups have since utilized the high mass resolving power capabilties of FTMS and FT-Orbitrap technology to analyze a variety of systems, ranging from the study of Crab neuropeptides by MALDI-FT profiling[204] to human tissue sections.[207]

Linear Ion Traps. Modern linear ion traps (LIT) are improving throughput and sensitivity for the identification of tryptic peptides in shotgun proteomics.[208] Their operating principle, a linear quadrupole ion trap in combination with a high performance mass spectrometer such as FTICR MS or FT-Orbitrap, provides the capabilities to multiplex mass spectral analysis. This approach has several advantages for MSI and has been described for example by the groups of Cooks[209] and Yost.[210] A new intermediate-pressure MALDI LIT mass spectrometer and its capabilities for imaging mass spectrometry are described by Garret et al.[211] The instrument design is described and is characterized in terms of four performance issues: (1) MALDI performance at intermediate pressure; (2) analysis of samples on nonconductive and conductive glass slides; (3) critical importance of tandem mass spectrometry (both MS^2 and MS^3) for identification of analyte species and imaging of isobaric species; (4) capability for repeated analysis of the same tissue section. Application of the new instrument to imaging phospholipids in rat brain sections is described in detail.[211]

Triple Quadrupole Mass Analyzers. Triple quadrupole mass analyzers have long been thought not to be useful for imaging mass spectrometry. The rationale behind this was the lack of speed combined with the low transmission efficiency of scanning type mass spectrometers if the objective of the surface analysis targets the whole mass range. A quadrupole is a mass filter, transmitting only ions in a certain mass window, and obtaining a mass spectrum requires scanning the filter characteristics. This mode of operation is not compatible with a pulsed ionization technique such as MALDI, as most of the ions produced at the surface are not analyzed. The triple-quadrupole system is for that reason mainly used with continuous ionization sources for small, low molecular weight analysis such as ESI or atmospheric pressure chemical ionization (APCI). A new method was introduced that allows the useful combination of a pulsed MALDI source with a triple quadrupole linear ion trap (MALDI-QqQLIT) instrument for high throughput quantitative analysis of low M_w molecules.[212] This method allows rapid single or multiple reaction monitoring (SRM/MRM) of small molecules at surfaces and is as a result very useful for targeted pharmaceutical compound and metabolite imaging. The SRM/MRM involves the selection of one or more (but sequential) structure specific fragmentation channels. A SRM experiment involves the selection of a precursor mass (by the first quadrupole), a fragmentation step (in the second quadrupole), and the selection of a specific fragment mass (by the third quadrupole). The quadrupole settings are fixed and provide high ion transmission of the system, resulting in a sensitive analysis. In this mode the triple quad becomes a selective mass filter for a specific precursor molecule combined with a specific fragment of that precursor molecule. In MRM mode several SRM channels are automatically examined sequentially. The group of Hopfgartner has

elegantly demonstrated how this approach can be used for rapid, quantitative imaging of selected compounds in whole body tissue sections.[105]

Magnetic Sector Mass Analyzers. Magnetic sectors are also used for imaging mass spectrometry. They are employed mainly for high resolution elemental analysis using dynamic SIMS. In that case one or more selected ions are continuously imaged at high sensitivity. As a result most other ions are discarded and the overall transmission is low. In particular, the Cameca NanoSIMS 50[213] shows an instrumental configuration for high spatial resolution SIMS: the primary ions and secondary ions in this instrument are controlled by the same ion-optical elements near the sample. This allows perpendicular sample analysis with small spot sizes and high secondary-ion collection efficiency. The magnetic sector and several moveable detectors allow simultaneous detection of several elements or small molecules (within a narrow mass range) with high detection sensitivity.

2.2.2. Software for MSI

Data collected from MS imaging yield high resolution molecular profiles across the tissue with data files of up to a few gigabytes which requires complex visualization software.

MSI software controls data acquisition and processing in order to generate ion images. A comparison of several recently developed imaging mass spectrometry software packages was presented by Jardin-Mathé et al. in 2008.[214] Here, we will present a couple of examples of imaging software.

Biomap. Biomap (Novartis, Basel, Switzerland, www.maldi-msi.org) is an image processing application. BioMap was originally developed by Rausch for the evaluation of MRI data in biomedical research, and due to multiple modifications, it can now support many more imaging data formats, including optical, positron emission tomography (PET), computed tomography (CT), near-infrared fluorescence (NIRF), and MSI.[93] BioMap was written in IDL (Research Systems, Boulder, CO). Visualization is based on multiplanar reconstruction, allowing extraction of arbitrary slices from a 3D-volume. Other features linked to visualization are overlaying of two individual data sets or displaying the ROIs. It allows displaying the mass spectrum from selected single points or ROIs on the generated image. Another mode is to select on the mass spectrum the analyte of interest and to calculate by integration over the corresponding peak its distribution on the scanned area.[165] Routines for baseline correction of spectra, spatial filtering, and averaging of spectra enhance the information obtainable from a data set.[93] The software provides visualization and a storage platform, which can be easily extended by various software packages, individually designed for the analysis of specific data sets.

FlexImaging. FlexImaging 2.0 (Bruker Daltonics GmbH, Bremen, Germany, www.bdal.com) software is used for acquisition and evaluation of MALDI-TOF and TOF/TOF imaging data. This software allows color-coded visualization of the distribution of any ion detected during MSI and overlaying of the optical and MS images. Integrating statistical classifications such as hierarchical clustering, principal component analysis (PCA), or variance ranking, the software provides "Class Imaging", which allows the classification of tissue types and determination of the class membership of comparable tissue samples.

MALDI Imaging Team Imaging Computing System (MITICS). MITICS is new software compatible with many types of instruments developed for MALDI imaging.[214] MITICS is divided into two parts: MITICS control for data acquisition and MITICS Image for data processing and image reconstruction. MITICS control is available for Applied BioSystems MALDI-TOF instruments and MITICS Image for both Applied BioSystems and Bruker Daltonics ones.[214] MITICS Control is used for setting the acquisition parameters for the imaging sequence, such as creating the raster of acquisition and controlling post acquisition data processing. MITICS Image is used for image reconstruction.

Datacube Explorer. The Datacube Explorer (DCE, www.imzml.org>Software Tools), developed at the FOM-Institute AMOLF, is a lightweight visualization tool to explore imaging mass spectrometry data sets. It offers both an image-based and a spectrum-based view of the data, with an easy way to dynamically scroll through the masses in a data set. The DCE includes features such as on-the-fly spectral binning, ROI spectral analysis, and image smoothing. It also includes a self-organizing map feature for image classification. The DCE is able to read and write the AMOLF datacube data set format and read imzML. The lightweight nature of the application makes it possible to easily share the application among several partners in scientific collaborations.

The Volume Explorer, also developed at the AMOLF, is a software tool to create 3D volumes out of a set of several "image slices" for any *m/z* value. It uses the Visualization Toolkit (VTK, www.vtk.org) for 3D visualization.

Imaging and Database Searching. Mascot (www.matrixscience.com) is a powerful search engine, which uses mass spectrometry data to identify proteins from primary sequence databases.[215] To identify an unknown protein from the sample, the protein of interest must be first purified, usually by 2-dimensional polyacrylamide gel electrophoresis (2D-PAGE) or liquid chromatography (LC), and digested with a proteolytic enzyme, such as trypsin. The resulting digest mixture containing peptides obtained after digestion is analyzed by mass spectrometry. For MS/MS analysis of individual peptides, the digest mixture is separated by chromatography prior to analysis. The experimental mass values are then compared with calculated peptide mass or fragment ion mass values, obtained by applying cleavage rules to the entries in a comprehensive primary sequence database. By using an appropriate scoring algorithm, the closest match or matches can be identified. If the sequence database does not contain the unknown protein, then the aim is to pull out those entries which exhibit the closest homology, often equivalent proteins from related species. The sequence databases that can be searched on the Mascot server are MSDB, NCBInr, SwissProt, and dbEST.

imzML. In order to ensure flexible and fast handling of the MSI data, two separate files are used: a small (ini or XML) file for the metadata and a larger (binary) file for the mass spectral data (biomap, DCE, udp). The metadata file is based on the mass spectrometry standard mzML developed by the Human Proteome Organization-Proteomics Standards Initiative (HUPO-PSI). The MS imaging data is stored in a binary format in order to ensure the most efficient storage of these large data sets. A new controlled vocabulary was compiled for imzML to include parameters that are specific for imaging experiments. These parameters are stored in the imagingMS.obo file.

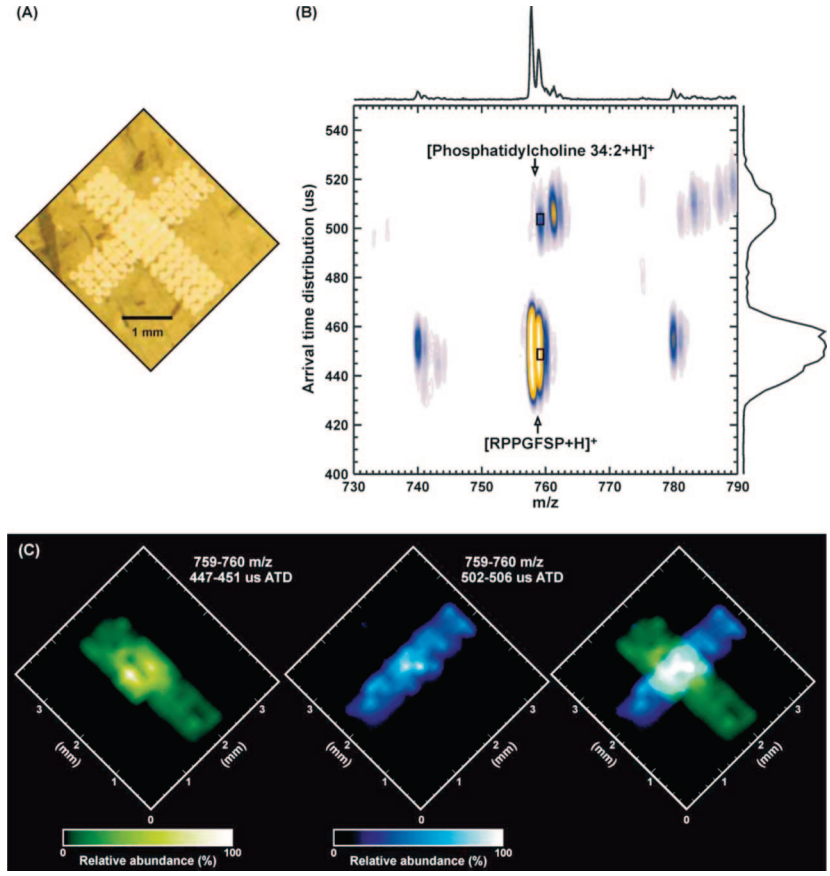

Figure 13. MS imaging in IMS mode of a nominally isobaric peptide (RPPGFSP) and lipid PC(34:2) deposited onto a mouse liver thin tissue section in the pattern of an X. (A) An optical image of the patterned matrix/analyte spots deposited on the tissue section. (B) A zoomed view in the region of PC(34:2) and RPPGFSP for a representative IMS of a mixture of the two analytes. (C) Extracted ion intensity maps for the peptide (left, green), the lipid (center, blue), and an overlay of the two maps at 50% transparency. Reprinted with permission from ref 225. Copyright 2007 Wiley Interscience.

Digital Staining Algorithms. MSI is at present one of many techniques used to visualize the spatial distribution of specific biomolecules from tissue sections. The main advantage of MSI over other techniques is its capability to monitor the distribution of a large number of different molecules in a broad mass range and at the same time. With thousands of mass spectra containing hundreds of peaks collected from one sample, the automated and reliable computational analysis of MSI data becomes indispensable.[216] These algorithms could in the future potentially constitute a valuable tool for pathologists or medical doctors that have to analyze large numbers of tissue samples. In that case, reliable classifiers can help minimize the risk of underdiagnosis.

Some applications of digital staining, namely hierarchical clustering and PCA, were used to analyze data collected from tissue sections of gastric cancer and non-neoplastic mucosa.[217] A PCA approach was also applied to the analysis of metabolites in starvation-induced fatty liver tissue sections.[218] A conceptual overview of PCA for MSI along with a demonstration of this approach on an MSI data set collected from a transversal section of the spinal cord of a standard control rat was published by Van de Plas et al. in 2007.[219]

2.3. Application of Ion Mobility Separation for Mass Spectrometric Imaging

Since its development in the 1970s, ion mobility separation (IMS), known also as plasma chromatography or ion chromatography, has mainly been applied to the analysis of volatile organic compounds and used as a tool to probe the electronic states of ions.[220] IMS is a gas phase separation method that adds new dimensions to mass spectrometry due to its capabilities to separate isobaric ions that cannot be separated by conventional TOF mass spectrometry.[91,221] Figure 13 shows an example of the separation of two spatially structured isobaric species, a peptide and a lipid, resolved in an imaging MALDI ion mobility mass spectrometric experiment. IMS separates ions based on their collision cross section and can be coupled with TOF mass spectrometry to yield a powerful tool used in the identification and characterization of biomolecules.[220] IMS adds an additional separation dimension which improves the molecular resolving power of imaging instruments and allows better characterization of detected biomolecules. IMS does not enhance the sensitivity of the instruments, since it does not modify the ionization conditions. Both (D)ESI and MALDI ionization sources can be coupled to IMS instruments for imaging purposes.

IMS has been applied to protein conformer differentiation, top-down protein sequencing, noncovalent protein complexes, isobaric compound identification, and mass spectrometry imaging.[221−223] It is necessary to develop the tools to interpret the additional ion mobility dimension introduced IMS-MSI data and gather valuable conformational information.

A fundamental introduction to ion mobility as it applies to macromolecules illustrated by a spectrum of a tryptic digest of bovine hemoglobin has been presented by Verbeck et al.[220]

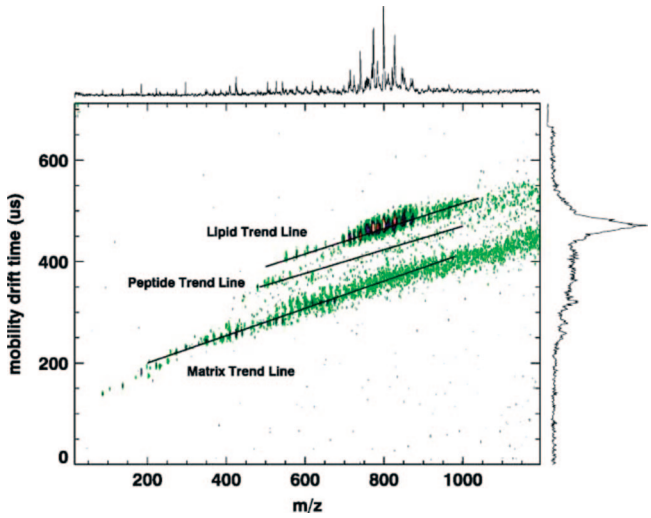

Figure 14. IMS diagram of ions detected from a rat brain tissue section covered with DHB. Ions of different drift time but overlapping *m*/*z* can be separated from each other. Reprinted with permission from ref 221. Copyright 2007 Wiley Interscience.

SYNAPT HDMS (Waters Corporation, Milford, MA) is at present the only commercially available instrument with IMS which can be used as a powerful tool for the identification and characterization of a variety of biomolecules.[224] This instrument has a quadrupole orthogonal acceleration TOF geometry and is equipped with an IMS device located between the quadrupole and the TOF analyzer. The ion mobility separator used consists of three consecutive traveling wave regions. The first traveling wave (trap) is used to store ions when an IMS is performed, to maximize the duty cycle of the IMS. Next is an actual ion mobility separation part of the T-wave. The final traveling wave device (transfer) is used to transfer ions from the ion mobility separator to the TOF mass analyzer maintaining the ions' separation. Collision induced dissociation (CID) can be achieved in either the trap or transfer T-wave or in both. The instrument is equipped with an interchangeable MALDI source, which can be replaced with AP ionization sources, such as ESI or APCI. MALDI is performed in an intermediate-pressure environment (9×10^{-2} mbar) using a frequency-tripled Nd:YAG laser (355 nm). Imaging data are obtained by moving the tissue sections in a raster pattern on an *x*/*y* stage relative to the laser beam position, which remains fixed.

MALDI-IMS-MSI has the ability to improve the imaging of some drugs, metabolites, lipids, and peptides by separating such ions from endogenous or matrix-related isobaric ions as shown in Figure 14. One such application is whole body imaging of rats dosed at 6 mg/kg with an anticancer drug, vinblastine.[91] The distribution of the precursor ion at *m*/*z* 811.4 and several product ions including *m*/*z* 793, 751, 733, 719, 691, 649, 524, and 355 has been investigated. Clearly demonstrated in these data are the removal of interfering isobaric ions within the images of *m*/*z* 811.4 and also of the fragment ion of *m*/*z* 751, resulting in a higher confidence in the imaging data. Within this work, IMS has been shown to be advantageous in both MS and MS/MS imaging experiments by separating vinblastine from an endogenous isobaric lipid.[91] The same combination of MALDI-IMS-MSI for improving the detection of low-abundance proteins that are difficult to detect by direct MALDI-MSI analysis was described by Djidja et al.[128] Both frozen as well as FFPE breast tumor tissue sections were subjected to a modified trypsin digestion followed by protein imaging and profiling. The advantages of imaging using ion mobility prior to MS analysis were also demonstrated for profiling of human glioma and selective lipid imaging from rat brain.[225] Also the distribution of phosphatidylcholine and cerebroside species was mapped from coronal rat brain sections using MALDI-IMS-MSI.[221] And most recently, the use of IMS coupled with MALDI-MSI enabled both the localization and *in situ* identification of a tumor biomarker, glucose regulated protein 78 kDa (Grp78), within FFPE pancreatic tumor tissue sections.[129]

2.4. Microscope vs Microprobe Mode of Image Acquisition

Microprobe and microscope modes of MS image acquisition are two different approaches of ion detection implemented in imaging instruments.[9] Figure 15 schematically illustrates the two different imaging approaches. Microprobe mode is the more widely used form of MSI data acquisition. The sample is rastered with a laser beam or primary ion beam, and the analyte ions are detected from each point separately. The laser beam or primary ion beam is highly focused in order to achieve maximum image resolution. In microscope mode the spatial relationship of ions desorbed from within the area irradiated by the defocused laser beam or primary ion beam is maintained from the moment of ion desorption until their detection on a 2D-detector.[9,226] This instrument is capable of resolving spatial features within the area irradiated by a laser beam to produce an effective spatial resolution of 4 μm.[226] The principle of position correlated ion detection instead of position correlated ion generation removes the need for a tightly focused microprobe for high lateral resolution imaging MS.[9] The speed of analysis is no longer limited by the large amounts of spots that need to be analyzed in a microprobe mode imaging experiment, and images can be generated at a speed limited by the repetition rate of the laser.[9]

2.5. Profiling vs Imaging

MSI experiments fall into two major groups: profiling (low spatial resolution) or imaging (high spatial resolution).[158] Profiling involves sampling of discrete areas of the tissue sections and subjecting the resulting protein profiles to statistical analysis. In a typical profiling experiment from the whole tissue section only for example 5−20 spots (approximately 1 mm in diameter) are analyzed. These experiments are designed to make comparisons between different types of tissue, such as normal versus tumor or control versus treated. Large numbers of samples are used to achieve statistical significance, and sophisticated data algorithms are required for meaningful data mining and classifications. Alternatively, imaging of a tissue requires an entire tissue section to be analyzed through an ordered array of spots, in which spectra are acquired at every 50−100 μm in both the *x* and the *y* directions. 2D ion intensity maps or images can then be created by plotting the intensities of any signal obtained as a function of its *x*,*y* coordinates. This array may contain several thousands to tens of thousands of pixels.[158] The resulting images allow comparison of molecular distributions between different regions of the sample as well as between the samples.[103] The size of the data files generated in imaging mode and the time required for data acquisition are much larger than those for profiling experiments. The sample preparation procedures for profiling and

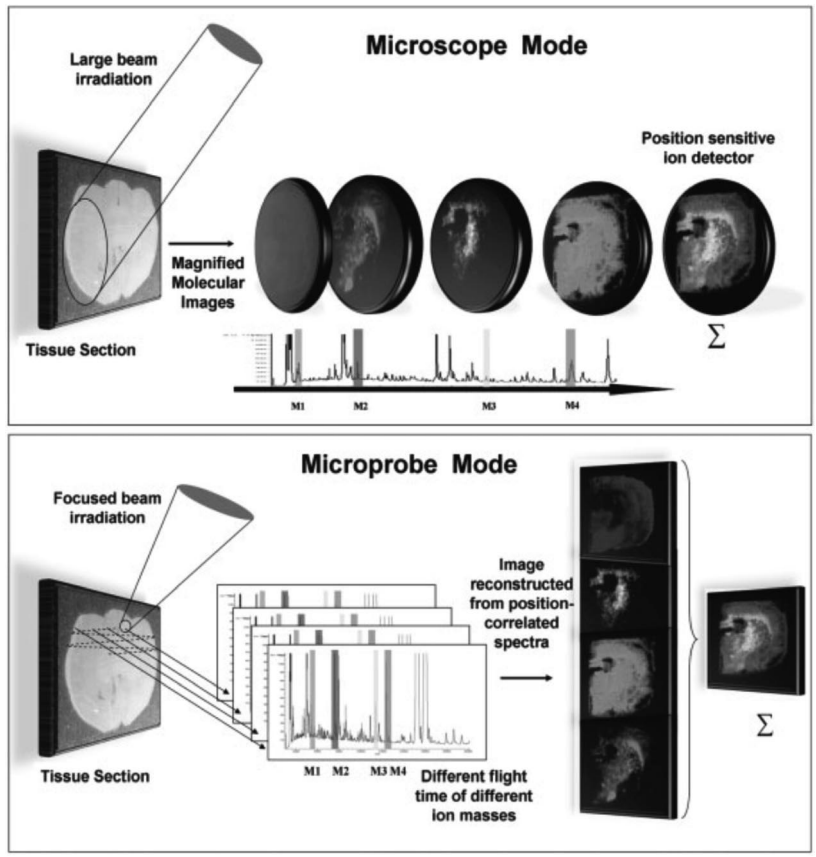

Figure 15. Schematic representation of the MS image acquisition process performed in (A) microscope mode and (B) microprobe mode. Reprinted with permission from ref 99. Copyright 2009 Wiley Interscience.

imaging experiments have been automated and allow correlation of matrix application with MS acquisition. The sample preparation methods are very similar for both types of imaging experiments, and the current matrix spotting instruments can print the matrix spots directly on a tissue section either as individual spots on selected sample features for profiling or as dense spot arrays over the entire tissue or as large ROI for imaging.[94]

Laser capture microdissection (LCM) is a specific cell isolation method used for tissue profiling experiments. In LCM a narrow infrared laser beam (7−10 μm diameter) is focused onto a heat sensitive, ethylene vinyl acetate (EVA) thermoplastic film. The laser light heats and locally deforms the polymer, enabling contact to the cell(s) of interest. The cell binds the polymer and is lifted from the tissue section when the polymer is removed. The polymer film containing the specific cells can be transferred to a MALDI-MS target plate using double-sided conductive tape. The "captured cells" are then spotted with matrix solution, and protein profiles are acquired by MALDI-MS. Several reports described the combination of LCM and MS technologies for the analysis of several types of cells, including normal breast stroma cells, normal breast epithelial cells, malignant invasive breast carcinoma cells, and malignant metastatic breast carcinoma cells from radical mastectomies.[227,228] Protein profiling showed unique protein patterns from these different disease subsets.

2.6. Tags

Photocleavable molecular tags have also been designed to enhance the specificity of MALDI-MSI analyses. In this strategy, the sample section is incubated with the tagging reagent and image analysis is performed on the low M_w tag compound instead of the target molecule.[229] The Tag-Mass strategy is based on the indirect MALDI imaging of mRNA or proteins using a probe labeled with a photocleavable linker, which is cleaved by the MALDI UV laser, releasing a Tag molecule. The Tag is a known molecule with a characteristic mass that can be detected efficiently during MSI, thus allowing for molecular images to be obtained more accurately and efficiently. Using this approach, proteins that are normally below the detection threshold of direct MALDI-MS imaging, such as synaptophysin in neuroendocrine cells in healthy human pancreatic tissue or the cancer markers PS100 and HMB45 from liver invaded by metastatic melanoma, can be visualized.[230]

3. Applications of Mass Spectrometric Imaging

After almost two decades of MSI developments, the technology is finding more and more applications in the life sciences. This is a marked difference from the initial development stages, where the images were taken from standard surfaces and well-known, well-defined substrates. More and more, applied MSI research is crossing the barriers between scientific disciplinces. This can be seen by the great variety in applications found in the current literature, ranging from disease pathology to molecular biology. In this section we have chosen to elaborate on a number of these different life-science oriented application domains of MSI. We realize that this list is not complete, but it does provide an overview of the MSI application domains that are receiving most attention throughout the scientific disciplines.

3.1. Application of MSI in Disease Pathology

MSI has been applied in a vast spectrum of disease pathology. A number of diseases, such as Parkinson's disease,[110,231] Alzheimer's disease,[165,232] Fabry's disease,[137,233] muscular dystrophy,[234] kidney diseases,[174,235,236] nonalcoholic fatty liver disease (NAFLD),[237] Tay-Sachs/Sandhoff's disease,[238] and cardiovascular disease,[59] have been investigated by the MSI technique.

Similarly, many cancer types, such as breast cancer,[128,135,239] prostate cancer,[112,240] ovarian cancer,[136] lung cancer,[122] glioma,[37,133] and colon cancer liver metastasis,[241] were analyzed using MSI. As the demand to understand cancer biology is constantly increasing, the number of projects being carried out in this field and the spectrum of applied techniques are also dramatically expanding. In this regard, MSI becomes a practical tool to study cancer biology. The availability of tumor tissue samples (biopsies, resected tumors, and xenograft models) increases the practicability of MSI in cancer biology, as they make good samples for MSI analysis.

Many molecular complexities, such as the transformation of cells from normal to malignant as well as the involved pathways, are important scientific questions at present. A number of MSI studies were carried out to compare the protein or lipid profiles obtained from normal and tumor tissue.[242−245] The objective of this comparative analysis is to distinguish cancer from normal tissue as well as classify different grades or subtypes of cancer on a molecular level.[103]

In this section of the review we present the application of MSI in current medical research.

In the first of the presented applications, a large series of quantitative element maps (such as Fe, Cu, Zn, and Mn) were produced in native brain sections of mice subchronically intoxicated with 1-methyl-4-phenyl-1,2,3,6-tetrahydropyridin (MPTP) as a model of Parkinson's disease by a newly developed LA-ICP-MS imaging technique.[246] Significant decreases of Cu concentrations in the periventricular zone and the fascia dentata at 2 h and 7 days and a recovery or overcompensation at 28 day, most pronounced in the rostral periventricular zone (+40%), were observed. In the cortex, Cu decreased slightly to −10%. Fe increased in the interpeduncular nucleus (+40%) but not in the substantia nigra. Some other model of neurodegenerative disease was recently investigated using MSI.[247] The analysis of the Scrapper-knockout (SCR-KO) mouse brain showed two types of neurodegenerative pathologies: spongiform neurodegeneration and shrinkage of neuronal cells. PCA revealed numerous alterations and their position in the KO mouse brain. In another study, TOF-SIMS was used to image the distribution of biochemical compounds on tissue sections of steatotic liver.[248] Fatty liver or steatosis is a frequent histopathological change, which is a precursor for steatohepatitis that may progress to cirrhosis and in some cases to hepatocellular carcinoma. The analysis of steatotic vesicles disclosed a selective enrichment in cholesterol as well as in diacylglycerol (DAG) species carrying long alkyl chains and demonstrated that DAG species C30, C32, C34, and C36 carrying at least one unsaturated alkyl chain were selectively concentrated in the steatotic vesicles. Moreover, investigations performed on the nonsteatotic part of the fatty livers despite exhibiting normal histological features revealed small lipid droplets corresponding most likely to the first steps of lipid accretion. Similar experiments were performed using TOF-SIMS with a bismuth cluster ion source to map lipids *in situ* at the micrometer scale and to simultaneously characterize their molecular distribution on liver sections obtained from patients suffering from NAFLD.[237] Accumulation of triacylglycerols (TAG), DAGs, monoacylglycerols, and fatty acids, with the apparition of myristic acid, together with a dramatic depletion of vitamin E and a selective macrovacuolar localization of cholesterol, were observed in steatosis areas of fatty livers compared to control livers. Finally, the analysis revealed lipid zonation in normal human liver and accumulation of very similar lipids to those detected in areas of fatty livers, which were not characterized as steatotic ones by the histological control performed on serial tissue sections. MSI potentially could be employed in early detection of steatosis, even before the pathological changes are detectable by histological examination.

In another example, MALDI-MSI was involved in studying the specific molecular profiles of ovarian cancer interface zones (IZ), which are the regions between tumors and normal tissues.[244] Unique profiles were identified for the tumors, the normal zone, and the IZ. Analysis identified two interface-specific proteins, plastin 2 and peroxiredoxin 1 (PRDX 1), which were differentially regulated between zones. The results were confirmed by fluorescence microscopy, which revealed high expression levels of plastin 2 and PRDX 1 along the IZ of ovarian tumors. This comparative proteomics study suggested that the IZ is different from the adjacent tumor and normal zones and that plastin 2 and PRDX 1 may be interface markers specific to ovarian tumors.

Cancer biology was also investigated by DESI-MSI used to image differential expression and the distribution of different classes of lipids in thin tissue sections of canine spontaneous invasive transitional cell carcinoma of the urinary bladder (a model of human invasive bladder cancer) as well as adjacent normal tissue from different dogs.[245] The tumor and adjacent normal tissue showed differences in the relative distributions of the lipid species. Increased absolute and relative intensities for at least five different GPLs and three free fatty acids in the negative ion mode and at least four different lipid species in the positive ion mode were seen in the tumor region of the samples in all four dogs. In addition, one sphingolipid species exhibited increased signal intensity in the positive ion mode in normal tissue relative to the diseased tissue.

The same imaging technique was also used for the profiling and imaging of arterial plaques.[249] Sodium (in positive ion mode) and chloride (in negative ion mode) adducts of diacyl glycerophosphocholines (GPChos), sphingomyelins (SMs), and hydrolyzed GPChos were detected. Additionally, cholesteryl esters were detected via adduct formation with ammonium cations. Finally, cholesterol was imaged in the atheroma by doping the charge labeling reagent betaine aldehyde directly into the DESI solvent spray, leading to *in situ* chemical derivatization of the otherwise nonionic cholesterol. The results revealed lipid rich regions of two different lipid profiles within the arterial walls. These lipid rich regions likely correspond to the areas of the tissue where lipoprotein particles accumulated. It is also possible that the different lipid distributions may correlate with the stability or vulnerability of that particular region of the plaque.

The MS profiling technique has been applied to detect the highly expressed proteins in human oral squamous cell carcinoma of tongue biopsy. In this study two distinct molecules at approximately 4500 Da and approximately 8360 Da were detected in cancer tissue.[250]

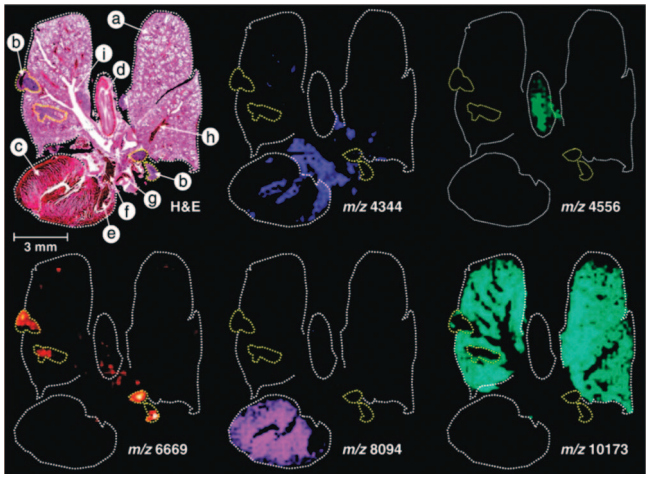

Figure 16. Analysis of a tissue section from an EPPE tumor bearing mouse lung specimen. The photomicrograph of the displayed section, which was H&E-stained following MSI acquisition and matrix removal, shows several histologically different regions: (a) lung, (b) lung tumors (areas in yellow dotted lines), (c) heart, (d) upper respiratory pathways, (e) left heart ventricle, (f) aorta, (g) right pulmonary artery, (h) artery, (i) bronchus. Five distinct ion density maps from proteins which distinctively localize in different areas of the section are displayed. Reprinted with permission from ref 123. Copyright 2008 American Chemical Society.

To study pancreas pathology, different regions of the pancreas of both control and obese mice were imaged by MALDI-MSI and peptide-specific profiling was performed.[111] The distribution of C-peptide of insulin and glicentin-related polypeptide displayed a striking resemblance with Langerhans islet's histology.

Recently, a new strategy in MSI was developed to use >9-year-old rat brain tissues of a Parkinson's disease animal model stored in FFPE blocks.[126] The method employed MALDI tissue profiling, combining the use of automatic spotting of the MALDI matrix with *in situ* tissue enzymatic digestion. The analyses confirmed that ubiquitin, transelongation factor 1 (eEF1), hexokinase, and Neurofilament M were down-regulated, as previously shown in human or animal models of Parkinson's disease. In contrast, peroxidoredoxin 6, F1 ATPase, and α-enolase were up-regulated. In addition, three novel putative biomarkers were uncovered from protein libraries: eEF1 and collapsin response mediator 1 and 2. Finally, the identity of CRMP-2 protein was validated using immunocytochemistry and MALDI imaging based on the different ions from tryptic digestion of the protein.

TOF-SIMS was used to obtain high-resolution ion images in ischemic retinal tissues.[251] Marked changes in Ca^{2+} distribution, compared with other fundamental ions, such as Na^+, K^+, and Mg^{2+}, were detected during the progression of ischemia. Furthermore, the Ca^{2+} redistribution pattern correlated closely with TUNEL-positive (positive for terminal deoxynucleotidyl transferase-mediated 2′-deoxyuridine 5′-triphosphate nick end-labeling) cell death in ischemic retinas. After treatment with a calcium chelator, Ca^{2+} ion redistribution was delayed, resulting in a decrease in TUNEL-positive cells. Results showed that ischemia-induced Ca^{2+} redistribution within retinal tissues was associated with the degree of apoptotic cell death, which possibly explains the different susceptibility of various types of retinal cells to ischemia.

MSI quickly became a very important tool for molecular histology. Pathologists have already recognized its potential and started exploring biological material collected from patients and stored in hospital tissue banks. Since these banks usually contain a large number of different samples, it became clear that MSI analysis of such material must be automated. The development of an automated setup for high throughput molecular histology MSI has been recently presented by McDonnell et al.[252] This device consists of a controlled environment sample storage chamber, a sample loading robot, and a MALDI TOF/TOF mass spectrometer, all controlled by a single user interface. The automated set up has the positional stability and experimental reproducibility necessary for its clinical application.

Figure 16 illustrates the use of MSI to image proteins from an ethanol-preserved and paraffin-embedded (EPPE) tumor bearing mouse lung section.[123] A clear distinction between tumurous tissue and healthy tissue is observed, indicating the applicability of MSI as a medical diagnostic imaging tool. An additional example in tumor biology is provided in Figure 17, where MSI is employed to study a MCF7 xenograft breast cancer model.[128] Both of these examples employ MSI to provide detailed molecular insight into tumor biology.

Along with advances in instrumentation, MSI became well recognized in the medical community. There are a number of MSI reviews dedicated to the application of MS imaging in disease and pathology.[93,253−257]

3.2. Application of MSI in Biological Sciences

MSI has numerous applications in the field of biological sciences. Direct tissue analysis from any type of biological material made this technique a powerful tool for life sciences. Here, we present some examples of MSI being applied to investigate biological samples of different origin.

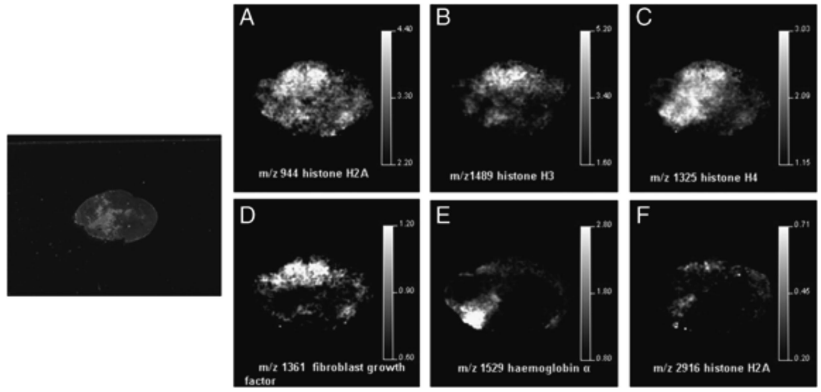

Figure 17. MALDI-MS images of peptide distributions within an MCF7 xenograft tissue section. Reprinted with permission from ref 128. Copyright 2009 Wiley Interscience.

An MSI technique was applied to investigate a novel family of antimicrobial peptides, named raniseptins present in the dorsal skin of a frog (*Hypsiboas raniceps*).[258] These studies demonstrated that the mature raniseptin peptides are in fact secreted as intact molecules within a defined glandular domain of the dorsal skin. *De novo* MS/MS sequencing and direct MALDI imaging experiments of the skin from another frog (*Phyllomedusa hypochondrialis*) identified 18 bradykinin related peptides (BRPs) along with their PTMs.[259]

Calf and mature bovine lenses were imaged by MALDI-MSI methods to obtain the distribution of lens α-crystallins and their modified forms.[260] The results from this study shed light on the physiological significance of the modified forms of the two α-Crystallin subunits. Another study, involved MSI to investigate the distribution of the age-related changes of human lens α-Crystallin including a novel L52F α-A-Crystallin mutation in a cataractous lens.[261] Application of this technique to lens biology enhanced the understanding of α-Crystallin protein processing in aging and diseased human lenses. Ocular lens and retinal tissues were used as model samples for developing a new MALDI-MSI tissue preparation protocol for integral membrane proteins.[262] Molecular images of full-length Aquaporin-0 (AQP0) and its most abundant truncation products were obtained from bovine and human lens sections. This tissue preparation protocol was also successfully applied to image the distribution of the G-protein coupled receptor, opsin, in the rabbit retina. In addition, both fresh and formaldehyde-fixed mammalian lenses were analyzed by direct profiling of two relevant phospholipid classes, phosphatidylcholines (PCs) and SMs.[263]

Neuropeptides are another class of biomolecules which can be investigated using an MSI technique. Neuropeptide distributions directly from rat, mouse, and human pituitary tissue sections were obtained using MALDI-MSI in microscope mode,[226] from crustacean neuronal tissues using an MALDI-FTMS instrument,[264] and from a wide variety of invertebrate samples such as tissues and ganglia, single neurons, or single vesicles using MALDI-MSI.[265] Distributions of peptide isoforms belonging to 10 neuropeptide families were investigated in the brain of the Jonah crab (*Cancer borealis*).[266] This study revealed the spatial relationships between multiple neuropeptide isoforms of the same family as well as the relative distributions of neuropeptide families. In addition, a MALDI ion trap was used to visualize neuropeptides from the dissected tissue of the house cricket (*Acheta domesticus*).[267] Tissue imaging together with tandem MS allowed successful identification of neuropeptides present in the corpora cardiaca and allata of the insect.

MSI was applied to obtain distributions of ganglioside molecular species in the mouse hippocampus.[268] In this study, the location of age-dependent C20-GD1 accumulation was successfully characterized. Another study of the gangliosides inside mouse brain tissue sections demonstrated that the N-fatty acyl chains of gangliosides were differentially distributed in mouse hippocampal regions, whereby the gangliosides with an N−C18 acyl chain were enriched in the CA1 region, while gangliosides with an N−C20 acyl chain were enriched in the dentate gyrus.[269] In this study, an ionic liquid matrix was used for MSI of gangliosides, which provided excellent sensitivity for ganglioside detection without significant loss of sialic acid residues.

Another class of lipids detected from rat brains was mapped by MSI to study the normal functioning of the brain. The differential distribution of PCs such as PC(32:0), PC(34:1), and PC(36:1) in different parts of the rat brain was successfully investigated by Mikawa et al. by using MALDI-MSI.[114] PC(32:0) and PC(34:1) were more abundantly observed in the gray matter areas than in the white matter areas, while PC(36:1) was evenly distributed throughout the central nervous system. In addition, PC(32:0) and PC(34:1) were mostly detected in the granular layer of the olfactory bulb, piriform cortex, insular cortex, and molecular layer of the cerebellum, regions known for high neuronal plasticity. In another study, the cell-selective distribution of polyunsaturated fatty acid-containing glycerol phospholipids in the mouse brain was presented.[107] The results showed that arachidonic acid- and docosahexaenoic acid-containing PCs were seen in the hippocampal neurons and cerebellar Purkinje cells, respectively.

Plant tissues of different origin can also be subjects for MSI. The first paper describing MALDI-MSI analysis of oligosaccharides in a plant system was published by Robinson et al.[270] Endogenous water-soluble oligosaccharides found in the stems of wheat (*Triticum aestivum*) were investigated as a potential indicator of grain yield. Water-soluble oligosaccharides up to 11 hexose residues were ionized as potassiated molecules and found to be located in the stem pith that is retained predominantly around the inner stem wall.

MALDI-MSI was applied by Mullen et al. in 2005 for imaging of the herbicide (mesotrione) and the fungicide (azoxystrobin) on the surface of the soya leaf and inside the stem of the soya plant.[271] This study demonstrated the applicability of MALDI imaging to the detection and imaging of small organic compounds in plant tissue. The same imaging technique provided new insights into the distribution of the pesticide nicosulfuron in sunflower plant tissue using direct tissue imaging following root and foliar uptake.[272] Images of fragment ions and alkali metal adducts were obtained which showed the distribution of the parent compound and a phase 1 metabolite in the plant. MALDI-MSI also enabled us to look at the distribution of metabolites within plant tissues such as wheat seeds.[273] Results showed the localization of metabolites such as amino acids, glucose-6-phosphate, and sucrose within seeds. Not only MALDI-TOF but also TOF-SIMS was used for imaging of biomolecules inside plant tissues. The movement of herbicide formulation components into and across plant cuticles was monitored at high spatial resolution by TOF-SIMS.[52] The studied components included the oligomeric ethoxylate surfactants Synperonic A7 and A20 and the active ingredient Sulfosate (trimesium glyphosate). Clear differences in the penetration/diffusion behavior of these molecules into the surface of *Prunus laurocerasus* leaves and across the isolated plant cuticle were identified. Colloidal silver LDI mass spectrometry was employed to directly profile and image epicuticular wax metabolites on leaves and flowers of a model organism *Arabidopsis thaliana*.[274] Silver adducts of major cuticular wax compounds, such as very long-chain fatty acids, alcohols, alkanes, and ketones, were successfully detected. For the first time the surface metabolites of different flower organs (carpels, petals, and sepals) were profiled at a spatial resolution of approximately 100 μm. Mass spectral profiles and images were collected from wild type and a mutant strain, which carried alleles affecting its surface constituents. Obtained data provided new insights into the complexity of epicuticular wax deposition in plants. In

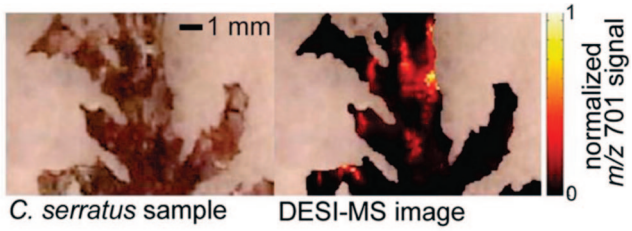

Figure 18. Negative-ion DESI mass spectra of bromophycolides. DESI-MS image (200 μm resolution) of a bromophycolide A/B chloride adduct ion *m/z* 701 on a *C. serratus* surface, indicating that bromophycolide "hot spots'' correspond to pale patches. Reprinted with permission from ref 78. Copyright 2009 PNAS.

addition, colloidal graphite-assisted LDI (GALDI) MSI was employed to map the location and the degree of light-induced accumulation of flavonoids in stem sections of *Arabidopsis thaliana*.[119] The main targeted metabolites were flavonoids and cuticular waxes. The mass spectral profiles revealed tissue-specific accumulation of flavonoids in flowers and petals. Conventional MALDI-MSI was employed to localize the major allergen present in peach in the outer part of the fruits.[275] The structure of this allergen, the lipid transfer protein (LTP), Pru p 3, was identified by ESI, coupled to single stage (quadrupole) or advanced (FT-HRMS) analyzers. The results showed the full potential of mass spectrometry for obtaining high quality structural data of relevant food proteins. MALDI-MSI was also used to study the spatial distribution of metabolites from the cyanobacteria *Lyngbya majuscula* 3L and JHB, *Oscillatoria nigro-viridis*, *Lyngbya bouillonii*, and a *Phormidium* species as well as the sponge *Dysidea herbacea*.[118]

The same ionization technique was employed to detect high concentrations of the marine alkaloid, norzoanthamine, present in the epidermal tissue in the colonial zoanthid *Zoanthus* sp.[276] The first examples of DESI imaging of metabolites on biological surfaces illustrated the potential of DESI-MS in understanding chemically mediated biological processes.[78] DESI-MSI was employed to investigate the concentrations of natural algal antifungal products such as bromophycolides from the red macroalga *Callophycus serratus*.[78] The analysis of the images shown in Figure 18 revealed that surface-associated bromophycolides were found exclusively in association with distinct surface patches at concentrations sufficient for fungal inhibition. A short review describing the application of DESI-MSI in probing marine natural product defenses was published by Esquenazi et al. in 2009.[77] DESI-MSI was also applied for *in situ* detection of alkaloids in the tissue of poison hemlock (*Conium maculatum*), jimsonweed (*Datura stramonium*), and deadly nightshade (*Atropa belladonna*).[74] Different types of plant material were analyzed, including seeds, stems, leaves, roots, and flowers.

MSI was used to investigate the biological processes occurring in the reproductory system of small rodents. For example, MALDI-MSI provided global and time-correlated information on the local proteomic composition of the sexually mature mouse epididymis.[120] Tissue sections, cells collected by LCM, and secretory products were analyzed, which resulted in detection of over 400 different proteins. In another study, MALDI-MSI technology was used to characterize the spatial and temporal distribution of phospholipid species associated with mouse embryo implantation.[277] The ion images showed that linoleate- and docosahexaenoate-containing phospholipids localized to regions destined to undergo cell death, whereas oleate-containing phospholipids localized to angiogenic regions. Molecular images revealed the dynamic complexity of lipid distributions in early pregnancy and shed light on the complex interplay of lipid molecules in uterine biology and implantation. Also, the molecular composition, relative abundance, and spatial distribution of a large number of proteins expressed during the periimplantation period were investigated by MALDI-MSI.[113] For the first time, *in situ* proteome profiles of implantation and interimplantation sites in mice in a region- and stage-specific manner with the progression of implantation were obtained. Cytosolic phospholipase A (2alpha) null females that show implantation defects were also investigated, which provided new insights regarding uterine biology. TOF-SIMS equipped with a gold ion gun was used to image mouse embryo sections and analyze tissue types such as brain, spinal cord, skull, rib, heart, and liver.[41] PCA was used to reduce the spectral data generated by TOF-SIMS. MALDI-MSI was also used to study the temporal diffusion of honeybee venom in envenomed tissue.[278]

3.3. Application of MSI in Proteomics/Peptidomics

Here, we briefly discuss the issue of peptide and protein detection directly from tissue sections. Topics such as bottom-up and top-down on-tissue proteomics, on-tissue protein digestion, and single-cell MALDI-MS profiling will be discussed.

Mass spectrometry evolved into an indispensable tool for proteomics research.[279] The demand for spatial information of detected proteins and peptides pushed the boundary of mass spectrometry capabilities and started a new era of MSI. Three strategies for protein identification and characterization are currently employed in proteomics: bottom-up proteomics, which analyzes proteolytic peptide mixtures, middle-down proteomics, which analyzes longer peptides, and top-down strategies, which analyze intact proteins.[280] It became clear that rapidly developing MSI instrumentation should allow detection, identification, and characterization of proteins directly from biological tissue also in terms of their interactions with other molecules, PTMs, and different isoforms expressed inside the cells.

In terms of the bottom-up approach, the proteins present in biological tissue must be first subjected to *in situ* digestion by proteolytic enzyme. The protocol designed for MSI was published by Groseclose et al. in 2007.[161] The method for on-tissue protein digestion involved a tissue washing step with organic solvents capable of removing lipids. Otherwise, the strong lipid signals in the same mass range as that of the obtained peptides interfere with peptide detection and identification. After removal of lipids, a tissue section should be sprayed or spotted with the solution of proteolytic enzyme, most commonly trypsin, and after the incubation time covered with matrix (usually DHB or CHCA).

The top-down approach allows detection of intact proteins directly from tissue sections. The upper mass range of the instruments used for MSI is the detection limiting factor. Therefore, efficient detection and identification of proteins with $M_w > 30$ kDa needs to be improved. MALDI also suffers from mass dependent sensitivity drop-off, which means that bigger proteins must be present at sufficient concentration in order to be detected and analyzed. One of the solutions for the sensitivity issue could be Tag-Mass (see Tags). The complexity of the sample and high M_w of the analyzed proteins, which very often limits detection of biomolecules

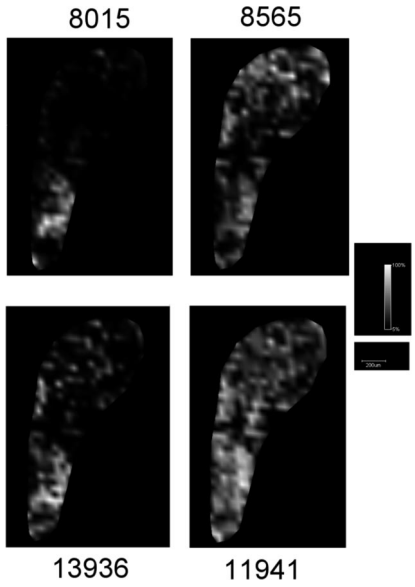

Figure 19. MALDI imaging of proteins from an *Anopheles gambiae* male antenna. Ion images of four proteins are reported, *m/z* 8015, *m/z* 8565, *m/z* 11941, and *m/z* 13936, respectively, in panels A, B, C, and D, showing different distributions across the antenna. Reprinted with permission from ref 285. Copyright 2008 Dani et al.

directly from tissue sections, can be reduced by simultaneous extraction, separation, and digestion of proteins from the tissue section while preserving their relative location. To reduce the complexity of the sample, contact blotting of fresh cut tissue sections on a surface of C18-coated resin beads[5] or on a polymeric conductive membrane[281] can be performed. The chemical properties of the blotting surface determine which analytes are detected during MSI. Typically, hydrophobic surfaces are used because they can be washed with water in order to remove salts before matrix application. More complex surfaces, such as Teflon plates or antibodies bound to surfaces, were also tested for extraction of specific proteins or a class of proteins from the tissue.[93] While the concept of blotting is quite straightforward, the process involves transfer of the proteins from the tissue into the methanol sprayed MALDI target, which requires diffusion of molecules, which can lead to loss of spatial resolution in the imaging experiment.[93] The molecular scanner approach, introduced by Hochstrasser and co-workers, combined both a blotting step and enzymatic digestion.[166,282,283] The molecular scanner was initially developed for 2D gels. It allows protein separation using 2D-PAGE with parallel digestion of the separated proteins and transfer of obtained peptides onto a membrane while keeping their relative positions. The membrane is then sprayed with a matrix solution and analyzed in a mass spectrometer.[284]

One of the interesting applications of MALDI-MSI for analyzing intact proteins directly from tissue sections was presented by Dani et al. in 2008.[285] MSI was applied to study *Anopheles gambiae* antennae, with the aim of analyzing the expression of soluble proteins involved in olfaction perireceptor events. Profiling of the proteins on the antennae surface, shown in Figure 19, revealed distinct protein profiles between male and female antennae, and imaging experiments showed differences in the localization of some of the detected proteins. High resolution measurement and top-down MS/MS experiments resulted in the identification of two proteins: a 8 kDa protein which matched with an unannotated sequence of the *A. gambiae* genome and odorant binding protein 9 (OBP-9). This work showed that MALDI-MS profiling is a technique suitable for the analysis and comparison studies of small and medium proteins in insect appendices.

A similar approach was used for comparison of the peptide profiles of the sea slug (*Aplysia californica*) neurons using MALDI-MSI which revealed distinct peptide profiles for each neuronal subtype analyzed and identification of previously unknown peptides.[286] In this study, individual F cells were isolated based on their position, size, and pigmentation and Tungsten needles were used to transfer each cell onto a MALDI target plate containing 0.5 mL of DHB solution.

Single-Cell MALDI-MS Profiling

A review presenting single-cell MALDI-MS peptide profiling from individual cells and other mass-limited tissue samples was published by Li et al. in 2000.[287] The most recent review presents the history of single-cell mass spectrometry with the emphasis on live single-cell MS.[288] Single-cell MALDI-MS has multiple advantages, such as the following: (1) compatibility with crude mixtures; (2) minimal sample clean up; (3) no need for tagging or preselecting the peptide of interest; (4) simple instrumentation; (5) high sensitivity; (6) complementary information to immunochemical methods; and (7) compatibility with PTMs.[287] One important characteristic of single-cell MALDI-MS is its ability to directly profile intact cell and tissue samples without any purification of peptides or proteins. Simplified sample preparation preserves spatial and biomolecular information within the cells, reducing degradation processes, dilution of biomolecules, or contamination from adjacent cells, which can have different sets of peptides or proteins. Among the disadvantages would be the following: (1) too low sensitivity of instruments to probe the entire content of a single cell and (2) too small size of the cell, making it hard to probe with a laser.[288]

The first MALDI-MS profiling analyses of peptides in single neurons were done by van Veelen et al. in 1993,[289] Jiménez et al. in 1994,[290] and Hsieh et al. in 1998.[291] Neuropeptides were directly detected in single neurons and the neurohemal area of peptidergic (neuroendocrine) systems in the *Lymnaea* brain.[290] The study of neuroendocrine systems revealed that processing of the complex prohormone expressed in this system occurred entirely in the soma. In addition, novel as well as previously identified peptides were detected. These experiments demonstrated that MALDI-MS was promising and a valuable approach to study of the synthesis and expression of bioactive peptides, with potential application to single-cell studies in vertebrates, including humans. Since then a number of single-cell MALDI-MS experiments was performed on cells of different origin, such as crayfish,[292] insects,[293] red blood cells,[294] single neurons,[290] mouse bone marrow-derived mast cells,[295] and individual rat pituitary cells.[296] The review article published by C. R. Jiménez and A. L. Burlingame provided an overview of MALDI as a tool for the direct analysis of peptide profiles contained in single cells from invertebrate (the pond snail), vertebrate species (*Xenopus* and rat), and tissue biopsies with a special emphasis on the sample handling required for each application.[297] MALDI-MS was successfully applied for profiling the proteome of single cells, but imaging is still not possible due to currently available laser spot sizes, which at present can be focused to a minimal diameter of 20 μm. Development of lasers capable of probing single cells, together with improved matrix application methods, deliver-

ing small crystals containing highly concentrated analytes, will open the gate for MALDI-MS imaging of single cells.

Obviously, single cells are routinely analyzed by TOF-SIMS, but the detection limit (upper mass <1000 Da), extensive in source fragmentation of secondary ions and lack of MS/MS capabilities of TOF-SIMS instruments, limits at present its application in proteomic studies.

The first application of MALDI-MSI to proteomics was presented by Caprioli et al. in 1997.[5] The analysis of regions of rat splenic pancreas and rat pituitary revealed many peptides and proteins detected from the C-18 blotted target.[5] The next paper showed direct profiling of proteins present in tissue sections for several organs of the mouse where over 100 peptide/protein signals in the 2000−30 000 Da range were observed after blotting of the tissue sections on a conductive polyethylene membrane and coating with SA.[281] Later, MALDI-MSI was used to determine peptide distributions directly from rat, mouse, and human pituitary tissue sections with high-resolution MSI, which allowed localization of neuropeptide distributions within different cell clusters of a pituitary tissue section.[226] MALDI-MS was also employed to detect and structurally characterize small cardioactive peptides in two functionally related neurons, which form a network involved in the modulation of heartbeat in freshwater snails *Lymnaea*.[298] MALDI-MS was also used to study the intricate processing pattern of a preprohormone expressed in neurons of this gastropod mollusk.[299] Isolated cells and tissues, including egg-laying hormone-releasing cells, from the central nervous systems of the model marine mollusks *Aplysia californica* and *Pleurobranchaea californica* were used to demonstrate the salt removal method and detect several neuroactive peptides previously characterized by conventional biochemical methods.[300] MALDI-MSI was applied to the study of amyloid β peptide distribution in brain sections from a mouse model of Alzheimer's disease.[186] A combination of MS profiling and LCM of normal breast stroma, normal ductal epithelium, ductal carcinoma *in situ*, and invasive ductal carcinoma microdissected from a single frozen section was presented by Palmer-Toy et al. in 2000.[228] Each tissue type, when analyzed separately, revealed characteristic peaks. Several prominent peaks in the 4500−7000 Da range distinguished the breast stroma from the ductal epithelium while high-mass peaks in the mass range of 45 to 60 kDa were characteristic only for the invasive carcinoma.[228] A recent review focused on four state of the art proteomic technologies applied in the discovery of potential tumor markers, namely, 2D difference gel electrophoresis, MALDI-MSI, electron transfer dissociation mass spectrometry, and a reverse-phase protein array technique, presenting progress in proteomic technologies from 1997 to 2008 was published by Wong et al. in 2009.[301]

3.4. Application of MSI in Metabolomics

The functional levels of biological cells or organisms can be separated into the genome, transcriptome, proteome, and metabolome. Here, we concentrate on applications of MSI for metabolomics. The term metabolism is derived from the Greek word $\mu\varepsilon\tau\alpha\beta^{\circ}\lambda\acute{\eta}$ (*metabolé*), meaning change. Metabolome is defined as the total quantitative collection of low M_w compounds (metabolites) present in cells or organisms which participate in metabolic reactions required for growth, maintenance, and normal function.[302] The metabolome is composed of small M_w organic and inorganic species, generally of a mass less than 1500 Da. The number of metabolites is generally 10-fold smaller compared to that of genes; for example, the yeast *S. cerevisiae* has a genome encoding more than 6600 genes and contains 584 identified metabolites.[206,303] But the number of metabolite molecules present within one cell can vary from just a few (signaling molecules) to millions (glucose). The concentration of metabolites depends on the metabolic state of the investigated cell. Metabolites can be of endogenous origin (synthesized or catabolized within the cell or organism) or of exogenous derivation (pharmaceuticals or food nutrients).[206]

Metabolomics is currently a rapidly developing discipline for the study of microbial, plant, and mammalian metabolomes. A recent review focused on the collection of analytical data for metabolomic studies was published by W. B. Dunn in 2008.[206] A review presenting the capabilities of current MSI techniques for imaging metabolite molecules and a summary of representative MSI studies of both endogenous and exogenous metabolites was recently published by Y. Sugiura and M. Setou.[304]

Here, some of the MSI applications for metabolomic studies of animals, plants, sponges, and cyanobacteria are presented. MSI has been recently employed for detection and identification of 13 primary metabolites, such as adenosine monophosphate (AMP), adenosine diphosphate (ADP), adenosine triphosphate (ATP), uridine diphosphate (UDP), or *N*-acetyl-D-glucosamine (GlcNAc), directly from rat brain sections using a 9-aminoacridine matrix.[305] The mass spectral images of the metabolites in Figure 20 clearly illustrate the usefulness of MSI in disease metabolomic studies. The combination of MALDI and SALDI, known as ME-SALDI-MS, enabled successful MSI of low mass species from mouse heart and brain tissues with improved detection sensitivity.[132] Two imaging instruments (MALDI-TOF and MALDI-FTICR) were used to image two HIV protease inhibitors, saquinavir and nelfinavir, in Mono Mac 6 cells.[193] A sublimation/deposition device for homogeneous matrix deposition was constructed which allowed imaging of these HIV protease inhibitors at clinically relevant concentrations. MALDI-TOF and cluster-TOF-SIMS imaging approaches were used to study the localization of lipids (cholesterol, cholesterol sulfate, vitamin E, glycosphingolipids) on skin and kidney sections of patients affected by the Fabry disease.[233] A number of plant metabolites, such as amino acids, sugars, and phosphorylated metabolites, in wheat seeds were imaged by using a combination of two matrices, CHCA and 9-aminoacridine.[273] MALDI-MSI was also used to image the distribution of the pesticide nicosulfuron (parent compound and a phase 1 metabolite) in plant tissue following root and foliar uptake.[272] The spatial distributions of natural products with potential therapeutic applications were characterized by a MALDI-MSI approach.[118] In this study, a number of metabolites from the cyanobacteria *Lyngbya majuscula*, *Oscillatoria nigro-viridis*, *Lyngbya bouillonii*, and a *Phormidium* species were identified. In addition to known natural products such as curacin A and curazole, a large number of unknown ions colocalized with the different cyanobacteria. MSI proved to be useful as a strategy for *de novo* drug discovery. The same technique was used to observe the secondary metabolites found within the sponge *Dysidea herbacea*. These data demonstrated the potential of MSI for providing spatial distribution of natural products, from single strands of cyanobacteria to the very complex marine assemblage of a sponge.[118]

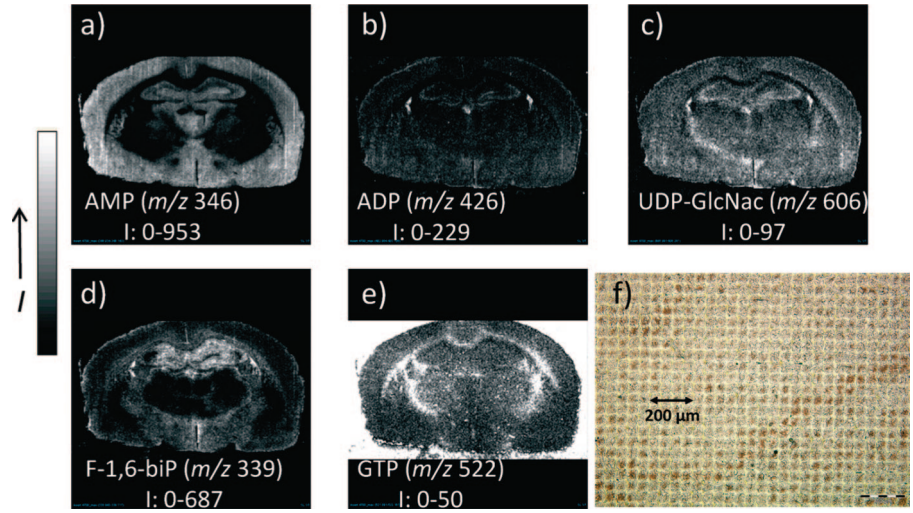

Figure 20. MALDI images of (A) AMP, (B) ADP, (C) UDP-GlcNac, (D) F-1,6-biP (fructose-1,6-bisphosphate), and (E) GTP (guanosine triphosphate) acquired in the negative ion mode from a rat brain section coated with a 9-AA matrix. (F) Optical image of a brain tissue section after 9-AA deposition and analysis by MALDI imaging with a 50 μm pixel size. Reprinted with permission from ref 305. Copyright 2009 American Chemical Society.

3.5. Application of MSI in Lipidomics

Lipids, important components of the cells, serve as the building blocks of cellular membranes (phospholipids, cholesterol), participate in many signaling pathways (diacylglycerol, ceramide, glycolipids, steroids, or prostaglandins),[306] and are stored as an energy source (triacylglycerols).[307] Various different types of lipids, such as glycerophospholipids, sphingolipids, sterol lipids, prenol lipids, saccharolipids, waxes, and fat-soluble vitamins, are found in biological systems. Some examples of common lipid structures are presented in Figure 21. Glycerophospholipids, the key components of the cellular membranes and also

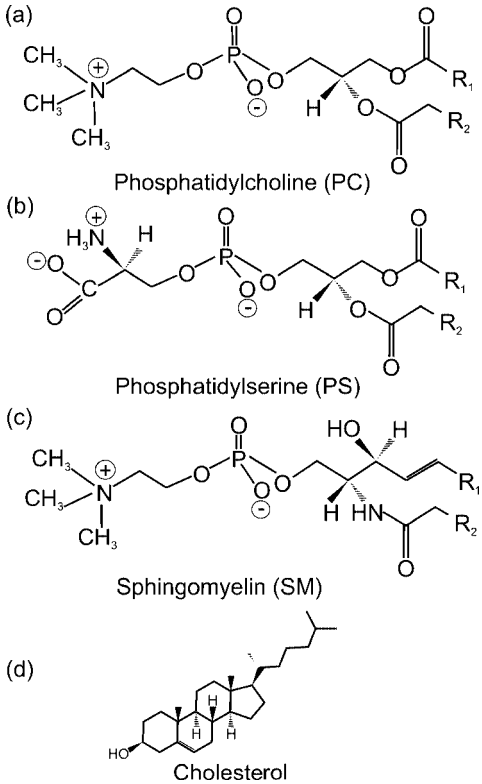

Figure 21. The most common (a, b) glycerophospholipids, (c) sphingolipid, and (d) sterol lipid structures.

important constituents of serum lipoproteins and pulmonary surfactant,[308] are the most abundant lipids in the brain,[309] and they play a role in metabolism and cell signaling. In glycerophospholipids, two hydroxyl groups of the glycerol are esterified by two different fatty acid chains. The third hydroxyl group of the glycerol backbone is esterified by phosphate. The phosphate group can be further esterified by inositol, glycerol, choline, serine, or ethanolamine. In the case of phosphatidic acid, phosphate remains in its unesterified form. Different subclasses of glycerophospholipids contain different types of bonds between the glycerol backbone and the fatty acid chain, e.g. acyl, alkyl, or alk-1′-enyl. The fatty acid chains in biomembranes usually contain an even number of carbon atoms, which can be saturated (e.g., 16:0, 18:0) or unsaturated (e.g., 16:1, 18:1, 18:2).[307]

Sterols are another important lipid constituent of biological membranes. For example, cholesterol is part of cellular membranes in animals, where it regulates the cellular membrane fluidity but also serves as a secondary messenger in developmental signaling.[310,311]

Researchers interested in lipid biology may visit a comprehensive Lipid Metabolites and Pathways Strategy Web site for more information about different classes of lipids and most recent discoveries in this field of science.[312]

Almost all types of ionization sources used for MSI have been successfully applied in the field of lipid imaging.[313] Lipids were imaged using MALDI,[114] DESI,[314] SIMS,[50] and also the recently developed nano-PALDI[82] ionization method. In general, most lipids present in tissues ionize easily due to their polar head groups[315] (e.g., phosphocholine $[M + H]^+$ m/z 184,[316] phosphoinositol $[M + H]^-$ m/z 241,[317] phosphoethanolamine $[M - H]^-$ m/z 140[318]). Phosphatidylcholines, sphingomyelins, and cholesterol ionize in positive ion mode, while phosphatidylinositols, phosphatidylserines, and sulfatides ionize in negative ion mode.[11] Phosphatidylethanolamine (PE) can be analyzed in both positive as well as negative ion mode.

Most biological samples subjected to MSI have a rich lipid content which manifests in a strong ion signal around m/z 800.[141] A commonly observed phospholipid in tissues is phosphatidylcholine PC (16:0/18:1) with an ion $[M + H]^+$

at *m/z* 760.5860 having the elemental composition of $C_{42}H_{83}NO_8P$.[108] Phosphatidylcholines are at present the most commonly detected and imaged lipid class.[50,55,58,61,249] They dominate mass spectra due to the presence of the positively charged quaternary ammonium group in the choline head.[11] Collisional activation and fragmentation of all phosphatidylcholines yield a major product of phosphocholine (PC) at *m/z* 184. However, when a phosphatidylcholine molecular species is cationized with either Na^+ or K^+, closely related but structurally quite different ions at *m/z* 147 and 163, respectively, are observed.[108] In fact, these product ions became very characteristic MS features by which cationized PC can be easily identified.

Lipids can also generate abundant negative ions. For phospholipids, such as PE, phosphatidylserine (PS), phosphatidic acid (PA), phosphatidylglycerol (PG), and phosphatidylinositol (PI), this is due to the presence of the phosphodiester moiety, which can exist as a very stable gas phase anion.[108] Other lipids, such as sphingomyelin (SM) (phosphodiester), sulfatides (sulfuric acid ester), and bacterial lipids related to lipid A (phosphate esters), also yield quite abundant $[M - H]^-$molecular anions. For some polyphosphate esters, doubly charged ions $[M - 2H]^{2-}$ can also be observed.[108] Phosphatidylinositol and lysophosphatidylinositol (LPI) yield a specific fragment ion at *m/z* 241; plasmenylethanolamine (PlsEtn) and PE yield one at *m/z* 196.[141]

The MS analysis of cellular membranes results in the detection of signals from hundreds of different phospholipid molecular species. In contrast, cholesterol is present in the plasma membrane as a single molecular species. During the MALDI desorption/ionization process, cholesterol undergoes dehydration, which results in detection of the $[M + H - H_2O]^+$ ion at *m/z* 369.3, instead of $[M + H]^+$ at *m/z* 387.3, $[H + NH_4]^+$ at *m/z* 404, or $[M + Na]^+$ at 409.3.[108]

A review of matrices used for the analysis of cellular phospholipids has been recently published by Kim et al.[319] Matrices such as 30 mg/mL DHA in 50:50 ethanol/water,[11] 5 mg/mL CHCA in 50:50 acetonitrile/0.1% TFAaq,[114] and 40 mg/mL DHB in 20 mM potassium acetate, 70:30 methanol/0.1% TFAaq[107] were used for imaging of lipids. The lipid spectra can be simplified by addition of potassium acetate[107] or LiCl[320] to the matrix solution, which results in the formation of exclusively potassium or lithium adducts of lipids, respectively. By changing the concentration of alkali metal salts in the matrix solution, it is also possible to selectively ionize either polar or nonpolar lipids. The presence of alkali metal salts in the matrix solution enhanced the detection of polar lipids, while a salt-free matrix solution was suitable for the detection of nonpolar lipids.[321]

The selection of the matrix must be tailored to the type of tissue examined and the class of lipids being analyzed. For MSI analysis of lipids in a lens, PNA (*p*-nitroaniline) at a concentration of 20 mg/mL resulted in improved sensitivity as compared to DHB.[263] The ionic liquid matrix offered excellent sensitivity for detection of gangliosides without significant loss of sialic acid residues.[269] The matrix application method should be carefully selected as well. The optimal matrix application should not cause any diffusion of lipids from their original position in the tissue section. Various matrix application methods have been examined for MSI of lipids. Among them are a spray-droplet method,[322] inkjet printing,[191] sublimation,[192] airbrush application,[241] and, most recently, an oscillating capillary nebulizer system[238] or a dry-coating technique.[175] Matrix application by direct sublimation of an organic matrix described by Hankin et al. provides multiple advantages.[108,192] Such a matrix deposition method prevents diffusion of the lipids, delivers extremely small matrix crystal sizes, and results in a substantial increase in sensitivity. Because no solvent is needed, this method provides enhanced purity of matrix applied to the sample and uniformity of deposition.[175,192] In terms of the tissue sample preparation method, the use of OCT is not recommended before lipid imaging due to a significant reduction in the quality of the mass spectra.[11]

Current, nonmass spectrometric approaches for phospholipid analysis include an extraction step and subsequent identification of the main phospholipid classes by either ^{31}P NMR (nuclear magnetic resonance) spectroscopy or chromatographic separation followed by mass spectrometric detection.[263] In comparison to these techniques, MSI offers a quick and easy method of lipid analysis. The summary of different analytical techniques used for the differentiation and quantification of phospholipids in biological samples was presented by Jones et al.[307] A review presenting MALDI-TOF MS as a technique suitable for all known lipid classes together with its advantages and disadvantages in comparison to other established lipid analysis methods was discussed by Schiller et al. in 2004.[313] A review presenting mass-spectrometry-based strategies for lipid analysis, including imaging, was published in 2007 by Isaac et al.[323]

Here, we will present some MSI applications for lipid analysis. Detection and imaging of lipid molecules was mostly studied using rodents brains. For example, whole normal rat brain sections were investigated by imaging technology to observe the distribution of three types of PCs such as PC(32:0), PC(34:1), and PC(36:1).[114] Age-dependent changes in the distribution and amount of PCs molecular species in a rat brain were also evaluated.[107] A number of other scientific questions, such as the distribution of gangliosides in different regions of mouse brain,[268] shown in Figure 22, the distribution of sulfatide in different layers of rat hippocampus,[82] the distribution of phosphatidylcholine and cerebroside species in rat brain sections,[221] and the cell-selective distribution of PUFA-containing glycerol phospholipids in a mouse brain section,[107] have been addressed. Atlases of lipid distributions in rat brain[209] and mouse brain[107] have been constructed. MSI was also successfully applied to rodent brain sections analyzed by intermediate-pressure MALDI on a linear ion trap (LIT) instrument[211] and by gold cluster focused ion beam TOF-SIMS.[47] Specific examples in the detection of phospholipids, sphingolipids, and glycerolipids were presented with images of mouse brain and kidney tissue slices.[108] In addition to this, some other samples, such as mouse heart and liver,[307] retina,[324] leg muscle,[54,234] and embryo,[277] have also been studied for the spatial and temporal distribution of phospholipid species. The localization of specific lipids and osmium oxide (OsO_4), a stain commonly used for unsaturated lipids in electron and optical microscopy of cells and tissues, was independently monitored in mouse adipose tissue by using TOF-SIMS with Bi cluster primary ions.[51] TOF-SIMS was also utilized to address the issue of localization of lipids and inorganic ions in healthy rat aorta and human atherosclerotic plaque.[58] Several frozen vessels bearing atherosclerotic lesion were analyzed by cluster TOF-SIMS to map lipid content at micrometric resolution.[59] Debois et al. performed the first *in situ* lipidomic analysis of human liver using TOF-SIMS imaging directly on tissue sections.[237]

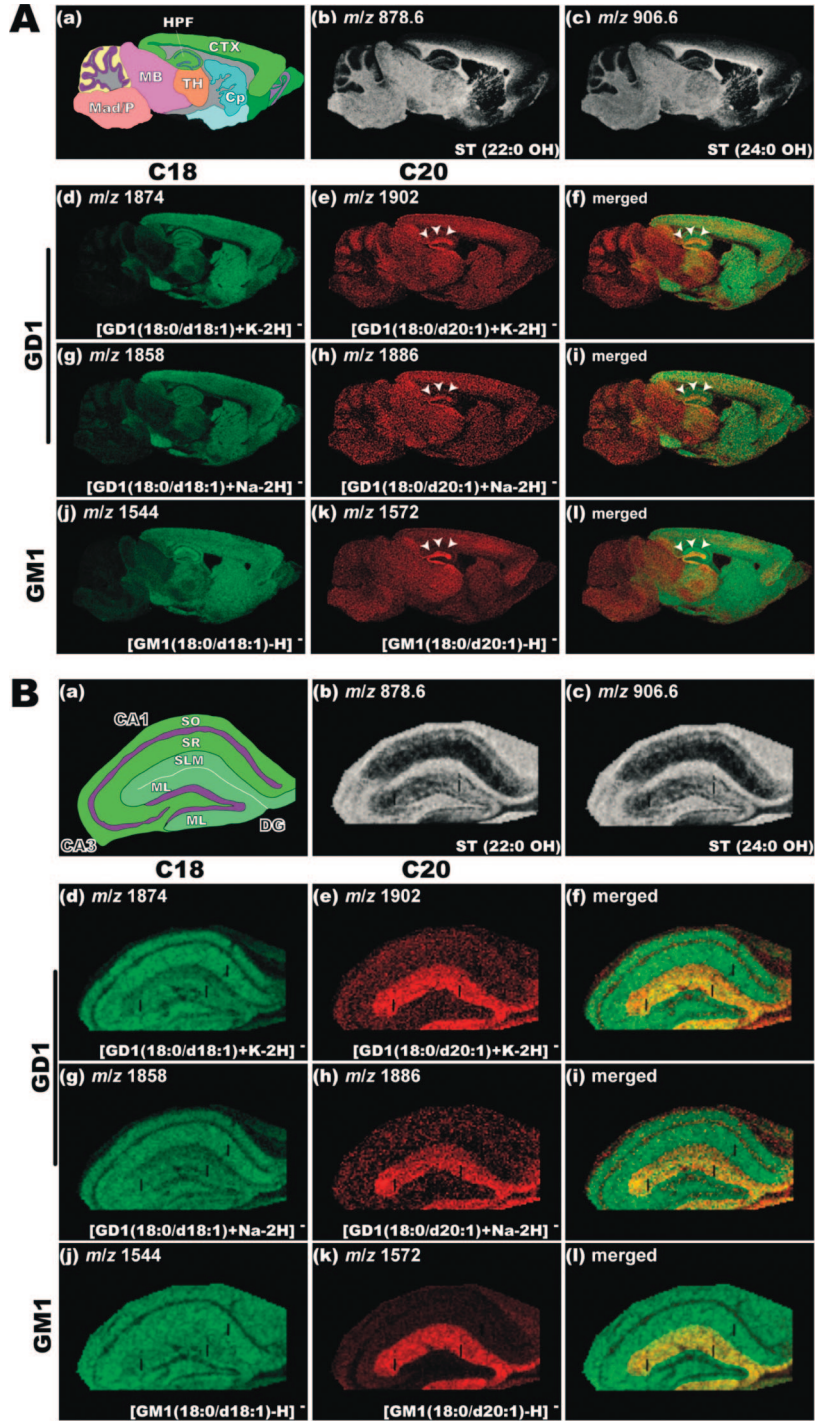

Figure 22. Imaging of the ganglioside distribution in different brain regions: (A) an overview of the ganglioside distribution in different brain regions; (B) the distribution pattern of gangliosides in the hippocampus. Reprinted with permission from ref 268. Copyright 2008 Sugiura et al.

In situ detection and structural analysis of phosphatidylcholine species in rat brain tissue was performed using a MALDI TOF/TOF mass spectrometer.[320] Initial profiling of lipids in tissue was conducted by MALDI-TOF and allowed for the assignment of phosphatidylcholine species. To confirm the structure, lithium adducts of phosphatidylcholine species were analyzed by MALDI-MS/MS and yielded fragments that allowed for the identification and positional assignment of acyl groups in phosphatidylcholine species.[320] The *in situ* analysis of two relevant phospholipid classes, phosphatidylcholines and sphingomyelins, in slices of fresh or fixed bovine lenses was also performed.[263] The methodologies for localization of phospholipids in flat-mounted eye segments from rhesus monkey using MSI have been recently described by Garrett and Dawson.[325] DESI-MS was also used to image a variety of tissue samples, including human liver adenocarcinoma, rat brain, human breast tissue, and canine abdominal tumor tissue.[314]

A new technical variation of NIMS has been recently presented by Patti et al. for analysis of carbohydrates and steroids, which can be challenging to detect with traditional mass spectrometric approaches.[326] The cation-enhanced NIMS was used to image the distribution of sucrose in a *Gerbera jamesonii* flower stem and the distribution of cholesterol in a mouse brain. The advantages of imaging using ion mobility prior to MS analysis were demonstrated

for profiling of human glioma and selective lipid imaging from rat brain.[225]

Lipids have been implicated in a number of human disease states, including cancer and cardiovascular disease. Different MSI ionization sources and mass analyzers offer a variety of possibilities for lipid analysis and practical tools to study lipidomics.

3.6. Application of MSI in Pharmacokinetic Studies

Pharmacokinetic studies are performed to examine the absorption, distribution, metabolism, and excretion of drugs in laboratory animals or humans. This procedure is mandatory for drug approval by the Food and Drug Administration (FDA). Pharmacokinetic studies employ many methods, such as whole-body autoradiography (WBA), tissue homogenization, and analysis by high performance liquid chromatography tandem mass spectrometry (HPLC MS/MS), and in the past decade also MSI.[98,327] WBA requires the compound of interest to be radioactively labeled. The compound is then administered to animals, which are sacrificed after different postdose time points. Whole-body sections of these animals are then exposed to a radioactivity detector or film, which allows visualizing the spatial radioactivity distribution. The WBA technique is used during early stage drug development, which provides many benefits, including parallel sample processing, standardized procedures, high sensitivity, and applicable quantification. However, this method has two major limitations, such as the expensive, time-consuming synthesis of radiolabeled drugs (labeled with e.g. ^{3}H, ^{14}C) and the incapability to distinguish between a parent drug and its metabolites.[98] While the first leads merely to more complexity and increased cost for each experiment, the last cannot be overcome by this technology and additional analysis of tissue homogenates by HPLC MS is required.[98] At present, WBA and MSI are two imaging techniques often used together to obtain the most reliable data for drug distribution in small animals.[327] MALDI imaging itself is an excellent tool for visualizing small molecules in tissue sections. Many biologically or pharmacologically relevant compounds are less than 1 kDa in size and can be easily detected by MS. These include both exogenous and endogenous molecules, such as pharmaceutical compounds and their metabolites, drugs of abuse, environmental toxins, and endogenous metabolites.[190] In pharmacokinetics, Troendle et al. were the first to demonstrate the use of MALDI-MSI by employing this technique to detect the anticancer drug paclitaxel in a human ovarian tumor and the antipsychotic drug spiperone in spiked sections of rat liver tissue.[328] The development of new MALDI-MS imaging methods adapted to animal whole-body sections allowed a specific and simultaneous detection of multiple analytes based on their molecular weights and fragmentation patterns.[98] This technique has potential to reveal data related to the drug's metabolism as well as obtain information on the organism's response to drug treatment.[103] On the other hand, MALDI low-molecular-weight imaging suffers from the interference of the ions derived from the matrix. This problem was overcome by applying tandem MS for imaging of drugs in tissue sections. For example, one study examined a distribution of a drug (SCH 226374) with a calculated protonated monoisotopic M_w that differed from the M_w of the SA matrix cluster ion by less than 0.2 amu.[329] In this case, collisionally activated dissociation (CAD) was employed to fragment the drug ion at *m*/*z* 695 into a dominant fragment ion at *m*/*z* 228. The SA cluster ion at *m*/*z* 695 fragmented into noninterfering ions at *m*/*z* 246 and *m*/*z* 471. Thus, MS/MS was used to indirectly localize the SCH 226374 compound in a mouse tumor sample. Another example of MALDI-MS/MS used to image drugs in tissue was performed on clozapine (*m*/*z* 327).[330] The MALDI-MS/MS image of the clozapine fragment ion (*m*/*z* 192) showed the most intense signal in the ventricle area, which was in agreement with autoradiography results. The role of the instrument as well as the method used for sample preparation is crucial with respect to the image quality obtained. MSI sample preparation procedures, including sample collection, the choice of matrix, extraction solvent, and matrix application method, must be optimized for each drug individually due to the wide variety of structures, solubilities, and physicochemical properties of drug compounds.[103] The matrix solution typically contains one or multiple matrices at different concentrations, organic solvent, water, and TFA. Standard matrix coating involves spraying saturated CHCA in 50:50 ACN/0.1% TFAaq with a pneumatic TLC sprayer.[98] Some other matrices, such as DHB (40 mg/mL) in 75:25 methanol/water[19] or CHCA (25 mg/mL) in 70:30 ethanol/0.1% TFAaq,[91] were also successfully used for imaging of different drug compounds. To improve the signal intensity in the low mass range, a thin (5 nm) layer of gold can also be sputter-deposited on top of the dried matrix layer.[27] In contrast to MALDI methods, DESI offers pharmacokinetic studies direct, high-throughput measurements of tissue sections at AP without any prior chemical treatment of the sample. This method was used to map the distribution of clozapine directly from rat brain, lung, kidney, and testis after an oral dose of 50 mg/kg.[76] Two reviews presenting various applications of MSI for drug imaging, biomarker discovery, and mapping were published in 2005 by Rohner et al.[165] and by Rubakhin.[331] Here, we present a short overview of the most recent applications of MSI in pharmacokinetic studies. MSI was used by different scientific groups all over the world to image the distribution of a number of pharmaceuticals, such as ketoconazole (an active ingredient in Nizoral),[332] the antipsychotic drugs clozapine[330] and olanzapine,[19,207] chlorisondamine and cocaine,[333] clioquinol as a potential drug for Alzheimer's disease,[232] the anticancer drugs banoxatrone,[334] vinblastine,[91] SCH 226374,[329] paclitaxel,[328] imatinib,[207] and oxaliplatin,[184] or the antiretroviral drugs saquinavir and nelfinavir.[193] The distribution of the anticancer drug SCH 226374 in mouse tumor tissue and rat brain was published by Reyzer et al. in 2003.[329] MALDI images were obtained by using the tandem mass spectrometric technique of selected reaction monitoring (SRM) to specifically monitor the drug under study. The SRM experiment is accomplished by specifying the parent mass of the compound for MS/MS fragmentation and then specifically monitoring for a single fragment ion. Such an approach minimized the potential for ions arising from either endogenous compounds or the interfering matrix ions. In another application of MALDI-MSI, the absorption of an antifungal agent, ketoconazole, into skin was examined by the use of an indirect tissue blotting approach.[332] This method can be used to study the absorption of a wide range of xenobiotics into skin. Additionally, some preliminary data from a combined solvent-assisted transfer/derivatization approach to sample preparation were also described. The distributions of chlorisondamine, a neuronal nicotinic ganglionic blocker, and cocaine into rat

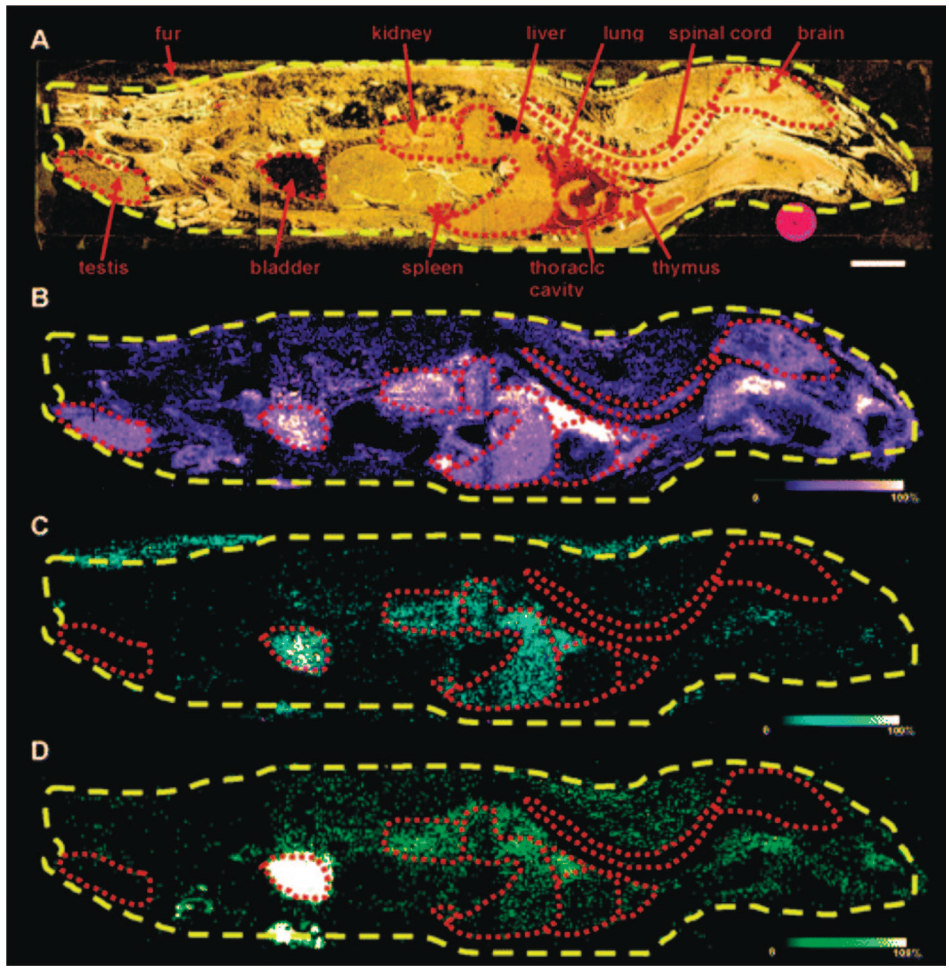

Figure 23. Detection of drug and metabolite distribution in a whole rat sagittal tissue section. (A) Optical image of a 2 h post OLZ (olanzapine) dosed rat tissue section across four gold MALDI target plates. (B) MS/MS ion image of OLZ (*m*/*z* 256). (C) MS/MS ion image of the *N*-desmethyl metabolite (*m*/*z* 256). (D) MS/MS ion image of the 2-hydroxymethyl metabolite (*m*/*z* 272). Bar, 1 cm. Reprinted with permission from ref 19. Copyright 2006 American Chemical Society.

brains were examined.[333] Both compounds were detected in the brains via MALDI-MS using CHCA and DHB as the matrices for chlorisondamine and cocaine, respectively. Tandem MS was employed to confirm the identity of the protonated ions.

The use of MALDI-MSI to study drug distribution in a whole-body mouse section was performed for the first time by Rohner et al. in 2005.[165] The first results showed a good correlation between WBA and MALDI-MSI data. This approach was extended by protein imaging to produce whole-body images, as illustrated by Figure 23, showing the location of drug, drug metabolites, and endogenous markers for various organs of the body.[19] In this study, olanzapine (brand name Zyprexa) was subjected to imaging. Zyprexa is generally used to treat mood disorders such as schizophrenia and acute mania in bipolar patients. MSI analysis of tissues from olanzapine dosed rats revealed the temporal distribution of the drug and metabolites, which was in agreement with previous quantitative WBA studies. MALDI-MS/MS analyses were performed on the whole-body sections to detect simultaneously olanzapine (*m*/*z* 313) and its fragment ion (*m*/*z* 256) and two first-pass metabolites, *N*-desmethylolanzapine (*m*/*z* 299) together with its fragment ion (*m*/*z* 256) and 2-hydroxymethylolanzapine (*m*/*z* 329) and its fragment ion (*m*/*z* 272). Both metabolites were detected in the liver and bladder, which was consistent with previous autoradiographic data and with the known metabolic pathways in rats. Detection of proteins from organs present in a whole-body sagittal tissue section showed the potential of MSI for the analysis of novel therapeutics with subsequent studies of therapeutic and toxicological processes at the molecular level. Some practical aspects of MALDI-MSI for drug and metabolite imaging in whole-body sections were described by Stoeckli et al. in 2007.[98] In another study, Atkinson et al.[334] applied MALDI-MSI to analyze the distribution of the bioreductive anticancer drug banoxatrone (AQ4N) in H460 lung tumor xenografts. In this study, imaging resulted in localization of the prodrug and its active form as well as ATP and the colocalization of the active reduced form of the drug in the hypoxic region of the tumor. In another MSI application, the anticancer drug vinblastine was imaged in rat whole-body sections by MALDI-MS.[91] Vinblastine is a chemical analogue of vincristine which was first isolated from the Madagascar periwinkle plant. The mechanism of action of these alkaloids is to arrest cell growth during the metaphase through binding to tubulin and inhibiting microtubule assembly.[335] The distribution of the vinblastine precursor ion *m*/*z* 811.4 together with several product ions, including *m*/*z* 793, 751, 733, 719, 691, 649, 524, and 355, was shown. IMS was employed to remove the interfering matrix ions.[91]

FTICR images of the antitumor drug imatinib (*m*/*z* 494.2664) and its des-methyl metabolite (*m*/*z* 480.2506) in mouse brain glioma were shown by Cornett et al. in 2008.[207]

The image showed almost none of the presumed imatinib ion distributed outside of the glioma, which indicated that this ion did not accumulate in normal brain. In another study, clioquinol (CQ) was administrated to a mouse model of Alzheimer's disease to study its potential therapeutic effect.[232] CQ is known to interfere with brain metal metabolism and ameliorate disease pathology through a mechanism that is not fully understood. The MSI results showed that CQ was mainly localized within the cortex and the hippocampus, which are brain areas primarily involved in cognitive functions. Recently, imaging of the HIV protease inhibitors saquinavir and nelfinavir in Mono Mac 6 cells by two types of mass spectrometry techniques, MALDI-TOF and MALDI-FTICR, was performed by Dekker et al. in 2009.[193] A sublimation/deposition device for homogeneous matrix deposition was constructed which allowed imaging of these HIV protease inhibitors at clinically relevant concentrations. MALDI-MSI has also been applied to assess the distribution of a novel potential therapeutic compound (β-peptide) in whole-body sections of mice.[106] β-Peptides display potent biological activity, such as somatostatin mimetics, and are resistant to the digestion by proteases and peptidases. Finally, a platinum anticancer drug, oxaliplatin, which is mainly used in the treatment of advanced colorectal cancer, was imaged by Bouslimani et al. in 2010.[184] In this study, the penetration of oxaliplatin in tissues from treated animals was investigated. Imaging experiments allowed the detection and localization of the drug and its metabolites, the monocysteine and monomethionine complexes, in kidney sections, where they localized exclusively in the cortex, suggesting that the drug did not penetrate deeply into the organ.

MALDI-MSI technology provides molecular images of resected organs or whole-body sections from small animals. It has attracted great interest of scientists interested in drug delivery and metabolism monitoring.[304] It provides *label free* tracking of both endogenous and exogenous compounds with spatial resolution and molecular specificity. In combination with WBA, this technology significantly improves the analysis of novel therapeutics. MSI is a powerful technique which provides deeper insight into therapeutic and toxicological processes such as metabolic changes or side effects often associated with drug administration.

3.7. MSI 3D Imaging

MSI provides two-dimensional distributions of multiple ions detected from biological samples. This technique has been recently extended to the third dimension. It provides 3D distributions of the selected molecules detected by MSI from biological samples. A stack of 2D MS images of a selected ion acquired from the same sample can be stitched together to reconstruct a 3D distribution map of that ion. This extension of a conventional MS imaging experiment provides more comprehensive information about the spatial distribution of selected molecules inside the whole sample. To perform MSI 3D reconstruction, the sample is cut into serial sections which are processed under identical conditions and imaged in MS. The acquired images are stitched together by software such as Image J[336] to obtain the 3D distribution of a particular ion.[156] Here, we present some practical aspects of 3D MSI, its applications and future perspectives of this youngest modification in the MSI family.

In terms of the sample, at the beginning of 3D MSI, the rodent brain was the most commonly chosen organ. This was due to its small size, well-defined internal/external

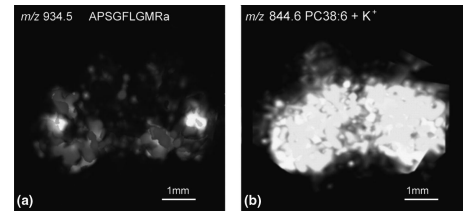

Figure 24. 3D reconstruction of images of (a) CabTRP 1a and (b) lipid PC(38:6) acquired from the brain of *C. borealis*. For the images shown in part a, tissue sections were prepared using the regular matrix coating method. In contrast, the images of part b were obtained from tissue sections prepared using a dry matrix spraying technique that favored detection of lipids. Reprinted with permission from ref 156. Copyright 2009 Elsevier.

structure, and an anatomical atlas which was used as reference for the methodology development. So far, 3D reconstructions have been performed for myelin basic protein (MBP) in the corpus callosum of a mouse brain,[131] Substance P and PEP-19 in the rat ventral midbrain,[162] neuropeptide (CabTRP 1a) and lipid PC(38:6) in the brain of the crab *Cancer borealis*,[156] and lipids in a mouse brain.[337] Figure 24 shows an example of the 3D distribution of a lipid and a peptide in a crab brain. A 3D construction of the distribution of lipids throughout the mouse brain has been recently presented by Eberlin et al.[337] These results represent the first 3D molecular reconstruction of mouse brain imaged by DESI-MS. Imaging of two lipids, PS (18:0/22:6) and ST (sulfatide) (24:1), allowed a full visualization of the gray-matter region as well as the white-matter region in the total volume of the brain. This allowed a complete view of substructures, such as the corpus callosum and anterior commissure, throughout the brain volume. Cross-sectional views of the 3D models can be used to investigate distributions of many additional molecules detected by MSI. The coregistration of MSI proteomic data from the whole mouse head with *in vivo* magnetic resonance imaging (MRI) data was reported by Sinha et al. in 2008.[338] A detailed procedure describing how to make 3D volume reconstructions of MALDI-MSI data was published by Andersson et al.[162]

On a subcellular scale, 3D MSI images of the mitotic spindle from T98G human glioblastoma tumor cells were acquired by TOF-SIMS.[36] This study demonstrated that 3D SIMS imaging was essential for the analysis of mitotic cells, where specialized regions such as the mitotic spindle were hidden beneath the cell surface. Another study applied TOF-SIMS to visualize the 3D distribution of phosphocholine and inorganic ions in single cells.[61]

Unlike *in vivo* tomographic imaging techniques, 3D MALDI-MS images require the specimen to be sliced into thin serial sections. Sectioning can lead to tissue tearing and deformation. Therefore, correlating consecutive 2D images to obtain a 3D reconstruction must be performed carefully. To properly reconstruct a 3D volume from 2D MSI data, the images must be coregistered. The coregistration can involve inter- and/or intrasection registration. The intersection registration provides alignment of optical images of the tissue sections, while the intrasection registration aligns the MALDI-MSI data to the corresponding optical image. Another coregistration technique involves the use of fiducial markers. The imaging of the sample includes the region containing the markers used as orientation and alignment points during the 3D reconstruction process.

One of the advantages of 3D MSI is the possibility to correlate distributions of the multiple biomolecular ions with

physiological and structural information observed by *in vivo* imaging techniques, such as CT, PET, and magnetic resonance spectrometric imaging (MRSI). These *in vivo* imaging techniques are limited to a few molecules and cannot show protein distributions. Of the current techniques, MSI can image the widest range of molecules.

4. Future Perspectives

MSI is becoming an established tool for imaging of the most complex biological samples. Its key applications are foreseen in a biomedical environment, more specifically in molecular histology. This *ex vivo* imaging technique provides a lot of information about the biomolecular composition of the tissue, without the need for labels, complicated sample preparation protocols, or staining procedures. No *a priori* knowledge about the sample is necessary, but for correct interpretation of results some MS knowledge is required. The instrumentation used for imaging has reached a degree of maturation, with ionization sources performing at high resolution and mass analyzers of broad mass range and high sensitivity. MSI is rapidly developing into an imaging tool used by pathologists, biologists, and biochemist. In the future it has the potential to become a routine tool for imaging of tissues dissected during surgerical operations or stored in tissue banks. MSI can help us to understand the link between the localization of certain molecules and their function during pathogenesis, disease progression, or treatment. It can accelerate our efforts to provide more effective therapeutics for a broad range of diseases, such as cancer, neurodegenerative diseases, or age-related problems.

Having said this, there are still areas of development needed. To make MSI a routine tool, the method needs to be validated on large patient or sample cohorts. This requires a higher degree of automation than currently available. Automation and robotics developments will improve the throughput of the MSI technologies, allowing a researcher to analyze more samples. The capability of high-throughput imaging also will drive the developments in sample preparation. The sample preparation protocols need to keep up with the speed of the new instruments. This requires automated sectioning, mounting, washing, and surface preparation. These tools are not available today.

High-throughput perspectives drastically increase the amount of data generated in MSI experiments. It will soon become difficult to keep all the raw data from a MSI validation study at high spatial resolution. On-the-fly data reduction and feature extraction protocols have to be developed that address this issue. In addition, multimodal imaging approaches will assist in the validation and acceptance of MSI technology in molecular biology. The increased throughput will also induce a larger demand for 3D MSI. The capabilities exisit already, but only a few good examples exist due to the lack of proper processing infrastructure. These prospective improvements in MSI technology put further strain on the data storage and processing resources. As a result, they pose new challenges for the bioinformaticians working in this field.

New desorption and ionization techniques in the ambient environment offer new application possibilities. They will migrate the MSI field from *ex vivo* analysis to *in vivo* analysis of living systems, such as bacterial colonies and living cells in aqueous environments. Given its current status and all of these high-end developments that lay ahead, MSI is strongly positioned to be an important molecular imaging tool for life sciences in the immediate future and many years to come.

5. Abbreviations

ADP	adenosine diphosphate
AMOLF	FOM—Institute for Atomic and Molecular Physics
AMP	adenosine monophosphate
AP	atmospheric pressure
APCI	atmospheric pressure chemical ionization
AQP0	Aquaporin-0
ATP	adenosine triphosphate
AuNPs	gold nanoparticles
BRPs	bradykinin related peptides
CAD	collisionally activated dissociation
CHCA	α-cyano-4-hydroxycinnamic acid
CID	collision induced dissociation
CMC	carboxymethylcellulose
CNTs	carbon nanotubes
CT	computed tomography
DAG	diacylglycerol
DART	direct analysis in real time
DESI	desorption electrospray ionization
DHA	2,6-dihydroxyacetophenone
DHB	2,5-dihydroxybenzoic acid
DI	desorption ionization
DIOS	desorption−ionization on silicon
2D-PAGE	2-dimensional polyacrylamide gel electrophoresis
EPPE	ethanol-preserved and paraffin-embedded
ESI	electrospray ionization
EVA	ethylene vinyl acetate
F-1,6-biP	fructose-1,6-bisphosphate
FAIMS	high-field asymmetric waveform ion mobility spectrometry
FDA	Food and Drug Administration
FFPE	formaldehyde-fixed and paraffin-embedded
FTICR	Fourier transform ion cyclotron resonance
FTMS	Fourier transform mass spectrometer
fwhm	full width at half-maximum
GALDI	graphite-assisted laser desorption/ionization
GlcNAc	*N*-acetyl-D-glucosamine
GPChos	glycerophosphocholines
GPLs	glycerophospholipids
GTP	guanosine triphosphate
H&E	hematoxylin and eosin
HPLC	MS/MS high performance liquid chromatography tandem mass spectrometry
HUPO-PSI	Human Proteome Organization-Proteomics Standards Initiative
HV	high vacuum
ICA	in-cell ion accumulation
ICR	ion cyclotron resonance
IMS	ion mobility separation
IR-MALDI	infrared MALDI
ITO	indium tin oxide
IZ	interface zones
kDa	kilo-Dalton
LAESI	laser ablation electrospray ionization
LA-ICP-MS	laser ablation inductively coupled plasma MS
LC	liquid chromatography
LCM	laser capture microdissection
LDI	laser desorption ionization
LIT	linear ion trap
LMIG	liquid metal ion guns
LPI	lisophosphatidylinositol
LTP	lipid transfer protein
LTQ	linear trap quadrupole

m/*z*	mass over charge ratio
MALDESI	matrix assisted laser desorption electrospray ionization
MALDI	matrix-assisted laser desorption/ionization
MBP	myelin basic protein
ME-SALDI	matrix-enhanced surface-assisted laser desorption/ionization
ME-SIMS	matrix enhanced SIMS
MetA-SIMS	metal assisted SIMS
MMA	mass measurement accuracy
MRI	magnetic resonance imaging
MRM	multple reaction monitoring
MRSI	magnetic resonance spectrometric imaging
MS	mass spectrometry
MSI	mass spectrometric imaging
M_w	molecular weight
NAFLD	nonalcoholic fatty liver disease
nano-PALDI	nanoparticle-assisted laser desorption/ionization
Nd:YAG	neodymium-doped yttrium aluminum garnet
NIMS	nanostructure−initiator mass spectrometry
NIRF	near-infrared fluorescence
NMR	nuclear magnetic resonance
oa-TOF	orthogonal acceleration
OBP-9	odorant binding protein 9
OCT	optimal cutting temperature polymer
OLZ	olanzapine
PA	phosphatidic acid
PC	phosphocholine
PCA	principal component analysis
PE	phosphatidylethanolamine
PEG	polyethylene glycol
PET	positron emission tomography
PG	phosphatidylglycerol
PI	phosphatidylinositol
pL	picoliter
PLAs	phospholipases A
PlsEtn	plasmenylethanolamine
PMI	post-mortem interval
PS	phosphatidylserine
PTMs	post-translational modifications
PVDF	polyvinylidene fluoride transfer membrane
Q	quadrupole
rf	radio frequency
ROIs	regions of interest
RT	room temperature
SA	sinapinic acid
SALDI	surface-assisted laser desorption/ionization
SELDI	surface-enhanced laser desorption
SIMS	secondary ion mass spectrometry
SMs	sphingomyelins
SRM	selected reaction monitoring
TAG	triacylglycerols
TFA	trifluoroacetic acid
TLC	thin-layer chromatography
TOF	time-of-flight
UDP	uridine diphosphate
UHV	ultrahigh vacuum
WBAvwhole-body	autoradiography

6. Acknowledgments

This work was supported by "Stichting voor Fundamenteel Onderzoek der Materie (FOM)", which is financially supported by the "Nederlandse organisatie voor Wetenschappelijk Onderzoek (NWO)". We also gratefully acknowledge financial support from NIH Grant R01 CA134695. The authors are indebted to Donald Smith for providing the unpublished FT-ICR data and Iliya Cerjak for graphical design of the cover art.

7. References

(1) Siuzdak, G. *The Expanding Role of Mass Spectrometry in Biotechnology*; MCC Press: San Diego, CA, 2006; p 11.
(2) Fenn, J. B.; Mann, M.; Meng, C. K.; Wong, S. F.; Whitehouse, C. M. *Science* **1989**, *246*, 64.
(3) Karas, M.; Bachmann, D.; Hillenkamp, F. *Anal. Chem.* **1985**, *57*, 2935.
(4) Leinweber, B. D.; Tsaprailis, G.; Monks, T. J.; Lau, S. S. *J. Am. Soc. Mass Spectrom.* **2009**, *20*, 89.
(5) Caprioli, R. M.; Farmer, T. B.; Gile, J. *Anal. Chem.* **1997**, *69*, 4751.
(6) Stoeckli, M.; Chaurand, P.; Hallahan, D. E.; Caprioli, R. M. *Nat. Med.* **2001**, *7*, 493.
(7) Colliver, T. L.; Brummel, C. L.; Pacholski, M. L.; Swanek, F. D.; Ewing, A. G.; Winograd, N. *Anal. Chem.* **1997**, *69*, 2225.
(8) Clerc, J.; Fourre, C.; Fragu, P. *Cell Biol. Int.* **1997**, *21*, 619.
(9) Heeren, R. M. A.; McDonnell, L. A.; Amstalden, E.; Luxembourg, S. L.; Altelaar, A. F. M.; Piersma, S. R. *Appl. Surf. Sci.* **2006**, *252*, 6827.
(10) Takats, Z.; Wiseman, J. M.; Gologan, B.; Cooks, R. G. *Science* **2004**, *306*, 471.
(11) Woods, A. S.; Jackson, S. N. *AAPS J.* **2006**, *8*, 391.
(12) Tanaka, K.; Ido, Y.; Akita, S.; Yoshida, Y.; Yoshida, T. *Proc. Japan-China Joint Symp. Mass Spectrom., 2nd* **1987**, 185.
(13) Karas, M.; Hillenkamp, F. *Anal. Chem.* **1988**, *60*, 2299.
(14) McDonnell, L. A.; Heeren, R. M. *Mass Spectrom. Rev.* **2007**, *26*, 606.
(15) Todd, P. J.; Schaaff, T. G.; Chaurand, P.; Caprioli, R. M. *J. Mass Spectrom.* **2001**, *36*, 355.
(16) Spengler, B.; Hubert, M. *J. Am. Soc. Mass Spectrom.* **2002**, *13*, 735.
(17) Chaurand, P.; Schriver, K. E.; Caprioli, R. M. *J. Mass Spectrom.* **2007**, *42*, 476.
(18) Holle, A.; Haase, A.; Kayser, M.; Hohndorf, J. *J. Mass Spectrom.* **2006**, *41*, 705.
(19) Khatib-Shahidi, S.; Andersson, M.; Herman, J. L.; Gillespie, T. A.; Caprioli, R. M. *Anal. Chem.* **2006**, *78*, 6448.
(20) Slaveykova, V. I.; Guignard, C.; Eybe, T.; Migeon, H. N.; Hoffmann, L. *Anal. Bioanal. Chem.* **2009**, *393*, 583.
(21) Pacholski, M. L.; Winograd, N. *Chem. Rev.* **1999**, *99*, 2977.
(22) Kaletas, B. K.; van der Wiel, I. M.; Stauber, J.; Guzel, C.; Kros, J. M.; Luider, T. M.; Heeren, R. M. *Proteomics* **2009**, *9*, 2622.
(23) Weibel, D.; Wong, S.; Lockyer, N.; Blenkinsopp, P.; Hill, R.; Vickerman, J. C. *Anal. Chem.* **2003**, *75*, 1754.
(24) Klerk, L. A.; Lockyer, N. P.; Kharchenko, A.; MacAleese, L. P.; Dankers, P. Y. W.; Vickerman, J. C.; Heeren, R. M. A. *Anal. Chem.* **2010**, *82*, 801.
(25) Altelaar, A. F.; Luxembourg, S. L.; McDonnell, L. A.; Piersma, S. R.; Heeren, R. M. *Nat. Protoc.* **2007**, *2*, 1185. Altelaar, A. F.; van Minnen, J.; Jimenez, C. R.; Heeren, R. M.; Piersma, S. R. *Anal. Chem.* **2005**, *77*, 735.
(26) McDonnell, L. A.; Piersma, S. R.; MaartenAltelaar, A. F.; Mize, T. H.; Luxembourg, S. L.; Verhaert, P. D.; van Minnen, J.; Heeren, R. M. *J. Mass Spectrom.* **2005**, *40*, 160.
(27) Altelaar, A. F.; Klinkert, I.; Jalink, K.; de Lange, R. P.; Adan, R. A.; Heeren, R. M.; Piersma, S. R. *Anal. Chem.* **2006**, *78*, 734.
(28) Delcorte, A.; Bour, J.; Aubriet, F.; Muller, J.-F.; Bertrand, P. *Anal. Chem.* **2003**, *75*, 6875.
(29) Wu, K. J.; Odom, R. W. *Anal. Chem.* **1996**, *68*, 873.
(30) Francese, S.; Dani, F. R.; Traldi, P.; Mastrobuoni, G.; Pieraccini, G.; Moneti, G. *Comb. Chem. High Throughput Screening* **2009**, *12*, 156.
(31) Nakata, Y.; Honda, Y.; Ninomiya, S.; Seki, T.; Aoki, T.; Matsuo, J. *J. Mass Spectrom.* **2009**, *44*, 128.
(32) Nygren, H.; Malmberg, P. *Trends Biotechnol.* **2007**, *25*, 499.
(33) Pumphrey, G. M.; Hanson, B. T.; Chandra, S.; Madsen, E. L. *Environ. Microbiol.* **2009**, *11*, 220.
(34) Finzi-Hart, J. A.; Pett-Ridge, J.; Weber, P. K.; Popa, R.; Fallon, S. J.; Gunderson, T.; Hutcheon, I. D.; Nealson, K. H.; Capone, D. G. *Proc. Natl. Acad. Sci. U. S. A.* **2009**, *106*, 6345.
(35) Ostrowski, S. G.; Kurczy, M. E.; Roddy, T. P.; Winograd, N.; Ewing, A. G. *Anal. Chem.* **2007**, *79*, 3554.
(36) Chandra, S. *Appl. Surf. Sci.* **2004**, *231*−*232*, 467.
(37) Kabalka, G. W.; Yao, M. L.; Marepally, S. R.; Chandra, S. *Appl. Radiat. Isot.* **2009**, *67*, S374.
(38) Chandra, S.; Morrison, G. H. *Int. J. Mass Spectrom.* **1995**, *143*, 161.
(39) Pacholski, M. L.; Cannon, D. M., Jr.; Ewing, A. G.; Winograd, N. *Rapid Commun. Mass Spectrom.* **1998**, *12*, 1232.
(40) Strick, R.; Strissel, P. L.; Gavrilov, K.; Levi-Setti, R. *J. Cell Biol.* **2001**, *155*, 899.
(41) Wu, L.; Lu, X.; Kulp, K. S.; Knize, M. G.; Berman, E. S.; Nelson, E. J.; Felton, J. S.; Wu, K. J. *Int. J. Mass Spectrom.* **2007**, *260*, 137.
(42) Nygren, H.; Borner, K.; Malmberg, P.; Tallarek, E.; Hagenhoff, B. *Microsc. Res. Technol.* **2005**, *68*, 329.

(43) Nygren, H.; Malmberg, P.; Kriegeskotte, C.; Arlinghaus, H. F. *FEBS Lett.* **2004**, *566*, 291.
(44) Nygren, H.; Johansson, B. R.; Malmberg, P. *Microsc. Res. Technol.* **2004**, *65*, 282.
(45) Jones, E. A.; Lockyera, N. P.; Vickerman, J. C. *Int. J. Mass Spectrom.* **2007**, *260*, 146.
(46) McCandlish, C. A.; McMahon, J. M.; Todd, P. J. *J. Am. Soc. Mass Spectrom.* **2000**, *11*, 191.
(47) Touboul, D.; Halgand, F.; Brunelle, A.; Kersting, R.; Tallarek, E.; Hagenhoff, B.; Laprevote, O. *Anal. Chem.* **2004**, *76*, 1550.
(48) Sjovall, P.; Lausmaa, J.; Johansson, B. *Anal. Chem.* **2004**, *76*, 4271.
(49) Todd, P. J.; McMahon, J. M.; McCandlish, C. A., Jr. *J. Am. Soc. Mass Spectrom.* **2004**, *15*, 1116.
(50) Malmberg, P.; Nygren, H.; Richter, K.; Chen, Y.; Dangardt, F.; Friberg, P.; Magnusson, Y. *Microsc. Res. Technol.* **2007**, *70*, 828.
(51) Belazi, D.; Sole-Domenech, S.; Johansson, B.; Schalling, M.; Sjovall, P. *Histochem. Cell Biol.* **2009**, *132*, 105.
(52) Perkins, M. C.; Bell, G.; Briggs, D.; Davies, M. C.; Friedman, A.; Hart, C. A.; Roberts, C. J.; Rutten, F. J. *Colloids Surf., B* **2008**, *67*, 1.
(53) Ameen, A. P.; Short, R. D.; Johns, R.; Schwach, G. *Clin. Oral Implants Res.* **1993**, *4*, 144.
(54) Touboul, D.; Brunelle, A.; Halgand, F.; De La Porte, S.; Laprevote, O. *J. Lipid Res.* **2005**, *46*, 1388.
(55) Tahallah, N.; Brunelle, A.; De La Porte, S.; Laprevote, O. *J. Lipid Res.* **2008**, *49*, 438.
(56) Kishikawa, Y.; Gong, H.; Kitaoka, T.; Amemiya, T.; Takaya, K.; Tozu, M.; Hoshi, T.; Ohashi, Y. *J. Electron Microsc.* **2003**, *52*, 349.
(57) Gong, H.; Takami, Y.; Amemiya, T.; Tozu, M.; Ohashi, Y. *Ophthalmic Res.* **2004**, *36*, 129.
(58) Malmberg, P.; Borner, K.; Chen, Y.; Friberg, P.; Hagenhoff, B.; Mansson, J. E.; Nygren, H. *Biochim. Biophys. Acta* **2007**, *1771*, 185.
(59) Mas, S.; Touboul, D.; Brunelle, A.; Aragoncillo, P.; Egido, J.; Laprevote, O.; Vivanco, F. *Analyst* **2007**, *132*, 24.
(60) Kulp, K. S.; Berman, E. S.; Knize, M. G.; Shattuck, D. L.; Nelson, E. J.; Wu, L.; Montgomery, J. L.; Felton, J. S.; Wu, K. *J. Anal. Chem.* **2006**, *78*, 3651.
(61) Nygren, H.; Hagenhoff, B.; Malmberg, P.; Nilsson, M.; Richter, K. *Microsc. Res. Technol.* **2007**, *70*, 969.
(62) Fletcher, J. S.; Lockyer, N. P.; Vaidyanathan, S.; Vickerman, J. C. *Anal. Chem.* **2007**, *79*, 2199.
(63) Smith, D. R.; Chandra, S.; Barth, R. F.; Yang, W.; Joel, D. D.; Coderre, J. A. *Cancer Res.* **2001**, *61*, 8179.
(64) Chandra, S.; Kabalka, G. W.; Lorey, D. R., 2nd; Smith, D. R.; Coderre, J. A. *Clin. Cancer Res.* **2002**, *8*, 2675.
(65) Monroe, E. B.; Jurchen, J. C.; Lee, J.; Rubakhin, S. S.; Sweedler, J. V. *J. Am. Chem. Soc.* **2005**, *127*, 12152.
(66) Kempson, I. M.; Skinner, W. M.; Kirkbride, P. K.; Nelson, A. J.; Martin, R. R. *Eur. J. Mass Spectrom.* **2003**, *9*, 589.
(67) Mazel, V.; Richardin, P.; Debois, D.; Touboul, D.; Cotte, M.; Brunelle, A.; Walter, P.; Laprevote, O. *Anal. Chem.* **2007**, *79*, 9253.
(68) Brunelle, A.; Laprevote, O. *Anal. Bioanal. Chem.* **2009**, *393*, 31.
(69) Ifa, D. R.; Wiseman, J. M.; Song, Q.; Cooks, R. G. *Int. J. Mass Spectrom.* **2007**, *259*, 8.
(70) Dole, M.; Mack, L. L.; Hines, R. L.; Mobley, R. C.; Ferguson, L. D.; Alice, M. B. *J. Chem. Phys.* **1968**, *49*, 2240.
(71) Iribarne, J. V.; Thomson, B. A. *J. Chem. Phys.* **1976**, *64*, 2287.
(72) Dill, A. L.; Ifa, D. R.; Manicke, N. E.; Ouyang, Z.; Cooks, R. G. *J. Chromatogr., B: Anal. Technol. Biomed. Life Sci.* **2009**, *877*, 2883.
(73) Wiseman, J. M.; Puolitaival, S. M.; Takats, Z.; Cooks, R. G.; Caprioli, R. M. *Angew. Chem., Int. Ed. Engl.* **2005**, *44*, 7094.
(74) Talaty, N.; Takats, Z.; Cooks, R. G. *Analyst* **2005**, *130*, 1624.
(75) Kertesz, V.; Van Berkel, G. J. *Rapid Commun. Mass Spectrom.* **2008**, *22*, 2639.
(76) Wiseman, J. M.; Ifa, D. R.; Zhu, Y.; Kissinger, C. B.; Manicke, N. E.; Kissinger, P. T.; Cooks, R. G. *Proc. Natl. Acad. Sci. U. S. A.* **2008**, *105*, 18120.
(77) Esquenazi, E.; Dorrestein, P. C.; Gerwick, W. H. *Proc. Natl. Acad. Sci. U. S. A.* **2009**, *106*, 7269.
(78) Lane, A. L.; Nyadong, L.; Galhena, A. S.; Shearer, T. L.; Stout, E. P.; Parry, R. M.; Kwasnik, M.; Wang, M. D.; Hay, M. E.; Fernandez, F. M.; Kubanek, J. *Proc. Natl. Acad. Sci. U. S. A.* **2009**, *106*, 7314.
(79) Myung, S.; Wiseman, J. M.; Valentine, S. J.; Takats, Z.; Cooks, R. G.; Clemmer, D. E. *J. Phys. Chem. B* **2006**, *110*, 5045.
(80) Berry, J. I.; Sun, S.; Dou, Y.; Wucher, A.; Winograd, N. *Anal. Chem.* **2003**, *75*, 5146.
(81) Bouamrani, A.; Ternier, J.; Ratel, D.; Benabid, A. L.; Issartel, J. P.; Brambilla, E.; Berger, F. *Clin. Chem.* **2006**, *52*, 2103.
(82) Ageta, H.; Asai, S.; Sugiura, Y.; Goto-Inoue, N.; Zaima, N.; Setou, M. *Med. Mol. Morphol.* **2009**, *42*, 16.
(83) Liu, Q.; Xiao, Y.; Pagan-Miranda, C.; Chiu, Y. M.; He, L. *J. Am. Soc. Mass Spectrom.* **2009**, *20*, 80.
(84) Yanes, O.; Woo, H. K.; Northen, T. R.; Oppenheimer, S. R.; Shriver, L.; Apon, J.; Estrada, M. N.; Potchoiba, M. J.; Steenwyk, R.; Manchester, M.; Siuzdak, G. *Anal. Chem.* **2009**, *81*, 2969.
(85) Becker, J. S.; Zoriy, M.; Matusch, A.; Wu, B.; Salber, D.; Palm, C.; Becker, J. S. *Mass Spectrom. Rev.* **2009**, *29*, 156.
(86) Sampson, J. S.; Hawkridge, A. M.; Muddiman, D. C. *J. Am. Soc. Mass Spectrom.* **2006**, *17*, 1712.
(87) Nemes, P.; Woods, A. S.; Vertes, A. *Anal. Chem.* **2010**, *82*, 982. Nemes, P.; Vertes, A. *Anal. Chem.* **2007**, *79*, 8098.
(88) Li, Y.; Shrestha, B.; Vertes, A. *Anal. Chem.* **2008**, *80*, 407. Li, Y.; Shrestha, B.; Vertes, A. *Anal. Chem.* **2007**, *79*, 523.
(89) Goodwin, R. J.; Pennington, S. R.; Pitt, A. R. *Proteomics* **2008**, *8*, 3785.
(90) Taban, I. M.; Altelaar, A. F.; van der Burgt, Y. E.; McDonnell, L. A.; Heeren, R. M.; Fuchser, J.; Baykut, G. *J. Am. Soc. Mass Spectrom.* **2007**, *18*, 145.
(91) Trim, P. J.; Henson, C. M.; Avery, J. L.; McEwen, A.; Snel, M. F.; Claude, E.; Marshall, P. S.; West, A.; Princivalle, A. P.; Clench, M. R. *Anal. Chem.* **2008**, *80*, 8628.
(92) Northen, T. R.; Yanes, O.; Northen, M. T.; Marrinucci, D.; Uritboonthai, W.; Apon, J.; Golledge, S. L.; Nordstrom, A.; Siuzdak, G. *Nature* **2007**, *449*, 1033.
(93) Sanchez, J. C.; Corthals, G. L.; Hochstrasser, D. F. *Biomedical Applications of Proteomics*; Wiley-VCH Verlag Gmbh Weinheim: 2004; p 373.
(94) Aerni, H. R.; Cornett, D. S.; Caprioli, R. M. *Anal. Chem.* **2006**, *78*, 827.
(95) Schwartz, S. A.; Reyzer, M. L.; Caprioli, R. M. *J. Mass Spectrom.* **2003**, *38*, 699.
(96) Kim, J. S.; Kim, J. Y.; Kim, H. *J. Anal. Chem.* **2005**, *77*, 7483.
(97) Mas, S.; Perez, R.; Martinez-Pinna, R.; Egido, J.; Vivanco, F. *Proteomics* **2008**, *8*, 3735.
(98) Stoeckli, M.; Staab, D.; Schweitzer, A. *Int. J. Mass Spectrom.* **2007**, *260*, 195.
(99) MacAleese, L.; Stauber, J.; Heeren, R. M. *Proteomics* **2009**, *9*, 819.
(100) Chaurand, P.; Norris, J. L.; Cornett, D. S.; Mobley, J. A.; Caprioli, R. M. *J. Proteome Res.* **2006**, *5*, 2889.
(101) Ayorinde, F. O.; Hambright, P.; Porter, T. N.; Keith, Q. L., Jr. *Rapid Commun. Mass Spectrom.* **1999**, *13*, 2474.
(102) Wisztorski, M.; Croix, D.; Macagno, E.; Fournier, I.; Salzet, M. *Dev. Neurobiol.* **2008**, *68*, 845.
(103) Reyzer, M. L.; Caprioli, R. M. *Curr. Opin. Chem. Biol.* **2007**, *11*, 29.
(104) Rubakhin, S. S.; Greenough, W. T.; Sweedler, J. V. *Anal. Chem.* **2003**, *75*, 5374.
(105) Hopfgartner, G.; Varesio, E.; Stoeckli, M. *Rapid Commun. Mass Spectrom.* **2009**, *23*, 733.
(106) Stoeckli, M.; Staab, D.; Schweitzer, A.; Gardiner, J.; Seebach, D. *J. Am. Soc. Mass Spectrom.* **2007**, *18*, 1921.
(107) Sugiura, Y.; Konishi, Y.; Zaima, N.; Kajihara, S.; Nakanishi, H.; Taguchi, R.; Setou, M. *J. Lipid Res.* **2009**, *50*, 1776.
(108) Murphy, R. C.; Hankin, J. A.; Barkley, R. M. *J. Lipid Res.*, in press.
(109) Monroe, E. B.; Annangudi, S. P.; Hatcher, N. G.; Gutstein, H. B.; Rubakhin, S. S.; Sweedler, J. V. *Proteomics* **2008**, *8*, 3746.
(110) Skold, K.; Svensson, M.; Nilsson, A.; Zhang, X.; Nydahl, K.; Caprioli, R. M.; Svenningsson, P.; Andren, P. E. *J. Proteome Res.* **2006**, *5*, 262.
(111) Minerva, L.; Clerens, S.; Baggerman, G.; Arckens, L. *Proteomics* **2008**, *8*, 3763.
(112) Schwamborn, K.; Krieg, R. C.; Reska, M.; Jakse, G.; Knuechel, R.; Wellmann, A. *Int. J. Mol. Med.* **2007**, *20*, 155.
(113) Burnum, K. E.; Tranguch, S.; Mi, D.; Daikoku, T.; Dey, S. K.; Caprioli, R. M. *Endocrinology* **2008**, *149*, 3274.
(114) Mikawa, S.; Suzuki, M.; Fujimoto, C.; Sato, K. *Neurosci. Lett.* **2009**, *451*, 45.
(115) Fletcher, J. S. *Analyst* **2009**, *134*, 2204.
(116) Debois, D.; Hamze, K.; Guerineau, V.; Le Caer, J. P.; Holland, I. B.; Lopes, P.; Ouazzani, J.; Seror, S. J.; Brunelle, A.; Laprevote, O. *Proteomics* **2008**, *8*, 3682.
(117) Yang, Y. L.; Xu, Y.; Straight, P.; Dorrestein, P. C. *Nat. Chem. Biol.* **2009**, *5*, 885.
(118) Esquenazi, E.; Coates, C.; Simmons, L.; Gonzalez, D.; Gerwick, W. H.; Dorrestein, P. C. *Mol. BioSyst.* **2008**, *4*, 562.
(119) Cha, S.; Zhang, H.; Ilarslan, H. I.; Wurtele, E. S.; Brachova, L.; Nikolau, B. J.; Yeung, E. S. *Plant J.* **2008**, *55*, 348.
(120) Chaurand, P.; Fouchecourt, S.; DaGue, B. B.; Xu, B. J.; Reyzer, M. L.; Orgebin-Crist, M. C.; Caprioli, R. M. *Proteomics* **2003**, *3*, 2221.
(121) Chaurand, P.; Rahman, M. A.; Hunt, T.; Mobley, J. A.; Gu, G.; Latham, J. C.; Caprioli, R. M.; Kasper, S. *Mol. Cell. Proteomics* **2008**, *7*, 411.

(122) Yanagisawa, K.; Shyr, Y.; Xu, B. J.; Massion, P. P.; Larsen, P. H.; White, B. C.; Roberts, J. R.; Edgerton, M.; Gonzalez, A.; Nadaf, S.; Moore, J. H.; Caprioli, R. M.; Carbone, D. P. *Lancet* **2003**, *362*, 433.
(123) Chaurand, P.; Latham, J. C.; Lane, K. B.; Mobley, J. A.; Polosukhin, V. V.; Wirth, P. S.; Nanney, L. B.; Caprioli, R. M. *J. Proteome Res.* **2008**, *7*, 3543.
(124) Groseclose, M. R.; Massion, P. P.; Chaurand, P.; Caprioli, R. M. *Proteomics* **2008**, *8*, 3715.
(125) Ronci, M.; Bonanno, E.; Colantoni, A.; Pieroni, L.; Di Ilio, C.; Spagnoli, L. G.; Federici, G.; Urbani, A. *Proteomics* **2008**, *8*, 3702.
(126) Stauber, J.; Lemaire, R.; Franck, J.; Bonnel, D.; Croix, D.; Day, R.; Wisztorski, M.; Fournier, I.; Salzet, M. *J. Proteome Res.* **2008**, *7*, 969.
(127) Lemaire, R.; Desmons, A.; Tabet, J. C.; Day, R.; Salzet, M.; Fournier, I. *J. Proteome Res.* **2007**, *6*, 1295.
(128) Djidja, M. C.; Francese, S.; Loadman, P. M.; Sutton, C. W.; Scriven, P.; Claude, E.; Snel, M. F.; Franck, J.; Salzet, M.; Clench, M. R. *Proteomics* **2009**, *9*, 2750.
(129) Djidja, M. C.; Claude, E.; Snel, M. F.; Scriven, P.; Francese, S.; Carolan, V.; Clench, M. R. *J. Proteome Res.* **2009**, *8*, 4876.
(130) Stauber, J.; Macaleese, L.; Franck, J.; Claude, E.; Snel, M.; Kukrer Kaletas, B.; Wiel, I. M.; Wisztorski, M.; Fournier, I.; Heeren, R. M. *J. Am. Soc. Mass Spectrom.* **2010**, *21*, 338.
(131) Crecelius, A. C.; Cornett, D. S.; Caprioli, R. M.; Williams, B.; Dawant, B. M.; Bodenheimer, B. *J. Am. Soc. Mass Spectrom.* **2005**, *16*, 1093.
(132) Liu, Q.; Xiao, Y.; Pagan-Miranda, C.; Chiu, Y. M.; He, L. *J. Am. Soc. Mass Spectrom.* **2009**, *20*, 80.
(133) Schwartz, S. A.; Weil, R. J.; Thompson, R. C.; Shyr, Y.; Moore, J. H.; Toms, S. A.; Johnson, M. D.; Caprioli, R. M. *Cancer Res.* **2005**, *65*, 7674.
(134) Seeley, E. H.; Caprioli, R. M. *Proc. Natl. Acad. Sci. U. S. A.* **2008**, *105*, 18126.
(135) Cornett, D. S.; Mobley, J. A.; Dias, E. C.; Andersson, M.; Arteaga, C. L.; Sanders, M. E.; Caprioli, R. M. *Mol. Cell. Proteomics* **2006**, *5*, 1975.
(136) Lemaire, R.; Menguellet, S. A.; Stauber, J.; Marchaudon, V.; Lucot, J. P.; Collinet, P.; Farine, M. O.; Vinatier, D.; Day, R.; Ducoroy, P.; Salzet, M.; Fournier, I. *J. Proteome Res.* **2007**, *6*, 4127.
(137) Roy, S.; Touboul, D.; Brunelle, A.; Germain, D. P.; Prognon, P.; Laprevote, O.; Chaminade, P. *Ann. Pharm. Fr.* **2006**, *64*, 328.
(138) Berman, E. S.; Fortson, S. L.; Checchi, K. D.; Wu, L.; Felton, J. S.; Wu, K. J.; Kulp, K. S. *J. Am. Soc. Mass Spectrom.* **2008**, *19*, 1230.
(139) Guo, J.; Colgan, T. J.; DeSouza, L. V.; Rodrigues, M. J.; Romaschin, A. D.; Siu, K. W. *Rapid Commun. Mass Spectrom.* **2005**, *19*, 2762.
(140) Chaurand, P.; Sanders, M. E.; Jensen, R. A.; Caprioli, R. M. *Am. J. Pathol.* **2004**, *165*, 1057.
(141) Lemaire, R.; Wisztorski, M.; Desmons, A.; Tabet, J. C.; Day, R.; Salzet, M.; Fournier, I. *Anal. Chem.* **2006**, *78*, 7145.
(142) Crecelius, A.; Gotz, A.; Arzberger, T.; Frohlich, T.; Arnold, G. J.; Ferrer, I.; Kretzschmar, H. A. *Proteomics* **2008**, *8*, 1276.
(143) Svensson, M.; Skold, K.; Nilsson, A.; Falth, M.; Nydahl, K.; Svenningsson, P.; Andren, P. E. *Anal. Chem.* **2007**, *79*, 15.
(144) Jia, X.; Hollung, K.; Therkildsen, M.; Hildrum, K. I.; Bendixen, E. *Proteomics* **2006**, *6*, 936.
(145) Svensson, M. S. K.; Svenningsson, P.; Andren, P. E. *J. Proteome Res.* **2003**, *2*, 213.
(146) O'Callaghan, J. P.; Sriram, K. *J. Neurosci. Methods* **2004**, *135*, 159.
(147) Ferrer, I.; Santpere, G.; Arzberger, T.; Bell, J.; Blanco, R.; Boluda, S.; Budka, H.; Carmona, M.; Giaccone, G.; Krebs, B.; Limido, L.; Parchi, P.; Puig, B.; Strammiello, R.; Strobel, T.; Kretzschmar, H. *J. Neuropathol. Exp. Neurol.* **2007**, *66*, 35.
(148) Fountoulakis, M.; Hardmeier, R.; Hoger, H.; Lubec, G. *Exp. Neurol.* **2001**, *167*, 86.
(149) Franzen, B.; Yang, Y.; Sunnemark, D.; Wickman, M.; Ottervald, J.; Oppermann, M.; Sandberg, K. *Proteomics* **2003**, *3*, 1920.
(150) Goodwin, R. J.; Dungworth, J. C.; Cobb, S. R.; Pitt, A. R. *Proteomics* **2008**, *8*, 3801.
(151) Skold, K.; Svensson, M.; Norrman, M.; Sjogren, B.; Svenningsson, P.; Andren, P. E. *Proteomics* **2007**, *7*, 4445.
(152) O'Callaghan, J. P.; Sriram, K. *J. Neurosci. Methods* **2004**, *135*, 159.
(153) Svensson, M.; Skold, K.; Svenningsson, P.; Andren, P. E. *J. Proteome Res.* **2003**, *2*, 213.
(154) Svensson, M.; Boren, M.; Skold, K.; Falth, M.; Sjogren, B.; Andersson, M.; Svenningsson, P.; Andren, P. E. *J. Proteome Res.* **2009**, *8*, 974.
(155) Mange, A.; Chaurand, P.; Perrochia, H.; Roger, P.; Caprioli, R. M.; Solassol, J. *J. Proteome Res.* **2009**, *8*, 5619.
(156) Chen, R.; Hui, L.; Sturm, R. M.; Li, L. *J. Am. Soc. Mass Spectrom.* **2009**, *20*, 1068.
(157) Sugiura, Y.; Shimma, S.; Setou, M. *J. Mass Spectrom. Soc. Jpn.* **2006**, *54*, 45.
(158) Caldwell, R. L.; Caprioli, R. M. *Mol. Cell. Proteomics* **2005**, *4*, 394.
(159) Chaurand, P.; Schwartz, S. A.; Crecelius, A.; Caprioli, R. M. *51st ASMS Conference on Mass Spectrometry and Allied Topics*; ASMS: Montreal, Canada, 2003.
(160) Chaurand, P.; Schwartz, S. A.; Billheimer, D.; Xu, B. J.; Crecelius, A.; Caprioli, R. M. *Anal. Chem.* **2004**, *76*, 1145.
(161) Groseclose, M. R.; Andersson, M.; Hardesty, W. M.; Caprioli, R. M. *J. Mass Spectrom.* **2007**, *42*, 254.
(162) Andersson, M.; Groseclose, M. R.; Deutch, A. Y.; Caprioli, R. M. *Nat. Methods* **2008**, *5*, 101.
(163) Brocchieri, L.; Karlin, S. *Nucleic Acids Res.* **2005**, *33*, 3390.
(164) Duncan, R.; McConkey, E. H. *Clin. Chem.* **1982**, *28*, 749.
(165) Rohner, T. C.; Staab, D.; Stoeckli, M. *Mech. Ageing Dev.* **2005**, *126*, 177.
(166) Binz, P. A.; Muller, M.; Hoogland, C.; Zimmermann, C.; Pasquarello, C.; Corthals, G.; Sanchez, J. C.; Hochstrasser, D. F.; Appel, R. D. *Curr. Opin. Biotechnol.* **2004**, *15*, 17.
(167) Stauber, J.; Macaleese, L.; Franck, J.; Claude, E.; Snel, M.; Kukrer Kaletas, B.; Wiel, I. M.; Wisztorski, M.; Fournier, I.; Heeren, R. M. *J. Am. Soc. Mass Spectrom.* **2010**, *21*, 338.
(168) Gluckmann, M.; Pfenninger, A.; Kruger, R.; Thierolf, M.; Karas, M.; Horneffer, V.; Hillenkamp, F.; Strupat, K. *Int. J. Mass Spectrom.* **2001**, *210/211*, 121.
(169) Zenobi, R.; Knochenmuss, R. *Mass Spectrom. Rev.* **1998**, *17*, 227.
(170) Beavis, R. C.; Chait, B. T. *Rapid Commun. Mass Spectrom.* **1989**, *3*, 432.
(171) Beavis, R. C.; Chait, B. T. *Rapid Commun. Mass Spectrom.* **1989**, *3*, 436.
(172) Tang, K.; Taranenko, N. I.; Allman, S. L.; Chang, L. Y.; Chen, C. H. *Rapid Commun. Mass Spectrom.* **1994**, *8*, 727.
(173) Wu, K. J.; Steding, A.; Becker, C. H. *Rapid Commun. Mass Spectrom.* **1993**, *7*, 142.
(174) Herring, K. D.; Oppenheimer, S. R.; Caprioli, R. M. *Semin. Nephrol.* **2007**, *27*, 597.
(175) Puolitaival, S. M.; Burnum, K. E.; Cornett, D. S.; Caprioli, R. M. *J. Am. Soc. Mass Spectrom.* **2008**, *19*, 882.
(176) Heeren, R. M. A.; Smith, D. F.; Stauber, J.; Kükrer-Kaletas, B.; Macaleese, L. A. *J. Am. Soc. Mass Spectrom.* **2009**, *20*, 1006.
(177) Lemaire, R.; Tabet, J. C.; Ducoroy, P.; Hendra, J. B.; Salzet, M.; Fournier, I. *Anal. Chem.* **2006**, *78*, 809.
(178) Dreisewerd, K. *Chem. Rev.* **2003**, *103*, 395.
(179) Chen, Y. T.; Ling, Y. C. *J. Mass Spectrom.* **2002**, *37*, 716.
(180) Ling, Y. C.; Lin, L.; Chen, Y. T. *Rapid Commun. Mass Spectrom.* **1998**, *12*, 317.
(181) McLean, J. A.; Stumpo, K. A.; Russell, D. H. *J. Am. Chem. Soc.* **2005**, *127*, 5304.
(182) Su, C. L.; Tseng, W. L. *Anal. Chem.* **2007**, *79*, 1626.
(183) Feng, C. H.; Lu, C. Y. *Anal. Chim. Acta* **2009**, *649*, 230.
(184) Bouslimani, A.; Bec, N.; Glueckmann, M.; Hirtz, C.; Larroque, C. *Rapid Commun. Mass Spectrom.* **2010**, *24*, 415.
(185) Norris, J. L.; Porter, N. A.; Caprioli, R. M. *Anal. Chem.* **2003**, *75*, 6642.
(186) Stoeckli, M.; Staab, D.; Staufenbiel, M.; Wiederhold, K. H.; Signor, L. *Anal. Biochem.* **2002**, *311*, 33.
(187) Luxembourg, S. L.; McDonnell, L. A.; Duursma, M. C.; Guo, X.; Heeren, R. M. *Anal. Chem.* **2003**, *75*, 2333.
(188) Lipton, M. S.; Pasa-Tolic, L. *Mass Spectrometry of Proteins and Peptides: Methods and Protocols*; Humana Press: 2009; p 295.
(189) Franck, J.; Arafah, K.; Barnes, A.; Wisztorski, M.; Salzet, M.; Fournier, I. *Anal. Chem.* **2009**, *81*, 8193.
(190) Cornett, D. S.; Reyzer, M. L.; Chaurand, P.; Caprioli, R. M. *Nat. Methods* **2007**, *4*, 828.
(191) Baluya, D. L.; Garrett, T. J.; Yost, R. A. *Anal. Chem.* **2007**, *79*, 6862.
(192) Hankin, J. A.; Barkley, R. M.; Murphy, R. C. *J. Am. Soc. Mass Spectrom.* **2007**, *18*, 1646.
(193) Dekker, L. J.; van Kampen, J. J.; Reedijk, M. L.; Burgers, P. C.; Gruters, R. A.; Osterhaus, A. D.; Luider, T. M. *Rapid Commun. Mass Spectrom.* **2009**, *23*, 1183.
(194) Liu, Q.; Guo, Z.; He, L. *Anal. Chem.* **2007**, *79*, 3535.
(195) Mengistu, T. Z.; DeSouza, L.; Morin, S. *J. Chromatogr., A* **2006**, *1135*, 194.
(196) Wei, J.; Buriak, J. M.; Siuzdak, G. *Nature* **1999**, *399*, 243.
(197) Zhang, H.; Cha, S.; Yeung, E. S. *Anal. Chem.* **2007**, *79*, 6575.
(198) Pan, C.; Xu, S.; Zou, H.; Guo, Z.; Zhang, Y.; Guo, B. *J. Am. Soc. Mass Spectrom.* **2005**, *16*, 263.
(199) Pan, C.; Xu, S.; Hu, L.; Su, X.; Ou, J.; Zou, H.; Guo, Z.; Zhang, Y.; Guo, B. *J. Am. Soc. Mass Spectrom.* **2005**, *16*, 883.
(200) Keller, B. O.; Sui, J.; Young, A. B.; Whittal, R. M. *Anal. Chim. Acta* **2008**, *627*, 71.
(201) Aebersold, R.; Mann, M. *Nature* **2003**, *422*, 198.
(202) Stephens, W. E.; Serin, B.; Meyerhof, W. E. *Phys. Rev.* **1946**, *69*, 42.

(203) Schwieters, J.; Cramer, H. G.; Heller, T.; Jurgens, U.; Niehuis, E.; Zehnpfenning, J.; Benninghoven, A. *J. Vac. Sci. Technol., A* **1991**, *9*, 2864.
(204) Kutz, K. K.; Schmidt, J. J.; Li, L. *Anal. Chem.* **2004**, *76*, 5630.
(205) Laiko, V. V.; Dodonov, A. F. *Rapid Commun. Mass Spectrom.* **1994**, *8*, 720.
(206) Dunn, W. B. *Phys. Biol.* **2008**, *5*, 11001.
(207) Cornett, D. S.; Frappier, S. L.; Caprioli, R. M. *Anal. Chem.* **2008**, *80*, 5648.
(208) Wolters, D. A.; Washburn, M. P.; Yates, J. R. *Anal. Chem.* **2001**, *73*, 5683.
(209) Wiseman, J. M.; Ifa, D. R.; Song, Q.; Cooks, R. G. *Angew. Chem., Int. Ed. Engl.* **2006**, *45*, 7188.
(210) Landgraf, R. R.; Prieto Conaway, M. C.; Garrett, T. J.; Stacpoole, P. W.; Yost, R. A. *Anal. Chem.* **2009**, *81*, 8488.
(211) Garrett, T. J.; Prieto-Conaway, M. C.; Kovtoun, V.; Bui, H.; Izgarian, N.; Stafford, G.; Yost, R. A. *Int. J. Mass Spectrom.* **2007**, *260*, 166.
(212) Panos, H.; Stephan, B.; Jay, C.; Peter, K.; Dietrich, A. V. *Rapid Commun. Mass Spectrom.* **2003**, *17*, 2303.
(213) Slodzian, G.; Daigne, B.; Girard, F.; Boust, F.; Hillion, F. *Biol. Cell* **1992**, *74*, 43.
(214) Jardin-Mathe, O.; Bonnel, D.; Franck, J.; Wisztorski, M.; Macagno, E.; Fournier, I.; Salzet, M. *J. Proteomics* **2008**, *71*, 332.
(215) Perkins, D. N.; Pappin, D. J.; Creasy, D. M.; Cottrell, J. S. *Electrophoresis* **1999**, *20*, 3551.
(216) Hanselmann, M.; Kothe, U.; Kirchner, M.; Renard, B. Y.; Amstalden, E. R.; Glunde, K.; Heeren, R. M.; Hamprecht, F. A. *J. Proteome Res.* **2009**, *8*, 3558.
(217) Deininger, S. O.; Ebert, M. P.; Futterer, A.; Gerhard, M.; Rocken, C. *J. Proteome Res.* **2008**, *7*, 5230.
(218) Zaima, N.; Matsuyama, Y.; Setou, M. *J. Oleo Sci.* **2009**, *58*, 267.
(219) Van de Plas, R.; Ojeda, F.; Dewil, M.; Van Den Bosch, L.; De Moor, B.; Waelkens, E. *Pac. Symp. Biocomput.* **2007**, 458.
(220) Verbeck, G.; Ruotolo, B.; Sawyer, H.; Gillig, K.; Russell, D. *J. Biomol. Technol.* **2002**, *13*, 56.
(221) Jackson, S. N.; Ugarov, M.; Egan, T.; Post, J. D.; Langlais, D.; Albert Schultz, J.; Woods, A. S. *J. Mass Spectrom.* **2007**, *42*, 1093.
(222) van Duijn, E.; Barendregt, A.; Synowsky, S.; Versluis, C.; Heck, A. J. *J. Am. Chem. Soc.* **2009**, *131*, 1452.
(223) Stauber, J.; van der Wiel, I. M.; Snel, M.; Claude, E.; Heeren, R. M. A. *Proc. ASMS Conf., 56th* 2008.
(224) Pringlea, S. D.; Gilesa, K.; Wildgoosea, J. L.; Williamsb, J. P.; Sladeb, S. E.; Thalassinosb, K.; Batemana, R. H.; Bowersc, M. T.; Scrivens, J. H. *Int. J. Mass Spectrom.* **2007**, *261*, 1.
(225) McLean, J. A.; Ridenour, W. B.; Caprioli, R. M. *J. Mass Spectrom.* **2007**, *42*, 1099.
(226) Altelaar, M. A.; Taban, I. M.; McDonnell, L. A.; de Lange, R. P.; Adan, R. A.; Mooi, W. J.; Heeren, R. M.; Piersma, S. R. *Int. J. Mass Spectrom.* **2006**, *260*, 203.
(227) Xu, B. J.; Caprioli, R. M.; Sanders, M. E.; Jensen, R. A. *J. Am. Soc. Mass Spectrom.* **2002**, *13*, 1292.
(228) Palmer-Toy, D. E.; Sarracino, D. A.; Sgroi, D.; LeVangie, R.; Leopold, P. E. *Clin. Chem.* **2000**, *46*, 1513.
(229) Lemaire, R.; Stauber, J.; Wisztorski, M.; Van Camp, C.; Desmons, A.; Deschamps, M.; Proess, G.; Rudlof, I.; Woods, A. S.; Day, R.; Salzet, M.; Fournier, I. *J. Proteome Res.* **2007**, *6*, 2057.
(230) Thiery, G.; Shchepinov, M. S.; Southern, E. M.; Audebourg, A.; Audard, V.; Terris, B.; Gut, I. G. *Rapid Commun. Mass Spectrom.* **2007**, *21*, 823.
(231) Pierson, J.; Norris, J. L.; Aerni, H. R.; Svenningsson, P.; Caprioli, R. M.; Andren, P. E. *J. Proteome Res.* **2004**, *3*, 289.
(232) Grossi, C.; Francese, S.; Casini, A.; Rosi, M. C.; Luccarini, I.; Fiorentini, A.; Gabbiani, C.; Messori, L.; Moneti, G.; Casamenti, F. *J. Alzheimer's Dis.* **2009**, *17*, 423.
(233) Touboul, D.; Roy, S.; Germain, D. P.; Chaminade, P.; Brunelle, A.; Laprévote, O. *Int. J. Mass Spectrom.* **2007**, *260*, 158.
(234) Touboul, D.; Piednoel, H.; Voisin, V.; De La Porte, S.; Brunelle, A.; Halgand, F.; Laprevote, O. *Eur. J. Mass Spectrom.* **2004**, *10*, 657.
(235) Meistermann, H.; Norris, J. L.; Aerni, H. R.; Cornett, D. S.; Friedlein, A.; Erskine, A. R.; Augustin, A.; De Vera Mudry, M. C.; Ruepp, S.; Suter, L.; Langen, H.; Caprioli, R. M.; Ducret, A. *Mol. Cell. Proteomics* **2006**, *5*, 1876.
(236) Xu, B. J.; Shyr, Y.; Liang, X.; Ma, L. J.; Donnert, E. M.; Roberts, J. D.; Zhang, X.; Kon, V.; Brown, N. J.; Caprioli, R. M.; Fogo, A. B. *J. Am. Soc. Nephrol.* **2005**, *16*, 2967.
(237) Debois, D.; Bralet, M. P.; Le Naour, F.; Brunelle, A.; Laprevote, O. *Anal. Chem.* **2009**, *81*, 2823.
(238) Chen, Y.; Allegood, J.; Liu, Y.; Wang, E.; Cachon-Gonzalez, B.; Cox, T. M.; Merrill, A. H., Jr.; Sullards, M. C. *Anal. Chem.* **2008**, *80*, 2780.
(239) Quonga, J. N.; Knizeb, M. G.; Kulpb, K. S.; Wu, K. J. *Appl. Surf. Sci.* **2004**, *231/232*, 424.
(240) Cazares, L. H.; Troyer, D.; Mendrinos, S.; Lance, R. A.; Nyalwidhe, J. O.; Beydoun, H. A.; Clements, M. A.; Drake, R. R. *Clin. Cancer Res.* **2009**, *15*, 5541.
(241) Shimma, S.; Sugiura, Y.; Hayasaka, T.; Hoshikawa, Y.; Noda, T.; Setou, M. *J. Chromatogr., B: Anal. Technol. Biomed. Life Sci.* **2007**, *855*, 98.
(242) Schwartz, S. A.; Weil, R. J.; Johnson, M. D.; Toms, S. A.; Caprioli, R. M. *Clin. Cancer Res.* **2004**, *10*, 981.
(243) Sanders, M. E.; Dias, E. C.; Xu, B. J.; Mobley, J. A.; Billheimer, D.; Roder, H.; Grigorieva, J.; Dowsett, M.; Arteaga, C. L.; Caprioli, R. M. *J. Proteome Res.* **2008**, *7*, 1500.
(244) Kang, S.; Shim, H. S.; Lee, J. S.; Kim, D. S.; Kim, H. Y.; Hong, S. H.; Kim, P. S.; Youn, J. H.; Cho, N. H. *J. Proteome Res.* **2010**, *9*, 1157.
(245) Dill, A. L.; Ifa, D. R.; Manicke, N. E.; Costa, A. B.; Ramos-Vara, J. A.; Knapp, D. W.; Cooks, R. G. *Anal. Chem.* **2009**, *81*, 8758.
(246) Matusch, A.; Depboylu, C.; Palm, C.; Wu, B.; Hoglinger, G. U.; Schafer, M. K.; Becker, J. S. *J. Am. Soc. Mass Spectrom.* **2009**, *21*, 161.
(247) Yao, I.; Sugiura, Y.; Matsumoto, M.; Setou, M. *Proteomics* **2008**, *8*, 3692.
(248) Le Naour, F.; Bralet, M. P.; Debois, D.; Sandt, C.; Guettier, C.; Dumas, P.; Brunelle, A.; Laprevote, O. *PLoS One* **2009**, *4*, 7408.
(249) Manicke, N. E.; Nefliu, M.; Wu, C.; Woods, J. W.; Reiser, V.; Hendrickson, R. C.; Cooks, R. G. *Anal. Chem.* **2009**, *81*, 8702.
(250) Patel, S. A.; Barnes, A.; Loftus, N.; Martin, R.; Sloan, P.; Thakker, N.; Goodacre, R. *Analyst* **2009**, *134*, 301.
(251) Kim, J. H.; Kim, J. H.; Ahn, B. J.; Park, J. H.; Shon, H. K.; Yu, Y. S.; Moon, D. W.; Lee, T. G.; Kim, K. W. *Biophys. J.* **2008**, *94*, 4095.
(252) McDonnell, L. A.; van Remoortere, A.; van Zeijl, R. J.; Dalebout, H.; Bladergroen, M. R.; Deelder, A. M. *J. Proteomics*, in press.
(253) Fournier, I.; Wisztorski, M.; Salzet, M. *Expert Rev. Proteomics* **2008**, *5*, 413.
(254) Wisztorski, M.; Lemaire, R.; Stauber, J.; Menguelet, S. A.; Croix, D.; Mathe, O. J.; Day, R.; Salzet, M.; Fournier, I. *Curr. Pharm. Des.* **2007**, *13*, 3317.
(255) Caprioli, R. M. *Proteomics* **2008**, *8*, 3679.
(256) Cobb, S. R.; Pitt, A. *Expert Rev. Proteomics* **2008**, *5*, 393.
(257) Jaffer, F. A.; Libby, P.; Weissleder, R. *Arterioscler., Thromb., Vasc. Biol.* **2009**, *29*, 1017.
(258) Magalhaes, B. S.; Melo, J. A.; Leite, J. R.; Silva, L. P.; Prates, M. V.; Vinecky, F.; Barbosa, E. A.; Verly, R. M.; Mehta, A.; Nicoli, J. R.; Bemquerer, M. P.; Andrade, A. C.; Bloch, C., Jr. *Biochem. Biophys. Res. Commun.* **2008**, *377*, 1057.
(259) Brand, G. D.; Krause, F. C.; Silva, L. P.; Leite, J. R.; Melo, J. A.; Prates, M. V.; Pesquero, J. B.; Santos, E. L.; Nakaie, C. R.; Costa-Neto, C. M.; Bloch, C., Jr. *Peptides* **2006**, *27*, 2137.
(260) Han, J.; Schey, K. L. *Invest. Ophthalmol. Visual Sci.* **2006**, *47*, 2990.
(261) Grey, A. C.; Schey, K. L. *Invest. Ophthalmol. Visual Sci.* **2009**, *50*, 4319.
(262) Grey, A. C.; Chaurand, P.; Caprioli, R. M.; Schey, K. L. *J. Proteome Res.* **2009**, *8*, 3278.
(263) Rujoi, M.; Estrada, R.; Yappert, M. C. *Anal. Chem.* **2004**, *76*, 1657.
(264) Kutz, K. K.; Schmidt, J. J.; Li, L. *Anal. Chem.* **2004**, *76*, 5630.
(265) Hummon, A. B.; Amare, A.; Sweedler, J. V. *Mass Spectrom. Rev.* **2006**, *25*, 77.
(266) DeKeyser, S. S.; Kutz-Naber, K. K.; Schmidt, J. J.; Barrett-Wilt, G. A.; Li, L. *J. Proteome Res.* **2007**, *6*, 1782.
(267) Verhaerta, P. D.; Prieto Conawaye, M. C.; Pekare, T. M.; Miller, K. *Int. J. Mass Spectrom.* **2006**, *260*, 177.
(268) Sugiura, Y.; Shimma, S.; Konishi, Y.; Yamada, M. K.; Setou, M. *PLoS ONE* **2008**, *3*, 3232.
(269) Chan, K.; Lanthier, P.; Liu, X.; Sandhu, J. K.; Stanimirovic, D.; Li, J. *Anal. Chim. Acta* **2009**, *639*, 57.
(270) Robinson, S.; Warburton, K.; Seymour, M.; Clench, M.; Thomas-Oates, J. *New Phytol.* **2007**, *173*, 438.
(271) Mullen, A. K.; Clench, M. R.; Crosland, S.; Sharples, K. R. *Rapid Commun. Mass Spectrom.* **2005**, *19*, 2507.
(272) Anderson, D. M.; Carolan, V. A.; Crosland, S.; Sharples, K. R.; Clench, M. R. *Rapid Commun. Mass Spectrom.* **2009**, *23*, 1321.
(273) Burrell, M.; Earnshaw, C.; Clench, M. *J. Exp. Bot.* **2007**, *58*, 757.
(274) Cha, S.; Song, Z.; Nikolau, B. J.; Yeung, E. S. *Anal. Chem.* **2009**, *81*, 2991.
(275) Cavatorta, V.; Sforza, S.; Mastrobuoni, G.; Pieraccini, G.; Francese, S.; Moneti, G.; Dossena, A.; Pastorello, E. A.; Marchelli, R. *J. Mass Spectrom.* **2009**, *44*, 891.
(276) Genji, T.; Fukuzawa, S.; Tachibana, K. *Mar. Biotechnol.* **2010**, *12*, 81.
(277) Burnum, K. E.; Cornett, D. S.; Puolitaival, S. M.; Milne, S. B.; Myers, D. S.; Tranguch, S.; Brown, H. A.; Dey, S. K.; Caprioli, R. M. *J. Lipid Res.* **2009**, *50*, 2290.

(278) Francese, S.; Lambardi, D.; Mastrobuoni, G.; la Marca, G.; Moneti, G.; Turillazzi, S. *J. Am. Soc. Mass Spectrom.* **2009**, *20*, 112.
(279) Wysocki, V. H.; Resing, K. A.; Zhang, Q.; Cheng, G. *Methods* **2005**, *35*, 211.
(280) Han, X.; Aslanian, A.; Yates, J. R., 3rd *Curr. Opin. Chem. Biol.* **2008**, *12*, 483.
(281) Chaurand, P.; Stoeckli, M.; Caprioli, R. M. *Anal. Chem.* **1999**, *71*, 5263.
(282) Bienvenut, W. V.; Sanchez, J. C.; Karmime, A.; Rouge, V.; Rose, K.; Binz, P. A.; Hochstrasser, D. F. *Anal. Chem.* **1999**, *71*, 4800.
(283) Binz, P. A.; Muller, M.; Walther, D.; Bienvenut, W. V.; Gras, R.; Hoogland, C.; Bouchet, G.; Gasteiger, E.; Fabbretti, R.; Gay, S.; Palagi, P.; Wilkins, M. R.; Rouge, V.; Tonella, L.; Paesano, S.; Rossellat, G.; Karmime, A.; Bairoch, A.; Sanchez, J. C.; Appel, R. D.; Hochstrasser, D. F. *Anal. Chem.* **1999**, *71*, 4981.
(284) Muller, M.; Gras, R.; Appel, R. D.; Bienvenut, W. V.; Hochstrasser, D. F. *J. Am. Soc. Mass Spectrom.* **2002**, *13*, 221.
(285) Dani, F. R.; Francese, S.; Mastrobuoni, G.; Felicioli, A.; Caputo, B.; Simard, F.; Pieraccini, G.; Moneti, G.; Coluzzi, M.; della Torre, A.; Turillazzi, S. *PLoS One* **2008**, *3*, 2822.
(286) Rubakhin, S. S.; Li, L.; Moroz, T. P.; Sweedler, J. V. *J. Neurophysiol.* **1999**, *81*, 1251.
(287) Li, L.; Garden, R. W.; Sweedler, J. V. *Trends Biotechnol.* **2000**, *18*, 151.
(288) Masujima, T. *Anal. Sci.* **2009**, *25*, 953.
(289) van Veelen, P. A.; Jiménez, C. R.; Li, K. W.; Wildering, W. C.; M., G. W. P.; Tjaden, U. R.; van der Greef, J. *Org. Mass Spectrom.* **1993**, *28*, 1542.
(290) Jimenez, C. R.; van Veelen, P. A.; Li, K. W.; Wildering, W. C.; Geraerts, W. P.; Tjaden, U. R.; van der Greef, J. *J. Neurochem.* **1994**, *62*, 404.
(291) Hsieh, S.; Dreisewerd, K.; van der Schors, R. C.; Jimenez, C. R.; Stahl-Zeng, J.; Hillenkamp, F.; Jorgenson, J. W.; Geraerts, W. P.; Li, K. W. *Anal. Chem.* **1998**, *70*, 1847.
(292) Redeker, V.; Toullec, J. Y.; Vinh, J.; Rossier, J.; Soyez, D. *Anal. Chem.* **1998**, *70*, 1805.
(293) Ma, P. W.; Garden, R. W.; Niermann, J. T.; Sweedler, J. V.; Roelofs, W. L. *J. Insect Physiol.* **2000**, *46*, 221.
(294) Whittal, R. M.; Keller, B. O.; Li, L. *Anal. Chem.* **1998**, *70*, 5344.
(295) Shimizu, M.; Levi-Schaffer, F.; Ojima, N.; Shingaki, T.; Masujima, T. *Anal. Sci.* **2002**, *18*, 107.
(296) Rubakhin, S. S.; Sweedler, J. V. *Nat. Protoc.* **2007**, *2*, 1987.
(297) Altelaar, A. F. M.; van Minnen, J.; Jimenez, C. R.; Heeren, R. M. A.; Piersma, S. R. *Anal. Chem.* **2005**, *77*, 735.
(298) Jimenez, C. R.; Li, K. W.; Dreisewerd, K.; Spijker, S.; Kingston, R.; Bateman, R. H.; Burlingame, A. L.; Smit, A. B.; van Minnen, J.; Geraerts, W. P. *Biochemistry* **1998**, *37*, 2070.
(299) Li, K. W.; Hoek, R. M.; Smith, F.; Jimenez, C. R.; van der Schors, R. C.; van Veelen, P. A.; Chen, S.; van der Greef, J.; Parish, D. C.; Benjamin, P. R.; et al. *J. Biol. Chem.* **1994**, *269*, 30288.
(300) Garden, R. W.; Moroz, L. L.; Moroz, T. P.; Shippy, S. A.; Sweedler, J. V. *J. Mass Spectrom.* **1996**, *31*, 1126.
(301) Wong, S. C.; Chan, C. M.; Ma, B. B.; Lam, M. Y.; Choi, G. C.; Au, T. C.; Chan, A. S.; Chan, A. T. *Expert Rev. Proteomics* **2009**, *6*, 123.
(302) Miura, D.; Fujimura, Y.; Tachibana, H.; Wariishi, H. *Anal. Chem.* **2010**, *82*, 498.
(303) Forster, J.; Famili, I.; Fu, P.; Palsson, B. O.; Nielsen, J. *Genome Res.* **2003**, *13*, 244.
(304) Sugiura, Y.; Setou, M. *J. Neuroimmune Pharmacol.* **2010**, *5*, 31.
(305) Benabdellah, F.; Touboul, D.; Brunelle, A.; Laprevote, O. *Anal. Chem.* **2009**, *81*, 5557.
(306) Lee, S. H.; Williams, M. V.; DuBois, R. N.; Blair, I. A. *Rapid Commun. Mass Spectrom.* **2003**, *17*, 2168.
(307) Jones, J. J.; Borgmann, S.; Wilkins, C. L.; O'Brien, R. M. *Anal. Chem.* **2006**, *78*, 3062.
(308) Nakanishi, H.; Shindou, H.; Hishikawa, D.; Harayama, T.; Ogasawara, R.; Suwabe, A.; Taguchi, R.; Shimizu, T. *J. Biol. Chem.* **2006**, *281*, 20140.
(309) O'Brien, J. S.; Sampson, E. L.; Stern, M. B. *J. Neurochem.* **1967**, *14*, 357.
(310) Woollett, L. A. *Curr. Opin. Lipidol.* **2001**, *12*, 305.
(311) Woollett, L. A. *Annu. Rev. Nutr.* **2008**, *28*, 97.
(312) Nature Publishing Group and the LIPID MAPS consortium. Lipidomics Gateway. http://www.lipidmaps.org.
(313) Schiller, J.; Suss, R.; Arnhold, J.; Fuchs, B.; Lessig, J.; Muller, M.; Petkovic, M.; Spalteholz, H.; Zschornig, O.; Arnold, K. *Prog. Lipid Res.* **2004**, *43*, 449.
(314) Dill, A. L.; Ifa, D. R.; Manicke, N. E.; Ouyang, Z.; Cooks, R. G. *J. Chromatogr., B: Anal. Technol. Biomed. Life Sci.* **2009**, *877*, 2883.
(315) Pulfer, M.; Murphy, R. C. *Mass Spectrom. Rev.* **2003**, *22*, 332.
(316) Malmberg, P.; Nygren, H.; Sjövall, P.; Lausmaa, J. *Spectroscopy* **2004**, *18*, 503.
(317) Hsu, F. F.; Turk, J.; Zhang, K.; Beverley, S. M. *J. Am. Soc. Mass Spectrom.* **2007**, *18*, 1591.
(318) Li, C.; Yergey, J. A. *J. Mass Spectrom.* **1997**, *32*, 314.
(319) Kim, Y.; Shanta, S. R.; Zhou, L. H.; Kim, K. P. *Exp. Mol. Med.* **2009**, *42*, 1.
(320) Jackson, S. N.; Wang, H. Y.; Woods, A. S. *J. Am. Soc. Mass Spectrom.* **2005**, *16*, 2052.
(321) Sugiura, Y.; Setou, M. *Rapid Commun. Mass Spectrom.* **2009**, *23*, 3269.
(322) Sugiura, Y.; Shimma, S.; Setou, M. *Anal. Chem.* **2006**, *78*, 8227.
(323) Isaac, G.; Jeannotte, R.; Esch, S. W.; Welti, R. *Genet. Eng.* **2007**, *28*, 129.
(324) Hayasaka, T.; Goto-Inoue, N.; Sugiura, Y.; Zaima, N.; Nakanishi, H.; Ohishi, K.; Nakanishi, S.; Naito, T.; Taguchi, R.; Setou, M. *Rapid Commun. Mass Spectrom.* **2008**, *22*, 3415.
(325) Garrett, T. J.; Dawson, W. W. *Methods Mol. Biol.* **2009**, *579*, 247.
(326) Patti, G. J.; Woo, H. K.; Yanes, O.; Shriver, L.; Thomas, D.; Uritboonthai, W.; Apon, J. V.; Steenwyk, R.; Manchester, M.; Siuzdak, G. *Anal. Chem.* **2010**, *82*, 121.
(327) Solon, E. G.; Schweitzer, A.; Stoeckli, M.; Prideaux, B. *AAPS J.* **2010**, *12*, 11.
(328) Troendle, F. J.; Reddick, C. D.; Yost, R. A. *J. Am. Soc. Mass Spectrom.* **1999**, *10*, 1315.
(329) Reyzer, M. L.; Hsieh, Y.; Ng, K.; Korfmacher, W. A.; Caprioli, R. M. *J. Mass Spectrom.* **2003**, *38*, 1081.
(330) Hsieh, Y.; Casale, R.; Fukuda, E.; Chen, J.; Knemeyer, I.; Wingate, J.; Morrison, R.; Korfmacher, W. *Rapid Commun. Mass Spectrom.* **2006**, *20*, 965.
(331) Rubakhin, S. S.; Jurchen, J. C.; Monroe, E. B.; Sweedler, J. V. *Drug Discovery Today* **2005**, *10*, 823.
(332) Bunch, J.; Clench, M. R.; Richards, D. S. *Rapid Commun. Mass Spectrom.* **2004**, *18*, 3051.
(333) Wang, H. Y.; Jackson, S. N.; McEuen, J.; Woods, A. S. *Anal. Chem.* **2005**, *77*, 6682.
(334) Atkinson, S. J.; Loadman, P. M.; Sutton, C.; Patterson, L. H.; Clench, M. R. *Rapid Commun. Mass Spectrom.* **2007**, *21*, 1271.
(335) Zhigaltsev, I. V.; Maurer, N.; Akhong, Q. F.; Leone, R.; Leng, E.; Wang, J.; Semple, S. C.; Cullis, P. R. *J. Controlled Release* **2005**, *104*, 103.
(336) Image Processing and Analysis in Java. USA. http://rsbweb.nih.gov/ij/.
(337) Eberlin, L. S.; Ifa, D. R.; Wu, C.; Cooks, R. G. *Angew. Chem., Int. Ed. Engl.* **2009**, *49*, 873.
(338) Sinha, T. K.; Khatib-Shahidi, S.; Yankeelov, T. E.; Mapara, K.; Ehtesham, M.; Cornett, D. S.; Dawant, B. M.; Caprioli, R. M.; Gore, J. C. *Nat. Methods* **2008**, *5*, 57.
(339) National High Magnetic Field Laboratory, FL, USA. gnet.fsu.edu.
(340) National ESCA and Surface Analysis Center for Biomedical Problems (NESAC/BIO), WA, USA. www.nb.engr.washington.edu.

CR100012C